STAT

On the Determination of Nuclear Spins by the Study of Neutron Capture Gamma Rays

by

GEORG TRUMPY

No. 13

JENER PUBLICATIONS

JOINT ESTABLISHMENT FOR NUCLEAR ENERGY RESEARCH

Kjeller per Lillestrøm, 1957

AKADEMISK TRYKNINGSSENTRAL · BLINDERN, OSLO 1957

On the Determination of Nuclear Spins by the Study of Neutron Capture Gamma Rays

by

GEORG TRUMPY

No. 13

JENER PUBLICATIONS

JOINT ESTABLISHMENT FOR NUCLEAR ENERGY RESEARCH

Kjeller per Lillestrøm, 1957

CONTENTS

ABSTRACT

Two types of experiments, studying angular momenta of γ-rays and of energy levels connected with radiative neutron capture, have been performed. Circular polarization of the γ-rays emitted from nuclei capturing polarized neutrons was studied by means of the dependence of the Compton cross section upon the relative spin direction of the photon and the electron. Thermal neutrons polarized by transmission through magnetized iron fell on the (n,γ)-target, and the γ-rays were detected by two NaI (Tl)-crystals after having passed through analyzers of iron magnetized in the direction of transmission. The degree of circular polarization was found to be in accordance with theory. Measurements were performed for the most intense neutron capture γ-rays from S, Ca, Ti, Cr, Fe, Ni, Cu, Zn and W.

Coincidence and angular correlation experiments were carried out using neutron capturing targets as sources. The existence of several γ-ray cascades was established. An earlier unobserved γ-ray of 0.60 ± 0.05 MeV in Cu^{64} was found. The most prominent γ-ray cascades of Cl, Cr, Ni and Cu were studied by the angular correlation method.

Combined results of these experiments yielded several spin values for the nuclei studied. The first part of the paper deals with theoretical aspects pertinent to methods of these kinds In particular, the degree of circular polarization of γ-rays emitted from nuclei capturing polarized neutrons has been calculated for various cases, including emission of mixed multipoles.

CHAPTER I

INTRODUCTION

The existing theories on nuclear structure have led to various predictions about nuclear properties. Particularly the nuclear shell model by Mayer (1950) and Haxel, Jensen and Suess (1950) together with the theory on collective motions in nuclei by Bohr and Mottelson (1952, 1953) have successfully accounted for a greater part of the existing data on nuclear energy level schemes. The spins x) and parities of stable nuclei are now very well understood, but compared to the large number of energy levels that have been observed, rather little has been experimentally determined about nuclear spins in excited states. From measurements on energies, spins and parities of excited nuclear levels the reliability of theoretical predictions can be checked. On the other hand, studies of cumulated experimental nuclear data may suggest new theoretical methods.

No generally useful method has been developed for the study of the spins of the nuclear energy levels. There are many different ways in which nuclear states can be observed, but any particular level is usually known from one or two types of reactions only.

Special conventional methods, primarily used for the study of the ground states of stable nuclei, are well developed. Among these are the measurement of the hyperfine structure of atomic spectra, the atomic and molecular beam methods, the nuclear induction methods and microwave spectroscopy. These techniques can also be applied to the measurement of the properties of relatively long-lived radioactive and isomeric states, provided that the excited nuclei can be obtained in sufficient quantity.

The spins of short-lived nuclear states must be studied by means of observation of their decay products. In some cases this can be done for random orientation of the exited nuclei, for example when one can measure the lifetime or internal conversion coefficient of γ-radiation, the lifetime and form of the spectrum for β-radiation, and the peak height and width of resonances for particle absorption and scattering. The theories for the lifetimes of γ- and β-rays and for the shape of β-spectra are, however, not complete and ambiguities may occur in the determination of nuclear spins with these methods.

The third group of experimental techniques consists of the measurement of angular distribution or polarization of the reaction products. Clearly, these properties, being dependent upon a preferred direction in space, require that the excited nuclei are polarized. Polarization here includes any deviation from the usual random orientation of the nuclear spin directions. Spiers (1948) first showed that the reaction products from aligned nuclei in general will be anisotropically distributed. The polarization and distribution of γ-rays was calculated by Tolhoek and Cox (1953).

x) According to current terminology, the total angular momentum of a nucleus in this paper will be referred to as "nuclear spin" in cases where no confusion with intrinsic spin of single particles should be possible.

The most straightforward way of polarizing nuclei is the alignment of nuclear magnetic moments in magnetic fields. This method, however, requires very low temperatures, $< 1^{o}$ K, combined with strong magnetic fields. The technique is very specialized and refined and it has hitherto found little application.

When the incident particles in a nuclear reaction have a definite spin direction or a definite angular momentum relative to the nucleus, the total angular momentum of the compound system will not be randomly oriented. Therefore, the reaction products may show a certain polarization or directional distribution with respect to the incident axis of spin or momentum. This will also be the case when no compound nucleus is formed, like in deuteron stripping, for example. The technique of measuring directional distributions of reaction products due to the angular momentum of the incident particles has been applied to nearly all types of nuclear reactions. Incidence or emission of polarized particles can give increased information, but the procedure may be rather complicated because of the difficulty of production and detection of polarized particles.

Finally, randomly oriented excited nuclei may become polarized by emission of radiation in a definite direction. If a nucleus decays by the emission of radiation in two rapidly consecutive steps, the observation of a fixed direction or polarization for the first reaction product will serve to select the disintegrations of nuclei with a certain spin orientation. The second disintegration then may have directional correlation or polarization correlation with respect to the first one. The first event may also consist in particle emission. A coincidence detection system is required for the selection of the pair of reaction products from the same nucleus. This principle is especially used for investigations of the spins of radioactive nuclei decaying by means of β - γ - or γ - γ -cascades.

The present work is concerned with the study of the spins of the nuclear energy levels that can be observed when the excitation of nuclei by the capture of neutrons is followed by γ-ray emission. This is a well known reaction which can take place in almost all nuclei. Some of the theoretical aspects pertinent to radiative neutron capture are treated in chapter II. Using a magnetic pair spectrometer, Kinsey, Bartholomew and Walker (1951 abc, 1952) and Kinsey and Bartholomew (1953 abcde) have carried out a very comprehensive study of the energies and intensities of the high energy neutron capture γ-rays from most of the elements of the periodic table. Another magnetic spectrometer, measuring the energy of Compton electrons, was used by Groshev, Adyasevich and Demidov (1955 ab) for the study of a smaller number of spectra. The latter instrument gives very good resolving power for all energies of interest, whereas the former one can not be used for energies below 3 MeV, and gives good resolution above 4.5 MeV γ-ray energy only. The most useful of other methods is the application of NaI(Tl)-scintillation crystals for the study of neutron capture γ-rays at low energy. Reier and Shamos (1955) and Braid (1956) successfully applied this technique.

From the knowledge on γ-ray energies and intensities, tentative decay schemes may be constructed, in many cases with great certainty, dependent upon the number of isotopes in the target and the complexity of the decay scheme. The γ-ray cascades can be followed in detail by coincidence measurements. A few studies of that kind are contained in chapter IV. In many cases the level scheme is known from (d,p)-reaction studies, and when the angular distribution of the protons has been measured, the orbital angular momentum of the level is known. It is more difficult to obtain the level spins from radiation intensities, since the connection between γ-ray emission probabilities and multipolarities are still not well known.

The measurement of internal conversion of γ-rays of low energy is a practical method for the determination of multipole orders, and it was applied by Muehlhause and Hibdon (1951 ab, 1952) to the study of radiation below 0.5 MeV following neutron capture. Since the conversion coefficient is decreasing rapidly as energy increases (Rose et al 1951), the principle is not very useful at higher energies of the capture radiation. In that case, the alternative method, internal pair formation, is more promising because its conversion coefficient is increasing with energy (Rose 1949). However, as the spectra of the pair electrons are continuous, it seems to be experimentally very hard to study the pairs originating from internal conversion of a definite γ-ray in the presence of a complicated distribution of radiation energies.

The interaction of polarized neutrons with samples polarized in magnetic fields has been studied

by Bernstein and co-workers (1954 ab, 1955). By means of measurements of the neutron transmission or the activity induced in the samples, they were able to determine whether the spin of the captured neutron was added to or subtracted from the spin of the target nucleus. As an apparatus for polarizing nuclei was not available for the present study, the useful methods would consist in polarization performed by the incident neutrons or by the emitted photons.

Polarized neutrons can be obtained from nuclear reactions, for example from the d-d-reaction as predicted by Wolfenstein (1949 a) and measured by Meier, Scherrer and Trumpy (1954). However, the fast neutrons have such a low capture cross section that they can hardly be used for the experimental study of neutron capture γ-rays. Polarized beams of thermal neutrons are fairly easily obtained, but their use is limited because only particles with angular momentum zero are captured. Halpern (1951 ab) was the first to suggest the measurement of circularly polarized γ-rays following the capture of polarized thermal neutrons. When the degree of circular polarization is measured, some information of the spin states of the emitting nucleus can be derived. This principle is discussed in chapter III together with the description of an experimental set-up and some measured results.

The second possibility, being the study of γ-ray cascades by means of the angular correlation method, is treated in chapter IV. An apparatus was built and a few experiments were performed.

Regarding the theoretical considerations of the following chapters, it should be pointed out that in several cases the use of the same symbol for different properties has been unavoidable. These symbols were, however, applied in such a way that no confusion should arise.

CHAPTER II

GENERAL THEORY

1. Thermal neutron capture

Neutrons of any velocity are easily introduced into the region of nuclear forces since there is no barrier like the Coulomb force acting upon them. The neutron may be scattered or absorbed by the nucleus. In the case of absorption, the resulting system will obtain an excitation energy that is equal to the binding energy of the neutron plus its kinetic energy. For thermal neutrons the kinetic energy is negligible compared with the binding energy which is of the order of 8 MeV The de-excitation may take place by re-emission of the neutron which is observed as scattering, by emission of a charged particle which only in a very few cases is energetically possible, or by a γ-ray disintegration to the ground state or to a lower excited state from which further de-excitation by γ-ray emission may occur.

The total angular momentum J of the nucleus is due to the combined action of the intrinsic spin of the nucleons and the orbital angular momentum of their motion. A thermal neutron has so low energy that no change in the orbital angular momentum is possible in a nucleus absorbing it. The intrinsic angular momentum of the neutron is $\frac{1}{2}$, x) and the quantum mechanical properties are such that when it is captured by a nucleus the value $+\frac{1}{2}$ or $-\frac{1}{2}$ will be added to the nuclear spin. This implies that the thermal neutron absorption by zero-spin nuclei will produce the compound state $J_c = \frac{1}{2}$, whereas for initial spin $J_i \neq 0$ there are two possibilities for the resulting spin: $J_c = J_i \pm \frac{1}{2}$. Accordingly, the nucleus may have two types of neutron resonances at thermal energies. No parity change of the nucleus takes place on absorption of particles with zero orbital angular momentum.

The capture cross section for thermal neutrons is determined by the shape and position of the nearest resonances. If the binding energy of a neutron happens to be equal to a resonance energy level of the compound nucleus, the thermal capture cross section will be extremely large. In the case that the influence of one single resonance predominates at thermal energies, the neutron cross section is given by the one-level Breit-Wigner formula (see Blatt and Weisskopf 1952) for the reaction product α:

$$\sigma(n,\alpha) = \pi \lambda\!\!\!^{-2}_n \, g \, \frac{\Gamma_n \Gamma_\alpha}{(E_n - E_r)^2 + (\Gamma/2)^2} \qquad (1.1)$$

where $\lambda\!\!\!^{-}$ is the neutron wavelength λ divided by 2π, Γ_n and Γ_α are the resonance widths for neutron and reaction product respectively, and $\Gamma = \Gamma_n + \Gamma_\alpha$ is the total width of the resonance. E_n is the energy of the incident neutron and E_r is the resonance energy. The statistical factor is:

$$g = \frac{1}{2}\left(1 \pm \frac{1}{2J_i + 1}\right) \qquad (1.2)$$

where the upper and lower signs correspond to the signs of $J_c = J_i \pm \frac{1}{2}$

---

x) Throughout the present paper, all spin and angular momentum values are referred to in units of $\hbar$.

Formula (1.1) is accurate near the resonance peak only. Other nearby resonances with the same spin J_c may produce large deviations of the cross section due to interference effects. Nevertheless, the one-level formula can be used to give a useful qualitative picture of the cross section for radiative capture of thermal neutrons. As the γ-ray energy is very large and the neutron energy very small, Γ_γ is essentially energy-independent in the region of thermal energies; one has a reaction width $\Gamma \ll E_\gamma$ and the denominator for formula (1.1) can be written E_r^2. From quantum mechanical considerations one finds for the width of neutrons with zero angular momentum:

$$\Gamma_n \propto D_n \, E_n^{1/2} \tag{1.3}$$

Here, D_n is the average spacing of resonances with the same spin. As $\lambda\!\!\!^{-}_n \propto E_n^{-1/2}$, formula (1.1) now becomes:

$$\sigma_{th}(n,\gamma) \propto g \, \frac{\Gamma_\gamma \, D_n}{E_r^2} \, E_n^{-1/2} \tag{1.4}$$

This is the well known 1/v-law for the absorption of thermal neutrons; v is the neutron velocity which is proportional to the square root of E_n.

The largest fluctuations of σ_{th} from one element to another are due to the variable magnitude of D_n, which in the regions of filled nucleon shells can be increased by several orders of magnitude with respect to the neighbouring elements. Outside these domains, the general trend is that D_n falls slightly off as the number of nucleons A is increased. Γ_γ is remarkably constant ($\cong$ 0.1 eV) and it only increases somewhat in the regions of closed shells as shown by Levin and Hughes (1956).

In the rare cases when thermal energies coincide with a resonance of the compound nucleus, a γ-ray observed corresponds to a unique transition between the state of the resonance and a lower state of the nucleus. When in that case the spin of the initial state is measured, this will be the spin of the resonance. If thermal energies do not fall on a peak, all the nearby resonances will contribute to the capture cross section. However, the E_r^{-2}-dependence of formula (1.4) shows that generally the nearest resonance will be major importance. This formula does not take account of interference effects which, according to Teichmann (1950), may give large positive or negative contributions to the cross section in regions where resonances with the same total angular momentum J_c contribute with the same order of magnitude. "Negative resonances" have energies smaller than the binding energy of a neutron in the compound nucleus. Their existence is not easily observed and of those occurring in the vicinity of thermal energies only very few are actually known. For thermal neutron reactions one may therefore not be able to tell which is the nearest resonance. The factor g implies that a resonance with spin $J_c = J_i + \frac{1}{2}$ gives a somewhat larger contribution to the cross section than does one with $J_c = J_i - \frac{1}{2}$ under equal conditions. One may conclude that there is a great chance of finding that the observed total angular momentum value of the composite initial state of a definite γ-ray transition, largely is due to one of the two possible combinations, but in many cases it will not be possible to ascribe this value to a definite resonance.

2. Electromagnetic radiation.

An electromagnetic wave moving in free space is described by the complex vector potential:

$$\left.\begin{aligned} &\vec{A} = \vec{A}_o \, e^{i(\vec{k}\vec{r}-\omega t)} + \vec{A}_o^{\,*} \, e^{-i(\vec{k}\vec{r}-\omega t)} \\ &\operatorname{div} \vec{A} = 0 \end{aligned}\right\} \tag{2.1}$$

Here t is time, ω is frequency of the oscillation, $\vec{r}$ is the vector from the origin and $\vec{k}$ is the

propagation vector. The wave number per unit length equals $|\vec{k}| = k = \omega/c$. Energy and momentum of the photon are then given by $\hbar$ ck and $\hbar$ k, respectively.

The electric and magnetic fields can be expressed in terms of $\vec{A}$:

$$\vec{E} = -\frac{1}{c}\frac{\partial \vec{A}}{\partial t} = ik\vec{A} \tag{2.2}$$

$$\vec{H} = \nabla \times \vec{A} = i(\vec{k} \times \vec{A}) \tag{2.3}$$

The condition div $\vec{A} = 0$ implies that $\vec{A}$ as well as $\vec{E}$ and $\vec{H}$ are perpendicular to the direction of propagation.

The state of polarization is given by the direction of the electric field vector:

$$\frac{\vec{E}_o}{|\vec{E}_o|} = \frac{\vec{A}_o}{|\vec{A}_o|} = a_1 \vec{e}_1 + a_2 \vec{e}_2 \tag{2.4}$$

Here, the unit vectors $\vec{e}_1$, $\vec{e}_2$ and $\vec{e}_3$ define an orthogonal co-ordinate system, where the photon is propagated along the 3-axis. The complex coefficients a_1 and a_2 are normalized by

$$|a_1|^2 + |a_2|^2 = 1$$

If a_1 and a_2 are both real or are both imaginary, the polarization is linear. If one is real and the other is imaginary, circular polarization will be obtained. This corresponds to a rotation of the vector $\vec{A}$ in space, as is seen by combination of equations (2.1) and (2.4). Generally, the polarization of a photon is defined by a unit vector $\vec{\xi}$ whose components in the co-ordinate system defined above are called the Stokes parameters. Their magnitudes have been given by Tolhoek and Cox (1953):

$$\left.\begin{aligned} \xi_1 &= |a_1|^2 - |a_2|^2 \\ \xi_2 &= a_1 a_2^* + a_2 a_1^* \\ \xi_3 &= i(a_1 a_2^* - a_2 a_1^*) \end{aligned}\right\} \tag{2.6}$$

Linear polarization is expressed by ξ_1 and ξ_2. The component ξ_3 along the propagation vector of the photon, gives the degree of circular polarization. ξ_3 is positive for left circular polarization, and vice versa. When the Stokes parameters are used to express the polarization of a photon beam, $|\vec{\xi}| \leqslant 1$.

The properties of the spin operator $\vec{S}$ for a vector field are given by Rose (1955):

$$\left.\begin{aligned} &\vec{S}^2 \vec{A} = S(S+1)\,\vec{A} \\ &\text{and of the z-component} \\ &S_z \begin{pmatrix} A_x \\ A_y \\ A_z \end{pmatrix} = \begin{pmatrix} -iA_y \\ iA_x \\ 0 \end{pmatrix} \end{aligned}\right\} \tag{2.7}$$

The eigenvectors of S^2 and S_z are:

$$\vec{X}_1 = -\frac{1}{\sqrt{2}}(\vec{e}_x + i\vec{e}_y), \quad \vec{X}_0 = \vec{e}_z, \quad \vec{X}_{-1} = \frac{1}{\sqrt{2}}(\vec{e}_x - i\vec{e}_y) \tag{2.8}$$

The eigenvalues are S = 1 and S_z = 1,0 or -1 as denoted by the index on $\vec{X}$. $\vec{e}_x$, $\vec{e}_y$ and $\vec{e}_z$ are unit vectors along the co-ordinate directions and $\vec{X}$ is normalized to unit length. If $\vec{A}$ has the form $\vec{X}_1$ or $\vec{X}_{-1}$, the photon propagated in the z-direction has left or right circular polarization respectively. $\vec{X} = \vec{e}_z$ is no solution for this photon, since the vector field must be transversal. Linear polarization is expressed by a combination of left and right circular polarization. The expectation value of the spin component in the direction of motion is then zero, i.e. S_z is not sharp. The fact that the photon has spin 1 with the two possible components ±1 in the direction of motion, corresponding to the two types of circular polarization, has also been pointed out by Heitler (1954, appendix 1).

A detailed account of the expansion of electromagnetic radiation into multipole fields has been given by Blatt and Weisskopf (1952). An arbitrary vector field is expressed by the series:

$$\vec{A}(\vec{r}) = \sum_{L=0}^{\infty} \sum_{M=-L}^{L} \vec{A}(L,M,\vec{r}) \tag{2.9}$$

Here, the terms $\vec{A}(L,M,\vec{r})$ are pure multipole fields, being functions of vector spherical harmonics. L is the angular momentum quantum number and M is the z-component thereof. Accordingly, also the electric field may be expanded into multipoles, and one gets:

$$\vec{E} = \sum_{L=1}^{\infty} \sum_{M=-L}^{L} \left[c_{el}(L,M)\vec{E}_{el}(L,M,\vec{r}) + c_{mag}(L,M)\vec{E}_{mag}(L,M,\vec{r}) \right] \tag{2.10}$$

where $\vec{E}_{el}$ and $\vec{E}_{mag}$ are electric vectors of the electric and magnetic multipole radiation respectively and the amplitudes are of the form:

$$c = \pm \frac{4\pi}{(2L+1)!!} \left(\frac{L+1}{L} \right)^{\frac{1}{2}} k^{L+2} Q_{LM} \tag{2.11}$$ x)

Here Q_{LM} is the multipole matrix element of the transition. It is dependent upon the convection currents and the varying magnetization density in the nucleus. An equation similar to (2.10) applies for the magnetic field H.

The parities for the two types of multipole radiation are:

$$\left.\begin{aligned} \Pi_{el}(L,M) &= (-1)^L \\ \text{and} \quad \Pi_{mag}(L,M) &= -(-1)^L \end{aligned}\right\} \tag{2.12}$$

Even and odd parities are denoted by Π = +1 and -1 respectively so that by the expansion of the electromagnetic fields according to equation (2.10), the radiation is classified in terms of the angular momentum and parity change it produces in the radiating system.

x) $(2L+1)!! = 1 \cdot 3 \cdot 5 \cdots (2L+1)$

Transitions of multipole radiation between nuclear levels with total angular momenta $\vec{J}_a$ and $\vec{J}_b$ are limited by the selection rule:

$$\vec{J}_a = \vec{J}_b + \vec{L} \tag{2.13}$$

or

$$|J_a - J_b| \leqslant L \leqslant J_a + J_b \tag{2.14}$$

and

$$m_a - m_b = M \tag{2.15}$$

where m is the z-component of the total angular momentum. The radiation at least carries away angular momentum 1, so that $L \geqslant 1$. Another selection rule follows from the parity of the radiation:

$$\Pi_a = \Pi_{rad}\ \Pi_b \tag{2.16}$$

TABLE 1

The lowest multipole order allowed by the selection rules

		Angular momentum carried away by radiation = L.					
		0	1	2	3	4	5
Parity of the radiation $= \Pi_{rad}$	-1	None	E1	M2	E3	M4	E5
	+1	None	M1	E2	M3	E4	M5

The lowest possible order of multipole radiation is given in table 1 as determined by the above-mentioned selection rules. We shall see that this radiation generally has the highest transition probability. Electric and magnetic 2^L-poles are denoted by the symbols EL and ML respectively.

The radiated energy is proportional to the square of the absolute value of the amplitude c, and one gets for the transition probability of a quantum per unit time:

$$w(L,M) = \frac{8\pi(L+1)}{L[(2L+1)!!]^2} \frac{k^{2L+1}}{\hbar} |Q_{LM}|^2 \tag{2.17}$$

The matrix element Q_{LM} can only be derived when the nuclear properties are completely known. On the basis of the individual particle model, Weisskopf (1951) obtained a rough estimate for the transition probability for the electric radiation of multipole order L:

$$w'_{el}(L) \cong \frac{4.4 \cdot 10^{21}(L+1)}{L[(2L+1)!!]^2} \left(\frac{3}{L+3} \right)^2 \left(\frac{\hbar c k}{197\ \text{MeV}} \right)^{2L+1} R^{2L}\ \text{sec}^{-1} \tag{2.18}$$

where the nuclear radius R is given in 10^{-13} cm.

An estimate for the magnetic radiation is obtained by a comparison between the matrix elements of the transitions, which are dependent upon the electric and magnetic moments of the nucleus. The electric moment is of the order of eR, and the magnitude of the magnetic moment is a few times $e\hbar/m_n c$ when the action of the orbital momentum and of the spins of the nucleons are added. Here m_n is the nucleon mass. The ratio of the transition probabilities is:

$$\frac{w'_{mag}(L)}{w'_{el}(L)} = \frac{|Q_{LMmag}|^2}{|Q_{LMel}|^2} \cong 10 \left(\frac{\hbar}{m_n c R}\right)^2 \qquad (2.19)$$

This quantity is approximately 10^{-2} for A = 100. The order of magnitude of the ratio between successive multipole orders is $(kR)^2$, which is as small as 10^{-5} for A = 100 and γ-energy = 0.5 MeV. According to these estimates the transition probability is quickly reduced for successive radiations of the series: E1, M1, E2, M2, · · · · · · · · ·

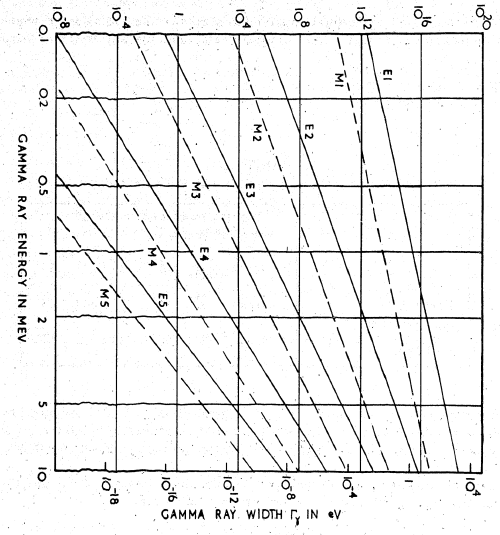

Figure 1.
Theoretical γ-ray transition probability for various multipole orders, as calculated from formulæ (2.18) and (2.19). For the nuclear radius was used the value $R = 6.73 \cdot 10^{-13}$ cm, corresponding to atomic weight A = 100.

Figure 1 is a graphical representation of the theoretical transition probability expressed by the formulæ (2.18) and (2.19). The magnitude of the resonance width for emission of γ-radiation $\Gamma_\gamma = w'_\gamma \hbar$ is also given in the figure. According to Weisskopf, formula (2.18) must be considered as an upper limit for the transition probability. In fact, practically all measurements of transition probabilities yield values which are several orders of magnitude smaller than w' (Goldhaber and Sunyar 1951). In spite of this, the theory accounts well for the ratio between different multipoles, and for the dependence upon energy and nuclear radius.

As seen from the selection rules illustrated in table 1 and in figure 1, the lowest allowed order of magnetic radiation will be very improbable when the most intense radiation is of the electric type. Mixing of two types of radiation is much more probable if the most intense γ-ray according to the above rules is a magnetic multipole. Electric radiation of one multipole order higher,

also being allowed, will in the region of 1 MeV be a factor 100 less probable. Most cases of mixing observed are of the type M1 + E2.

Mayer and Jensen (1955) derived a separate selection rule for the case that the transition is due to a single proton or a single neutron which changes its orbital angular momentum from ℓ_i to ℓ_f. In this case the additional condition is:

$$L \geq |\ell_i - \ell_f| \qquad (2.20)$$

Generally, this rule has not complete validity, but transitions violating the rule have a strongly reduced transition probability as compared with the expressions (2.18) and (2.19).

When a neutron is captured, the nucleus is excited to approximately 8 MeV, and the following γ-ray emission leads, either directly, or by successive γ-rays emitted in cascade, to the ground state of the compound nucleus. Blatt and Weisskopf (1952, chapter XII) have shown that for emission from highly excited states a more correct form of the transition probability is obtained when it is multiplied with a factor proportional to the average level spacing D_ℓ in the region of the initial state. Only levels from which radiative transitions of the same multipole order can produce the same final state are concerned. The authors proposed the proportionality constant $D_0 \cong 0.5$ MeV. Transition probabilities for high energy dipole and quadrupole radiation were determined by Kinsey and Bartholomew (1954), who found that the theoretical transition probability $w'' = (D_\ell/D_0)w'$ was too small by about a factor 10^{-2} for E1 radiation and somewhat larger for M1 radiation.

The γ-ray width, being proportional to the transition probability, is the sum of the partial widths for transitions to various lower levels:

$$\Gamma_\gamma = \sum_i \Gamma_{\gamma i} \qquad (2.21)$$

From a careful study of various neutron resonances Levin and Hughes (1956) found that Γ_γ was of the order of 0.1 eV for nearly all cases studied. As a general rule, Γ_γ is decreasing slowly with increasing A, but seems to increase somewhat in the regions of closed nucleon shells. Furthermore, Γ_γ is not varying strongly, if at all, amongst resonances of the same nucleus. A comparison of the measurements of Levin and Hughes with those of Kinsey and Bartholomew indicates that most of the radiation emitted in neutron capture is of the electric dipole type. This is a plausible result since generally the de-excitation may proceed by γ-ray emission to many lower levels, and there is a great chance that some of these levels can be reached by electric dipole radiation, which because of its high transition probability then will account for the greater part of the decay.

3. Nuclear energy levels.

The best general agreement with observed nuclear level data is obtained by the nuclear shell theory combined with the theory on collective motion of the nucleons.

In the shell model (Mayer 1950; Haxel, Jensen and Suess 1950) the nucleons are supposed to be moving in individual orbits. The eigenfunctions of the particle motion in the spherically symmetric potential chosen, are, analogous to the electron states of an atom, given by the quantum numbers n and ℓ, where n is the number of radial nodes of the eigenfunction and ℓ is the orbital angular momentum quantum number. In order to explain the experimental data it is necessary to add a spin-orbit-coupling potential which implies a splitting of the ℓ-levels due to the nucleon spin. The two total angular momentum states $J = \ell \pm \frac{1}{2}$ then have different energies, and contrary to the case of atomic spectra, the state with parallel spin and angular momentum, $J = \ell + \frac{1}{2}$, has the lower energy. Nucleon configurations are given by the quantum numbers $(n\ell j)^\nu$, where ν is the population of the level, and the value of ℓ is given by the usual letters s, p, d, f, · · · · · · The level degeneracy is $2(2\ell + 1)$, and the parity of the eigenfunction is $\Pi_\ell = (-1)^\ell$. When the parameters of the potentials are adjusted to give the best possible agreement between the theoretical and the existing experimental values of nuclear spins in ground states, one arrives at an energy level scheme of which the lowest part is shown in figure 2, taken from Klinkenberg (1952).

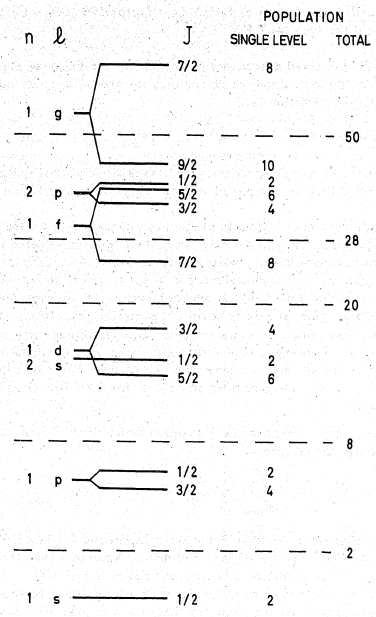

Figure 2.
Energy level scheme of the nuclear shell model.

In the ground state of the nucleus the nucleons are filling the lowest possible energy states of the level system. In order to excite the nucleus, one or more of them must be lifted to a higher level. For the nuclei with filled shells, i.e. for proton and neutron numbers 2, 8, 20, 28, 50, 82 and 126, comparatively high energies are required for the excitation of the system. These "closed shell" nuclei are therefore unusually stable.

The lowest energy states are obtained when pairs of protons and neutrons couple their angular momenta to zero with even parity. Thus even-even nuclei always have zero spin and even parity in the ground state. This rule has been verified in all cases experimentally studied. In nuclei with odd mass number A, there will be a core consisting of even numbers of protons and neutrons, and one extra nucleon which alone determines the spin and parity of the nucleus. This single particle model has given an extremely good explanation of the spins of stable odd-A nuclei. A few exceptions to this rule and to the sequence of levels in figure 2 must be explained by special coupling rules (Mayer and Jensen 1955). In an odd-odd nucleus one proton and one neutron couple their angular momenta to produce the total angular momentum of the nucleus. For this case, complete coupling rules have not been deduced.

In general, the excited states of nuclei are due to the combined action of the shell structure and the collective motion of the nucleons which has been treated by Bohr and Mottelson (1952, 1953). For the larger nuclei far from closed shells the collective motion of the particles in the deformed nucleus contributes appreciably to the properties of the excited states. This is an additional degree of freedom which gives rise to rotational and vibrational levels in analogy with rotational

bands in molecular spectra. The lowest excited states in the regions $155 < A < 185$ and $A > 225$ are very well explained by this theory. The quantum energies of collective motions are large for small nuclei and for systems in the vicinity of closed shells. In these cases, the nuclear shell levels account for the lowest excited states. Above the two or three lowest states one must expect contributions from combinations of single particle configurations which will be hard to predict or explain unambiguously. As the excitation energy increases, the number of combinations and the density of levels will increase rapidly. For odd-A nuclei, the single particle model applies, and the lowest energy levels are simply give by figure 2. Even-even nuclei can be excited when one nucleon pair obtains a change of the coupling in the same configuration as that of the ground state. The first excited state then becomes angular momentum 2, and the second has the possibilities 0,2 and 4. A change of coupling only, involves no change of parity. Also the first excited state of the collective motion in even-even nuclei has angular momentum 2 and no change of parity. In fact this rule has been confirmed in almost all cases studied (Scharff-Goldhaber 1953). For the more complicated case of excited states of odd-odd nuclei, no rules have been formed.

Generally the spacing of energy levels is decreasing as A increases, due to the action of collective motions in the nucleus. Because of this, most neutron capture γ-ray spectra for heavy nuclei have been resolved to a small extent only. Exceptions are encountered in the vicinity of closed nucleon shells, where the spectra clearly resemble those of light nuclei. For capture of thermal neutrons in even-even nuclei the spin of the compound nucleus has only one possible value, $J_c = \left| J_i \pm \frac{1}{2} \right| = \frac{1}{2}$, and the spectrum may then be fairly simple. If the ground level of the resulting nucleus is a p-state, which has spin $\frac{1}{2}$ or $\frac{3}{2}$ and odd parity, the disintegration to the ground state will be of electric dipole (E1)-type and of high intensity. For reasons of poor resolving power, most of the γ-rays experimentally studied in the present work were of the type mentioned, and all except one originated in light nuclei ($Z \lesssim 30$).

CHAPTER III

CIRCULAR POLARIZATION OF GAMMA-RAYS FOLLOWING CAPTURE OF POLARIZED NEUTRONS

Consider the reaction in which γ-rays are emitted from a target as a result of the absorption of polarized thermal neutrons. We shall in the following discuss the effects that the polarization may have upon the radiation, and the possibilities of detecting these effects. It shall also be investigated to what extent these detecting methods may be used for the determination of nuclear properties.

1. Main principles.

The polarization of a particle beam is generally defined as the net alignment of the particle spins:

$$P = \frac{I^+ - I^-}{I^+ + I^-} \tag{1.1}$$

where P is the polarization and I^+ and I^- are intensities of particles with spins parallel and antiparallel to a certain axis of reference. This definition is also valid for photons as far as circularly polarized radiation is concerned.

The experiment treated in the present chapter deals with polarized slow neutrons, which have zero angular momentum, and with circularly polarized γ-rays. Certain rules, which imply a limitation on the application of these effects to nuclear spectroscopy, may easily be deduced.

Consider a nuclear reaction induced by particles with angular momentum zero, and the net spin direction along the x-axis. The outgoing intensity must have symmetry about the x-axis, since no other direction is defined for the compound system. Accordingly the intensity I, emitted in a certain direction (x, y, z) is independent of a reversal of the y-co-ordinate:

$$I(x, y, z) = I(x, -y, z). \tag{1.2}$$

If we perform the transformation

$$x' = x, y' = -y, z' = z, \tag{1.3}$$

the polarization will reverse its direction since spin is an axial vector. The intensity will be unaltered and equal to

$$I(x', y', z') = I(x, -y, z) = I(x, y, z) \tag{1.4}$$

which means that the direction of polarization has no influence upon the distribution of the reaction products.

A similar restriction applies for the scattering of circularly polarized photons. If the radiation

is incident along the z-axis, this is the direction of polarization, and accordingly it is the axis of symmetry. Also in this case the transformation (1.3) will reverse the direction of polarization, while the intensity is unaltered as in equation (1.4). Therefore one cannot distinguish between left and right circular polarization of radiation purely by measurement of the scattered photons.

These two conclusions on the application of polarization are also contained in the polarization theorems number 2 and 3 formulated by Wolfenstein (1949 b).

Consider a material which mainly scatters particles having a definite spin direction. When there are only two possible orientations of the spin due to quantum mechanical requirements, the total cross section may be expressed by

$$\sigma_t = \sigma_o \pm \sigma_p \tag{1.5}$$

where σ_o is the cross section for unpolarized particles, and σ_p is the contribution that is added or subtracted, depending upon whether the particle spins are parallel or antiparallel to a certain axis of reference. The corresponding particle currents are I^+ and I^- respectively. The intensity transmitted through polarizing material is given by

$$I_1^{\pm} = I_o^{\pm} T_1^{\pm} = I_o^{\pm} \, e^{-\varrho(\sigma_o \pm \sigma_p)} \tag{1.6}$$

where T_1 is the transmission and I_o and I_1 are the intensities of the incident and the transmitted beams as indicated in the left part of figure 3. All the upper or all the lower signs should be chosen, indicating the spin direction of the particles considered. ϱ is the number of atoms per square centimetre of the beam.

An unpolarized incident beam is characterized by $I_o^+ = I_o^- = \frac{1}{2} I_o$. In this case, the combination of (1.1) and (1.6) gives:

$$P_1 = \frac{e^{-\varrho\sigma_p} - e^{\varrho\sigma_p}}{e^{-\varrho\sigma_p} + e^{\varrho\sigma_p}} \cong \frac{\varrho\sigma_p}{1 + \frac{\varrho^2\sigma_p^2}{2}} \tag{1.7}$$

The condition for the validity of the approximate formula is $\varrho\sigma_p \ll 1$. The relative difference between the transmission T_p and T_u, respectively, of the polarizer and of the same device without polarizing properties is called the "single transmission effect":

$$\left.\begin{aligned} \eta &= \frac{T_p - T_u}{T_u} = \frac{e^{-\varrho\sigma_p} + e^{\varrho\sigma_p}}{2} - 1 \\ &\cong \frac{\varrho^2 \sigma_p^2}{2} \quad \text{for } \varrho\sigma_p \ll 1 \end{aligned}\right\} \tag{1.8}$$

Polarization now becomes the form $P \cong \varrho\sigma_p / (1 + \eta)$. In many experiments the measurement of η can be used as a simple method for the determination of σ_p and the polarization P.

Equation (1.1) gives for unpolarized incident beam:

$$I_1^{\pm} = \frac{1}{2} I_o T_1 (1 \pm P_1) \tag{1.9}$$

Generally, the properties of a polarizer are completely described by the transmission T and by the polarization P of the emitted beam when the incident beam is unpolarized. The transmissions for the two components of the beam with opposite polarization directions are equal to $T(1 \pm P)$.

Figure 3 shows the principle of a double transmission polarization experiment, which means that the particle beam passes successively through two polarizers with properties T_1, P_1 and T_2, P_2 respectively. When the incident particles are unpolarized, the intensities emitted from the second polarizer are:

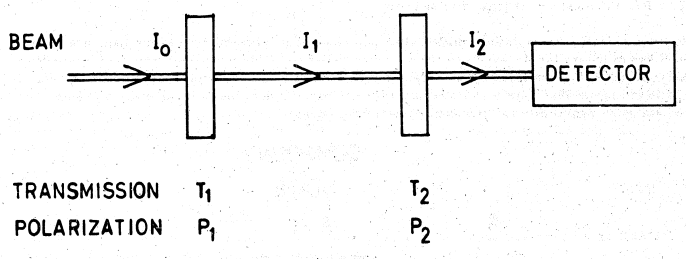

Figure 3.
Schematical double transmission experiment.

$$\left.\begin{aligned} I_2^+ &= I_1^+ T_2 (1 + P_2) = \frac{1}{2} I_o T_1 T_2 (1 + P_1)(1 + P_2) \\ I_2^- &= I_1^- T_2 (1 - P_2) = \frac{1}{2} I_o T_1 T_2 (1 - P_1)(1 - P_2) \end{aligned}\right\} \tag{1.10}$$

With a polarization-independent detector the intensity

$$I_2 = I_2^+ + I_2^- = I_o T_1 T_2 (1 + P_1 P_2) \tag{1.11}$$

is measured. If I_2' is the observed counting rate for parallel polarizers ($P_1 P_2 > 0$), and I_2'' is that obtained for antiparallel polarizers ($P_1 P_2 < 0$), we get the relation

$$P_1 P_2 = \frac{I_2' - I_2''}{I_2' + I_2''} \tag{1.12}$$

Thus, the polarization P_1 of a particle beam can be determined by means of an "analyzer" whose polarization P_2 is known.

In the production of polarized particles by passage through matter, a compromise must always be made between the increase in polarization and the decrease in intensity as the thickness of the polarizer is increased. When background counts are neglected, the standard deviation of a counting experiment measuring polarization is

$$\left.\begin{aligned} \Delta P &\propto \frac{\sqrt{I' + I''}}{I' - I''} = \frac{1}{P\sqrt{T I_o}} \\ &\cong \frac{1}{\sigma_p \varrho \sqrt{I_o \, e^{-\varrho\sigma_o}}} \propto \frac{\frac{\varrho\sigma_o}{e^2}}{\varrho} \quad \text{for } \varrho|\sigma_p \ll 1 \end{aligned}\right\} \tag{1.13}$$

The minimum value of this quantity is obtained for $\varphi\sigma_c = 2$. This means that the greatest statistical accuracy of a measurement carried out in a certain time is obtained when the length of the polarizer is equal to twice the mean free path in the polarizing material.

2. Polarization of the radiation.

In the discussion the radiation emitted after polarized neutron capture, one can make use of the well known theory for the angular correlation of radiation. This procedure was used by Biedenharn, Rose and Arfken (1951 a), who treated the possibility of linearly polarized radiation. In the following we shall give a short review of their theory, which then will be used to calculate the emission probability for circularly polarized photons.

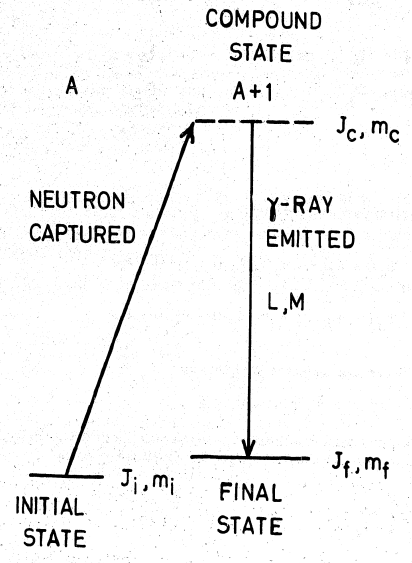

Figure 4.
Energy level scheme for (n,γ)-reaction.

The angular momentum quantities involved are shown in the simple decay scheme of figure 4. The target nucleus, having A nucleons, has total angular momentum J_i, with z-component m_i. The compound and final states of the nucleus have one nucleon more, and the total angular momenta are J_c and J_f with z-components m_c and m_f respectively. Since the transition between the compound and the final state is due to a single γ-ray with multipole order L and angular momentum in the z-direction M, we get the following relations between these quantities

$$\left.\begin{aligned} & J_i \pm \tfrac{1}{2} = J_c \\ & |J_f - L| \leqslant J_c \leqslant J_f + L \\ & m_i - \tfrac{1}{2} = m_c = m_f + M \end{aligned}\right\} \qquad (2.1)$$

The sign + or - depends upon the orientation of the neutron spin relative to $\vec{J}_i$ and to the z-axis.

The relative probability for the emission of a capture γ-ray in the $\vec{k}$-direction with circular polarization p following the capture of an s-neutron with polarization P_n is given by

$$w(P_n,p,\vec{k}) = \sum_{m_i m_f} \left| \sum_{m_c} \langle i | H_1 | c \rangle \langle c | H_2 | f \rangle^* \right|^2 \qquad (2.2)$$

Here, the probability amplitudes for the initial, compound and final states of the nucleus are simply denoted by i, c and f respectively. H_1 and H_2 are the Hamiltonians that effect the neutron capture and the γ-ray emission respectively. The quantity p equals +1 for left and -1 for right circular polarization of the γ-ray. If the z-direction is chosen as the quantization axis, no cross terms will be obtained from (2.2), and one gets

$$w(P_n,p,\vec{k}) = \sum_{m_i\, m_c\, m_f} \left|\langle i | H_1 | c \rangle\right|^2 \left|\langle c | H_2 | f \rangle\right|^2 \qquad (2.3)$$

The values of these matrix elements are given by Biedenharn, Rose and Arfken (1951 a). The first one is proportional to the occupation probability of the m_c-th sublevel:

$$\left|\langle i | H_1 | c \rangle\right|^2 \propto \frac{1}{2} + \frac{2(J_c - J_i)}{2J_i + 1}\, m_c\, P_n \qquad (2.4)$$

Here, P_n is defined by equation (1.1) when I^+ and I^- are the probabilities that the incident neutron has spin parallel and antiparallel to the z-axis respectively.

In order to calculate the second matrix element, they make use of the expansion of a circularly polarized plane wave as performed by Goertzel (1946):

$$\vec{A}(\vec{k},p) = \pi \sum_{L=1}^{\infty} \sum_{M=-L}^{L} i^L \sqrt{2L+1}\; D^{(L)}_{M,p}(\alpha\beta\gamma) \left[\vec{A}^m_{LM} + ip\vec{A}^e_{LM}\right] \qquad (2.5)$$

where $D^{(L)}_{M,p}(\alpha\beta\gamma)$ is the rotation matrix of the L-th order as defined by Wigner (1931, p. 180) and the superscripts e and m denote electric and magnetic multipoles respectively. The result is

$$\langle c | H_2 | f \rangle \propto \sum_L i^L (ip)^\lambda\, b(J_c J_f \Pi L)\, D^{(L)}_{M,p}(0\Theta 0)\quad (J_c J_f m_c(-m_f) \,|\, J_c J_f L(-M)) e^{-ip\tau} \qquad (2.6)$$

The symbol $(J_c J_f m_c(-m_f) \,|\, J_c J_f L(-M))$ is a Clebsch-Gordan or vector addition coefficient as defined by Condon and Shortley (1935). The amplitudes $b(J_c J_f \Pi L)$ of the waves may be chosen real, but the relative phase between two b's can be 0 or 180°, and their signs will not be known. Parity change due to the radiation is denoted by Π and is also contained in the exponent $\lambda = \frac{1}{2}(1 + \Pi(-1)^L)$ which equals 0 or 1. In the rotation matrix the values of the Euler angles α and γ are insignificant, and can be chosen equal to zero. Θ is the angle between the γ-ray and the z-axis; it corresponds to the Euler angle β. The angle τ is the phase of the circularly polarized wave. The sum over L implies coherent mixing of different multipole orders.

We shall here consider mixtures of radiation with a difference of multipole order one only, i.e. $L_2 = L_1 + 1$. Then the square of the second matrix element becomes:

$$\left|\left\langle c \left| H_2 \right| f \right\rangle\right|^2 \propto b_1^2 \, D^{(L_1)}_{M,p_1}(0\Theta 0) \left(J_c J_f m_c(-m_f) \,\middle|\, J_c J_f L_1(-M)\right)^2$$
$$+ b_2^2 \, D^{(L_2)}_{M,p_2}(0\Theta 0) \left(J_c J_f m_c(-m_f) \,\middle|\, J_c J_f L_2(-M)\right)^2$$
$$+ 2\, b_1 b_2 \, i^{L_1-L_2+\lambda_1-\lambda_2} \, D^{(L_1)}_{M,p_1}(0\Theta 0) \, D^{(L_2)}_{M,p_2}(0\Theta 0)$$
$$\left(J_c J_f m_c(-m_f) \,\middle|\, J_c J_f L_1(-M)\right)\left(J_c J_f m_c(-m_f) \,\middle|\, J_c J_f L_2(-M)\right)$$
$$\cdot\left(\delta^{p_2}_{p_1} + \delta^{-p_2}_{p_1} \cos 2\tau\right) \qquad (2.7)$$

where $\delta^{p_2}_{p_1}$ is the Kronecker symbol.

A plane polarized wave is equal to the sum of two circularly polarized waves:

$$\vec{A}_\tau = \vec{A}(p=1)e^{-i\tau} + \vec{A}(p=-1)e^{i\tau} \qquad (2.8)$$

The direction of linear polarization is given by the angle τ with respect to a fixed vector perpendicular to $\vec{k}$. The only term of equation (2.7) which may be dependent upon linear polarization gives the intensity

$$w_\tau \propto \cos 2\tau \sum_{p_1=-1}^{1} p_1 \, D^{(L_1)}_{M,p_1}(0\Theta 0) \, D^{(L_2)}_{M,-p_1}(0\Theta 0) \qquad (2.9)$$

Wigner (1931, p.204) has given the relation

$$D^{(L_1)}_{M,N}(\alpha\beta\gamma) \; D^{(L_2)}_{m,n}(\alpha\beta\gamma)$$
$$= \sum_{F=|L_1-L_2|}^{L_1+L_2} \left(L_2 L_1 \, m\,M \,\middle|\, L_2 L_1 F\,(m+M)\right) D^{(F)}_{M+m,N+n}(\alpha\beta\gamma) \left(L_2 L_1 \, n\,N \,\middle|\, L_2 L_1 F\,(n+N)\right) \qquad (2.10)$$

If one also makes use of the symmetry relations for the Clebsch-Gordan coefficients given by Biedenharn, Blatt and Rose (1952)

$$\left(L_2 L_1 \, mM \,\middle|\, L_2 L_1 F\,(m+M)\right) = (-1)^{L_1+L_2-F}\left(L_1 L_2 \, Mm \,\middle|\, L_1 L_2 F\,(m+M)\right) \qquad (2.11)$$

it is easily seen that

$$D^{(L_1)}_{M,p} \, D^{(L_2)}_{M,-p} = D^{(L_2)}_{M,p} \, D^{(L_1)}_{M,-p} \qquad (2.12)$$

Hence, the expression (2.9) is zero, and no linear polarization is obtained.

It is seen that if circular polarization occurs, this is the only additional property obtained from the capture of polarized thermal neutrons. The intensity of circularly polarized radiation is given by a combination of the formulæ (2.3), (2.4) and (2.7):

$$w(P_n, p_1, p_2, \vec{k}) \propto \sum_{m_c m_f} \left\{ \frac{1}{2} + \frac{2(J_c - J_i)}{2J_i + 1} m_c P_n \right\}$$
$$\left\{ b_1^2 \left[D^{(L_1)}_{M,p_1}(0\Theta 0) \right]^2 \left(J_c J_f m_c(-m_f) \,\middle|\, J_c J_f L_1(-M)\right)^2 \right.$$
$$+ b_2^2 \left[D^{(L_2)}_{M,p_2}(0\Theta 0) \right]^2 \left(J_c J_f m_c(-m_f) \,\middle|\, J_c J_f L_2(-M)\right)^2$$
$$- (-1)^{\lambda_1}(p_1 + p_2) b_1 b_2 \, D^{(L_1)}_{M,p_1}(0\Theta 0) \, D^{(L_2)}_{M,p_2}(0\Theta 0)$$
$$\left.\left(J_c J_f m_c(-m_f) \,\middle|\, J_c J_f L_1(-M)\right)\left(J_c J_f m_c(-m_f) \,\middle|\, J_c J_f L_2(-M)\right)\right\} \qquad (2.13)$$

In this formula the expression corresponding to the first term of the first factor is very easily deduced when one makes use of the simple sum rule for Clebsch-Gordan coefficients as given by Alder (1952):

$$\sum_{\alpha=-a}^{a} (ab\alpha\beta \,|\, abc(\alpha+\beta))(ab\alpha\beta \,|\, abd(\alpha+\beta)) = \delta^d_c \qquad (2.14)$$

We get for the polarization independent part of the intensity

$$w_o \propto \sum_{m_c m_f} \frac{1}{2} \left|\left\langle c \left| H_2 \right| f \right\rangle\right|^2 = b_1^2 + b_2^2 \qquad (2.15)$$

since D is a unitary matrix.

The other expression to be calculated is:

$$w_p \propto \sum_{m_c m_f} \frac{2(J_c + J_i)}{2J_i + 1} m_c P_n \left|\left\langle c \left| H_2 \right| f \right\rangle\right|^2 \qquad (2.16)$$

The relations $D^{(L)}_{M,p}(0\Theta 0) = (-1)^{M+p} D^{(L)}_{-M,-p}(0\Theta 0)$ and $D^{(L)}_{0,0}(0\Theta 0) = P_L(\cos\Theta)$, being the Legendre polynomial of order L, have been given by Alder (1952). Combined with the formula (2.10) they give

$$D^{(L_1)}_{M,p}(0\Theta 0) \, D^{(L_2)}_{M,p}(0\Theta 0)$$
$$= (-1)^{M+1} \sum_F \left(L_2 L_1 \, (-p)p \,\middle|\, L_2 L_1 F\, 0\right)\left(L_2 L_1 \, (-M)M \,\middle|\, L_2 L_1 F\, 0\right) P_F(\cos\Theta) \qquad (2.17)$$

One may also write the factor $m_c = \left[J_c(J_c+1)\right]^{\frac{1}{2}} \left(J_c l m_c 0 \,\middle|\, J_c \tfrac{1}{2} J_c m_c\right)$ according to Condon and Shortley (1935). The summations to be performed then read

$$\sum_F P_F(\cos\Theta)\ \left(L_2L_1(-p)p\ \middle|\ L_2L_1F\,0\right)\sum_M(-1)^M\ \left(L_2L_1(-M)M\ \middle|\ L_2L_1F\,0\right)$$

$$\sum_{m_c}\left(J_c1m_c0\ \middle|\ J_c1J_cm_c\right)\ \left(J_cJ_fm_c(-m_f)\ \middle|\ J_cJ_fL_1(-M)\right)\left(J_cJ_fm_c(-m_f)\ \middle|\ J_cJ_fL_2(-M)\right) \qquad (2.18)$$

To do this we make use of a summation formula given by Biedenharn, Blatt and Rose (1952)

$$\left(ab\alpha\beta\ \middle|\ abe(\alpha+\beta)\right)\left(ed(\alpha+\beta)(\gamma-\alpha-\beta)\ \middle|\ edc\gamma\right)\left(bd\beta(\gamma-\alpha-\beta)\ \middle|\ bdf(\gamma-\alpha)\right)$$
$$= (2e+1)^{\frac{1}{2}}\ (2f+1)^{\frac{1}{2}}\ \left(af\alpha(\gamma-\alpha)\ \middle|\ afc\gamma\right)\ W(abcd;ef) \qquad (2.19)$$

where W(abcd;ef) are Racah coefficients, which are tabulated in the paper mentioned. Also given are symmetry relations of the Clebsch-Gordan coefficients which are needed in the present calculations. Terms of the sum (2.18) having $F \neq 1$ become zero. This sum therefore is proportional to $P_1(\cos\Theta) = \cos\Theta$. The γ-ray emission probability then has the form

$$w = 1 + pP_nR\cos\Theta \qquad (2.20)$$

If w^+ and w^- are the intensities for left (p = 1) and right (p = -1) circularly polarized radiation respectively, the circular polarization of the γ-rays is

$$P_\gamma = \frac{w^+ - w^-}{w^+ + w^-} = P_n\,R\cos\Theta \qquad (2.21)$$

The reaction consisting of neutron absorption leading to emission of a γ-ray is schematically illustrated in figure 5. Clearly, the degree of circular polarization is largest in the direction of neutron polarization, i.e. for $\cos\Theta = \pm 1$. In these cases, the neutron and photon spins are parallel or antiparallel corresponding to R being positive or negative respectively.

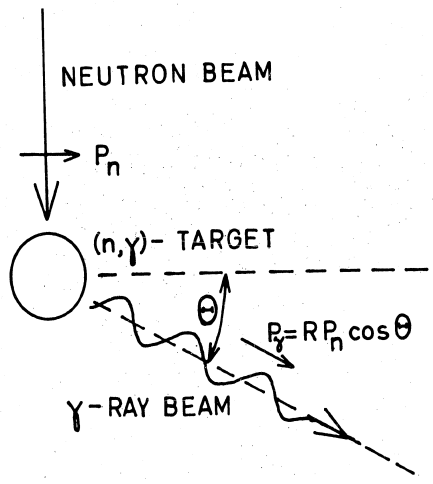

Figure 5.
Schematical (n,γ)-reaction.

The dependence of the polarization upon nuclear properties is expressed by the factor R:

$$R = \frac{b_1^2\,r(L_1,L_1) + b_2^2\,r(L_2,L_2) + 2b_1b_2r(L_1,L_2)}{b_1^2 + b_2^2} \qquad (2.22)$$

where the single terms are obtained by means of the summation (2.18):

$$r(L_1,L_2) = (-1)^{-J_f-J_c-L_2+1/2(L_1-L_2+\lambda_1-\lambda_2)}\ {}_p\lambda_1{}^+\ \lambda_2{}^{-1}\ \frac{4(J_c-J_i)}{2J_i+1}$$
$$\left[J_c(J_c+1)(2J_c+1)(2L_1+1)\right]^{\frac{1}{2}}\ \left(L_11(-p)0\ \middle|\ L_1L_2(-p)\right)\ W\left(L_1L_2J_cJ_c;1J_f\right) \qquad (2.23)$$

The practical forms of this formula are:

$$r(L,L) = \frac{2(J_c-J_i)}{2J_i+1}\ \frac{L(L+1) + J_c(J_c+1) - J_f(J_f+1)}{L(L+1)} \qquad (2.24)$$

and

$$r(L_1,L_2) = -(-1)^{\lambda_1}\ \frac{2(J_c-J_i)}{2J_i+1}\ \frac{1}{L_1+1}$$
$$\left[\frac{L_1(L_1+2)(J_c+J_f+L_1+2)\,(J_c-J_f+L_1+1)\,(-J_c+J_f+L_1+1)\,(J_c+J_f-L_1)}{(2L_1+1)(2L_1+3)}\right]^{\frac{1}{2}} \qquad (2.25)$$

In the case of pure multipole radiation one has $b_2 = 0$, and R = r(L,L). Formula (2.24), which is valid for this case, has also been quoted by Biedenharn, Rose and Arfken (1951 b). The numerical values of R are given in table 2 for the cases of greatest interest.

TABLE 2.

Numerical values of r(L,L), calculated from formula (2.24). For pure multipole radiation this equals the polarization ratio R.

J_i \ J_c	J_f / L	0			1			2			3			$\frac{1}{2}$	$\frac{3}{2}$		$\frac{5}{2}$	
		1	2	3	1	2	3	1	2	3	1	2	3	1	1	2	2	3
$\frac{1}{2}$	0				0			0			0							
	1	1			$\frac{1}{2}$	$\frac{1}{2}$		$-\frac{1}{2}$	$\frac{1}{6}$	$\frac{1}{3}$		$-\frac{1}{3}$	$\frac{1}{12}$					
$\frac{3}{2}$	1	$-\frac{1}{2}$			$-\frac{1}{4}$	$-\frac{1}{4}$		$\frac{1}{4}$	$-\frac{1}{12}$	$-\frac{1}{6}$		$\frac{1}{6}$	$-\frac{1}{24}$					
	2		$\frac{1}{2}$		$\frac{3}{4}$	$\frac{5}{12}$	$\frac{1}{3}$	$\frac{1}{4}$	$\frac{1}{4}$	$\frac{1}{4}$	$-\frac{1}{2}$	0	$\frac{1}{8}$					
$\frac{5}{2}$	2		$-\frac{1}{3}$		$-\frac{1}{2}$	$-\frac{5}{18}$	$-\frac{2}{9}$	$-\frac{1}{6}$	$-\frac{1}{6}$	$-\frac{1}{6}$	$\frac{1}{3}$	0	$-\frac{1}{12}$					
	3			$\frac{1}{3}$		$\frac{4}{9}$	$\frac{11}{36}$	$\frac{2}{3}$	$\frac{1}{3}$	$\frac{1}{4}$	$\frac{1}{6}$	$\frac{1}{6}$	$\frac{1}{6}$					
0	$\frac{1}{2}$													1	$-\frac{1}{2}$	$\frac{1}{2}$	$-\frac{1}{3}$	$\frac{1}{3}$

It is limited by

$$1 \geqslant R \geqslant -\frac{1}{2} \qquad (2.26)$$

When R = 1, the polarization of the γ-rays is equal to the polarization of the incident neutrons. It is seen from table 2 that if one or two of the spin values of the reaction are known in advance, a measurement of the ratio between γ-ray and neutron polarization may be sufficient to determine the other spin values unambiguously. Some applications of this method will be reported below.

In the formula for $r(L_1,L_2)$ the exponent $\lambda_1 = \frac{1}{2}\left[1 + (-1)^{L_1}\right]$ implies a dependence of the polarization direction upon parity and multipole order. Actually, $(-1)^{\lambda_1} = +1$ when L_1 is the multipole order of the magnetic radiation, and -1 when L_1 represents electric radiation. Since $L_1 = L_2 \pm 1$ we see from section II,2 that the former case will be the one of practical importance. The sign of the mixing term is also determined by the relative phases of the amplitudes b_1 and b_2, which are not known. Table 3 gives the magnitude of $r(L_1,L_2)$ for the lowest nuclear spins.

TABLE 3.

Numerical values of $r(L_1,L_2)$ calculated from formula (2.25) for the case of mixture of M1 and E2 radiation. When E1 and M2 radiations are mixed, all signs in the table are reversed.

Ji \ Jc \ Jf	1	2	3	3/2
1/2 — 0	0			
1/2 — 1	$-\frac{1}{2}$	$-\frac{3}{2\sqrt{5}}$		
3/2 — 1	$\frac{1}{4}$	$\frac{3}{4\sqrt{5}}$		
3/2 — 2	$-\frac{3}{4\sqrt{5}}$	$-\frac{1}{4}\sqrt{\frac{21}{5}}$	$-\frac{1}{2}\sqrt{\frac{6}{5}}$	
5/2 — 2	$\frac{1}{2\sqrt{5}}$	$\frac{1}{6}\sqrt{\frac{21}{5}}$	$\frac{1}{3}\sqrt{\frac{6}{5}}$	
5/2 — 3		$-\frac{1}{3}\sqrt{\frac{6}{5}}$	$-\frac{1}{2}$	
0 — 1/2				$-\sqrt{\frac{3}{2}}$

Only if all the spin values of the decay scheme are known can the intensity ratio $(b_1/b_2)^2$ and the phase difference of the mixed radiations be studied. Because of the uncertainty in the experimental determination of R, this method has not yet been attempted.

3. Polarized thermal neutron beams.

Two methods exist for the production of intense beams of polarized thermal neutrons.

The highest degree of polarization is obtained by selection of particles corresponding to a definite reflection from a magnetized, ferromagnetic single crystal. This method was applied by Shull, Wollan and Koehler (1951) who report that it is possible to obtain approximately 10^5 polarized neutrons per second in the (220) Fe_3O_4 reflection, using neutron radiation from a reactor with a central flux of 10^{12} neutrons/cm^2 sec.

Another polarizing principle consists in the transmission of neutrons through a magnetized block of iron which predominantly scatters particles with a definite spin direction. According to Stanford et al. (1954), neutrons passing through a 4 cm long iron sample magnetized to 11000 Oersted have a polarization of 32 %. Since such a polarizer has a total transmission of approximately 2 %, about 10^6 polarized neutrons per second should be obtainable with the kind of reactor mentioned above. The smaller total intensity in the former case will, in principle, contribute to better statistical results. This is, however, an unimportant point, as the background is very high for γ-ray counting equipment in the vicinity of a reactor, and the total counting rate would be of the same order of magnitude in the two cases. On the basis of these considerations, the transmission method was found to be best suited for the present purpose.

The cross section for thermal neutrons passing through a block of polycrystalline iron has the form (1.5), whereas equations (1.7) and (1.8) must be somewhat modified for this case. When the iron sample is not magnetized to saturation, the magnetic fields of the microcrystals are not completely aligned. In passing through domains with varying field directions, the neutrons may be depolarized. The theory for this effect has been considered in detail by Halpern and Holstein (1941). They introduce the depolarization coefficient σ_d which is proportional to the deviation from magnetic saturation. In the region of thermal neutrons, σ_d is essentially energy independent for polycrystalline iron. When $\rho\sigma_p \ll 1$, the formulæ (1.7) and (1.8) obtain the forms

$$P_n = \frac{\rho\sigma_p}{1+\eta}\, g(\rho\sigma_d) \qquad (3.1)$$

$$\eta = \frac{\rho^2\sigma_p^2}{2}\, f(\rho\sigma_d) \qquad (3.2)$$

where

$$g(x) = \frac{1-e^{-x}}{x} \qquad (3.3)$$

$$f(x) = \frac{2(x-1+e^{-x})}{x^2} \qquad (3.4)$$

The correction functions g and f are shown in figure 6, where the abcissa is proportional to the deviation from magnetic saturation. Since complete saturation is never obtained, g and f are always smaller than one. Even in the best transmission experiments performed, these corrections played a dominant role.

The transmission method utilizes the whole thermal neutron spectrum of the source. Because of neutron reflection from lattice planes in the polarizing iron block, both σ_o and σ_p are strongly energy dependent. Therefore the degree of polarization is varying according to energy and the neutron spectrum is altered by transmission through the polarizer. Neutrons passing through a device with transmission T(v) obtains the flux distribution $\Phi(v)\ T(v)$, where $\Phi(v)$ is the spectrum of the incident beam. These quantities are functions of the neutron velocity v. When the emitted neutron beam is studied by means of a detector with sensitivity $\varepsilon(v)$, the neutrons counted have the distribution $\Phi T\varepsilon$. In certain cases one detects the γ-rays resulting from neutron capture. Then ε is proportional to the absorption of neutrons in the target.

By setting $\Phi(v)\,\varepsilon(v) = \Phi'(v)$ and using the equation (3.1), we obtain for the average polarization of the neutrons detected after having passed through a magnetized block of iron

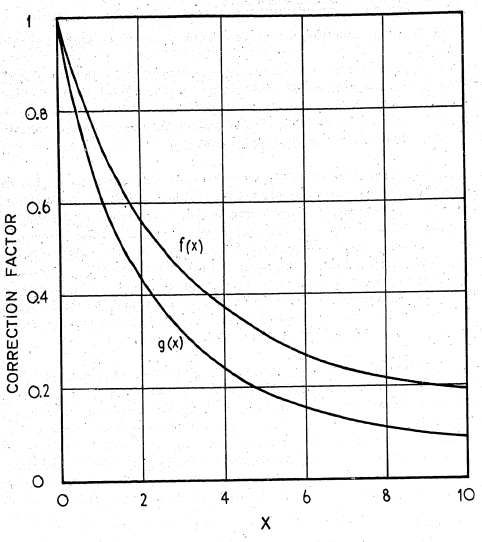

Figure 6. Correction functions g(x) and f(x), as calculated from formulæ (3.3) and (3.4).

$$\overline{P} = \varrho\, g\, \frac{\int \sigma_p \Phi' T \, dv}{(1 + \overline{\eta}) \int \Phi' T \, dv} \tag{3.5}$$

When σ_p, Φ' and T are known as functions of v, the integrations can be carried out.

The correction factor can be determined in two ways. If the average single transmission effect is measured, one can determine f from the relation

$$\overline{\eta} = \frac{I_m - I_u}{I_u} = f\, \frac{\varrho^2}{2}\, \frac{\int \sigma_p^2 \Phi' T \, dv}{\int \Phi' T \, dv} \tag{3.6}$$

where I_m and I_u are the transmitted intensities for the magnetized and unmagnetized block of iron respectively. The value of f determines g, as seen from figure 6. The factor g can also be evaluated from a double transmission experiment, as indicated in figure 3. When both polarizers are magnetized in the same direction, the counting rate $I_m^{(2)}$ is obtained. The superscript (2) indicates a double transmission experiment. In weak fields σ_d for iron is very large. A fraction of a millimetre of iron plate is sufficient to depolarize the neutrons completely, as shown by Burgy et al. (1950). Thus, when an iron shim with a thickness of about 0.5 mm is placed in field free space between the polarizers, the neutron beam is depolarized in passing through it. The counting rate after having been corrected for the attenuation of the beam in the shim, is denoted by $I_s^{(2)}$. For a definite neutron energy, equation (1.11) gives the relation $I_m^{(2)} = I_s^{(2)}(1 + P_1 P_2)$, and the double transmission effect averaged over the whole neutron spectrum has the form

$$\frac{I_m^{(2)} - I_s^{(2)}}{I_u^{(2)}} = g^2\, \varrho^2\, \frac{\int \sigma_p^2\, \Phi' T^2 \, dv}{\int \Phi' T^2 \, dv} \tag{3.7}$$

from which g can be calculated. $I_u^{(2)}$ is the intensity when none of the polarizers are magnetized. For the numerical evaluation of the equations (3.5), (3.6) and (3.7) the energy dependence of the quantities σ_o, σ_p, Φ and ε is needed.

Taking into account both nuclear and magnetic scattering of neutrons, Halpern and Johnson (1939) obtained for the differential coherent cross section of a single atom

$$d_s\sigma = \left[b^2 + 2\, b\, p\, \vec{q}\, \vec{e}_n + p^2 \left| \vec{q} \right|^2 \right] d\Omega \tag{3.8}$$

where b is the amplitude of the nuclear scattering, giving for the total coherent scattering of a single atom: ${}_s\sigma_{coh} = 4\pi b^2$. The magnetic scattering amplitude is p, $\vec{e}_n$ is a unit vector in the direction of polarization of the incident neutron, and $\vec{q} = \vec{e}_s(\vec{e}_s \vec{e}_a) - \vec{e}_a$ is the magnetic interaction vector, where $\vec{e}_s$ is the the unit scattering vector and $\vec{e}_a$ is a unit vector parallel to the atomic magnetic moment. By applying the methods indicated by Halpern, Hamermesh and Johnson (1941) and by Steinberger and Wick (1949) the total, atomic, elastic scattering cross section for magnetized crystalline material becomes

$$a\sigma_{el} = \frac{\lambda^2}{2a^2} \left\{ b^2 \sum_{\ell} \frac{N(\ell)}{\ell}\, e^{-2W} + \frac{2}{3} \left(\frac{e^2}{m_e c^2} \right)^2 \mu_n^2\, S_a^2 \sum_{\ell} \frac{N(\ell)}{\ell}\, F(\ell)^2\, e^{-2W} \right.$$
$$\left. \pm\, b\, \frac{e^2}{m_e c^2}\, \mu_n\, S_a \sum_{\ell} \frac{N(\ell)}{\ell}\, F(\ell) \left[1 + \left(\frac{\ell \lambda}{2a} \right)^2 \right] e^{-2W} \right\} \tag{3.9}$$

Here λ is neutron wavelength and a is the length of one side of the body-centred cubic unit cell of iron. The quantity ℓ takes all possible values $\ell = \sqrt{n_1^2 + n_2^2 + n_3^2}$ where the n's are Miller indices for a set of reflecting planes. $N(\ell)$ equals twice the value of the multiplicity of the set of planes corresponding to ℓ. The factor $e^{-2W(\ell)}$ is a correction for inelastic scattering due to thermal lattice vibrations. Its magnitude is given by Bacon (1955, p. 42). The magnetic form factor $F(\ell)$ for the set of planes ℓ in iron was calculated by Steinberger and Wick (1949) for two different assumptions regarding the 3d wave function of the iron atom. For the application in equation (3.9) the lower of the two values was chosen for $F(\ell)$, since this apparently gives the better agreement with the experimental data as shown by Stanford et al. (1954, fig. 2). S_a is the spin quantum number of the scattering atom, and μ_n is the neutron magnetic moment in nuclear magnetons. The first two terms are due to nuclear and magnetic scattering respectively. The last term in equation (3.9) is the polarization dependent cross section due to interference between elastic nuclear and magnetic scattering. It is preceded by the sign + or - corresponding to positive or negative neutron spin respectively in the direction of magnetization. The total cross section includes inelastic scattering which takes the form of a smaller correction to the above formula.

Cassels (1950) has evaluated the complete cross section for nuclear scattering of neutrons in iron in the region of neutron velocities between 900 and 2200 m/sec. Its magnitude is given in relation to the coherent and incoherent cross sections ${}_s\sigma_{coh}$ and ${}_s\sigma_{inc}$ for a single atom. Shull and Wollan (1951) have given for these quantities: ${}_s\sigma_{coh} = 11.7$ barns and ${}_s\sigma_{inc} = 0.3$ barns.

The magnetic elastic cross section was calculated from the second term of equation (3.9). According to Lowde (1954) the corresponding inelastic cross section is of the order of 10 millibarns, so that it can safely be neglected. Outside the energy region treated by Cassels, experimental values for the total cross section of iron are given in the compilation by Hughes and Harvey (1955). At the low energy side, the data indicate that the absorption of neutrons in iron obeys the 1/v-law, where

$$\sigma_{abs} = \frac{5830}{v} \text{ (barns)} \tag{3.10}$$

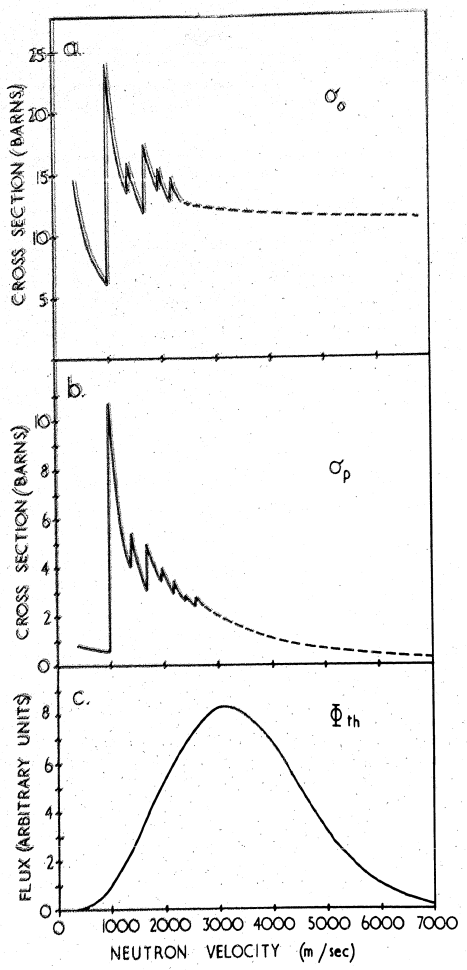

Figure 7.
The upper curve shows the total neutron cross section for iron, then follows the polarization cross section for iron, and the lowest curve gives the thermal neutron flux distribution from JEEP.

in which the neutron velocity v is inserted in m/sec. We are now able to form the total neutron cross section for unmagnetized polycrystalline iron

$$\sigma_o = \sigma_{nuc} + \sigma_{mag} + \sigma_{abs} \qquad (3.11)$$

which is illustrated in the upper diagram of figure 7. From 2200 m/sec upward a smooth curve is drawn through the above mentioned experimental points. Since it represents an average over many absorption edges, the curve is drawn as a broken line in the figure.

The polarization cross section σ_p was calculated by Stanford et al. (1954) for the neutron velocities between 980 m/sec and 2700 m/sec. They also quote observed values from various experiments. Above 2700 m/sec we apply a smooth curve drawn through these points. The corresponding line in figure 7b is broken. Below 980 m/sec the single transmission effect η for a single crystal of iron has been measured by Hughes, Burgy and Woolf (1950). From equation (3.2) we get

$$\sigma_p = \frac{1}{\varrho}\sqrt{\frac{2\eta}{f}} \qquad (3.12)$$

Because a single crystal was applied, f = 1; σ_p is then easily calculated for this region.

The curve thus obtained for the complete polarization cross section for iron at thermal energies is drawn in figure 7b. σ_p is positive, which means that the magnetization is parallel to the neutrons having the highest cross section, and antiparallel to the polarization of the transmitted beam.

The velocity distribution of the thermal neutrons emitted from the reactor JEEP was measured by Pelser (1954). In figure 7c is shown the Maxwell flux distribution Φ, which was adapted from his results.

In the evaluation of experimental results, the energy response of the neutron detector or the absorption of the target should also be known. For BF_3 counter tubes, having a pure 1/v cross section, the energy dependence of the absorption is easily calculated. Polycrystalline targets may present a greater difficulty, since both the strongly varying scattering cross section and the capture cross section should be taken into account. For "thin" targets, having $\varrho d_t \ll 1$ one can generally assume a 1/v-dependent absorption. Thicker targets will be 1/v-absorbers at high energies and total absorbers in the low energy region. Nearly complete absorption must be assumed for high capture cross sections and very thick targets.

4. Principles for the measurement of circular polarization.

For a beam of light, the degree of circular polarization can be determined by means of a "quarter wave plate", which utilizes the fact that the electric field vector of the photon is rotating in space. In the case of γ-rays, however, no similar detecting device exists. The methods for measuring circular polarization must, therefore, be based upon observation of the spin direction of the photon. As pointed out in section II,2 , the angular momentum is directed along the axis of propagation.

Using a mechanical method, Beth (1936) measured the angular momentum acting upon a disc irradiated with circularly polarized light. He was able to assign the spin +1 and -1 to left and right circularly polarized photons respectively, in accordance with theory. This method requires high photon intensity, and it is hardly applicable to γ-rays.

As shown in the first section of this chapter, ordinary angular distribution measurements can not be used to distinguish between spin directions parallel and antiparallel to the direction of incidence. This method can only be useful in the case that the target particles are also polarized. Gamma-rays interact with both nuclei and electrons, but the only easy way of polarizing matter is obviously by magnetization of ferromagnetic materials. In this method electrons of the outermost shell are aligned. These electrons are not concerned with the photodisintegration, photoelectric emission or pair formation processes. Only in the Compton scattering process can γ-rays interfere with electrons aligned by magnetic fields.

A practical form of the generalized Klein-Nishina formula for the Compton cross section of polarized photons interacting with polarized electrons, has been evaluated by Lipps and Tolhoek (1954 ab). They give the differential cross section for the scattering of a photon into the solid angle $d\Omega$ as a function of the polarization vector $\vec{\xi}$ for the photon as defined in section II,2, the unit vector $\vec{\zeta}$ directed along the spin of the electron, the momentum of the photon, $\vec{k} = k\vec{e}_3$, and the corresponding quantities for the emitted particles $\vec{\xi}'$, $\vec{\zeta}'$ and k'.

For the present purpose, this function should be averaged over all directions of the vectors $\vec{\xi}'$ and $\vec{\zeta}'$, since we are not interested in the polarization of the scattered photon and electron. Lipps and Tolhoek (1954 b) give for this case

$$d_e\tau\ (k,k',\vec{\xi},\vec{\zeta}) = d\ {}_e\tau_c + \xi_3\vec{\zeta}\ d\ {}_e\vec{\tau}_p \tag{4.1}$$

The symbol ${}_e\tau$ denotes the cross section for a single electron. For the sake of simplicity we shall in the following introduce the units: $m_e = 1$, $c = 1$, $\hbar = 1$. Then the scattering angle ϑ between the vectors $\vec{k}$ and $\vec{k}'$ is related to their magnitudes by

$$\cos\vartheta = 1 - \frac{k - k'}{kk'} \tag{4.2}$$

The azimuthal angle of the scattered photon with respect to the $(\vec{e}_1,\vec{e}_3)$-plane shall be called φ. In equation (4.1) the first term is the ordinary differential Compton cross section:

$$d\ {}_e\tau_c = \frac{e^2}{2}\frac{k'^2}{k^2}\left[1 + \cos^2\vartheta + (k - k')(1 - \cos\vartheta)\right] d\Omega \tag{4.3}$$

and the polarization dependent cross section is a vector:

$$d\ {}_e\vec{\tau}_p = -\frac{e^2}{2}\frac{k'^2}{k^2}(1 - \cos\vartheta)(\vec{k}\cos\vartheta + \vec{k}')\ d\Omega \tag{4.4}$$

in which e is the electronic charge.

In the two special cases of the electron being polarized parallel and perpendicular to the momentum of the incident photon we get

$$\vec{\zeta} = \vec{e}_3,\quad \vec{\xi}\,d\ {}_e\vec{\tau}_p = -\frac{e^2k'^2}{2k^2}(k + k')(1 - \cos\vartheta)\cos\vartheta\, d\Omega \tag{4.5}$$

$$\vec{\zeta} = \vec{e}_1,\quad \vec{\xi}\,d\ {}_e\vec{\tau}_p = \frac{e^2k'^3}{2k^2}(1 - \cos\vartheta)\sin\vartheta\cos\varphi\, d\Omega \tag{4.6}$$

These quantities change sign when $\vec{\zeta}$ is reversed. When scattered γ-radiation is measured, the ratio between scattering from polarized and unpolarized electrons is given by

$$\frac{N_{pol}}{N_{unpol}} = 1 + \xi_3\vec{\zeta}\,\frac{d\ {}_e\vec{\tau}_p}{d\ {}_e\tau_c} \tag{4.7}$$

where $1 \geqslant \xi_3 \geqslant -1$. In figures 8 and 9 is shown the ratio $\vec{\zeta}(d\ {}_e\vec{\tau}_p/d\Omega)/(d_e\tau_c/d\Omega)$ between the polarization dependent and the ordinary Compton cross section as function of the scattering angle, for the two above mentioned cases of electron polarization. The diagrams illustrate the large effects resulting from circular polarization of low energy γ-rays when the electrons are polarized transverse to the incident beam. When the photon and the electron are polarized along the same axis large effects can be obtained for all energies.

For the study of single γ-rays resulting from neutron capture, discrimination between various photon energies is required. When scattered quanta are studied, energy discrimination can only be performed if narrow γ-ray beams are available. In the present experiment rather large γ-ray sources must be used in order to obtain sufficient intensity. Therefore, a less

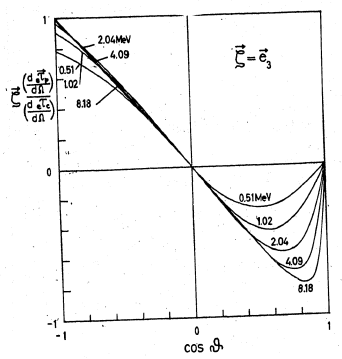

Figure 8.
The relative polarization dependent part of the differential Compton cross section for iron. The scattering electron is polarized in the propagation direction of the γ-ray.

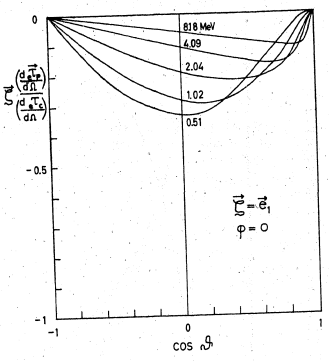

Figure 9.
The relative polarization dependent part of the differential Compton cross section for iron. The polarization vector of the scattering electron is in the same plane as the incident and the emitted γ-ray, and it is perpendicular to the incident beam.

polarization- sensitive method, which consists in measuring the transmission of γ-radiation through magnetized iron, was applied. In such an experiment one can, to some extent, distinguish between γ-rays of different energies by selecting pulses from a scintillation crystal.

The transmission for iron is given by the total cross section which can be obtained by integration of the differential cross section over the sphere. As a result of the integration over φ, components of the electron spin perpendicular to the axis of incidence will cancel out. The total Compton cross section for a single electron then becomes

$$\int \frac{d_e\tau}{d\Omega}\, d\Omega = {}_e\tau_c + \xi_3\zeta_3\ {}_e\tau_p \tag{4.8}$$

where the ordinary Compton cross section is

$${}_e\tau_c = 2\pi e^2\left\{\frac{1+k}{k^2}\left[\frac{2(1+k)}{1+2k} - \frac{1}{k}\ln(1+2k)\right] + \frac{1}{2k}\ln(1+2k) - \frac{1+3k}{(1+2k)^2}\right\} \tag{4.9}$$

and the polarization dependent part

$${}_e\tau_p = -2\pi e^2\left[\frac{1+k}{2k^2}\ln(1+2k) - \frac{1+4k+5k^2}{k(1+2k)^2}\right] \tag{4.10}$$

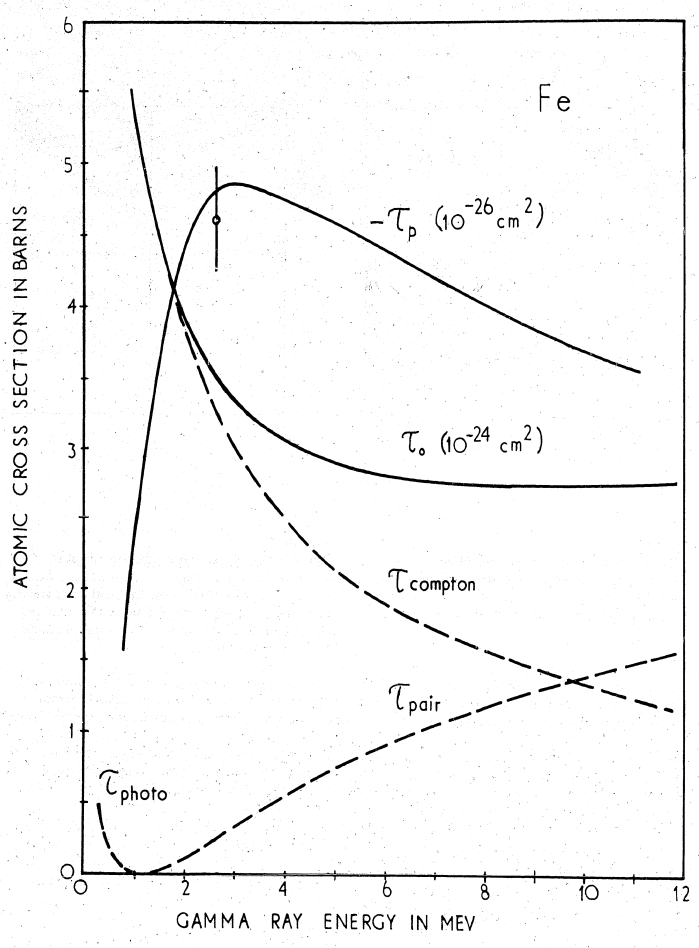

Figure 10.
γ-ray cross sections for iron. Note that the polarization cross section τ_p is on a hundred times larger scale than the other quantities. The experimental value was obtained by Gunst and Page (1953).

It is seen from figure 8 that the polarization effects of the forward and backward scattering give opposite contributions to the integral (4.8). The total polarization cross section ${}_e\tau_p$ becomes zero at about 0.65 MeV. It is positive for lower energy, and negative for higher energy photons, which are mainly scattered in the forward direction. This means that above 0.65 MeV the transmission is greatest when ξ_3 and ζ_3 have the same sign, i.e. when the photon spin is parallel to the electron spin and antiparallel to the magnetic field.

Atomic cross sections are obtained by multiplication with the number of electrons:

$$ {}_a\tau_c = Z\ {}_e\tau_c \qquad (4.11) $$

$$ {}_a\tau_p = \nu_{eff}\ {}_e\tau_p \qquad (4.12) $$

where Z = 26 is the atomic number for iron, and ν_{eff} is the effective number of polarized electrons in magnetized iron. The cross sections ${}_a\tau_c$ and ${}_a\tau_p$ are given in figure 10 as functions of energy. For the number of polarized electrons, the value for saturated iron, ν_{sat} = 2.06 was used, as reported by Argyres and Kittel (1953). The photodisintegration and pair formation cross sections for iron were taken from the tables of Davisson (1955). As seen from the figure, the polarization cross section is only about 1.5 % of the total cross section in the region of high energy neutron capture γ-rays. This low value is mainly due to the fact that only about two of the 26 electrons of the iron atom can be polarized. By performing a single transmission experiment for γ-radiation passing through magnetized iron, Gunst and Page (1953) have performed an experimental determination of the magnitude of ${}_a\tau_p$ at 2.62 MeV. Their result is indicated in figure 10.

5. Experimental set-up.

A schematical top view of the main apparatus is shown in figure 11. A neutron flux of about 10^7 neutrons/cm^2 sec is emitted from the collimator which "sees" a slug of graphite very near the reactor centre in one of the isotope channels of JEEP. At the collimator opening the slightly divergent beam has its narrowest cross section, which is 10 x 30 mm. After having passed through the polarizer, it hits the (n, γ)-target. The neutron polarizer is a 12 x 18 x 40 mm block of iron, joined to the pole faces of a magnet by the 40 x 18 mm planes. The neutrons pass through 18 mm of iron, which approximately satisfies the condition $\rho = 2/\sigma_o$ for optimum counting statistics. The block is cut from cold-rolled iron in such a way that the magnetic field is applied in the direction of rolling. According to Hughes, Wallace and Holtzmann (1948), this procedure gives the highest degree of polarization. The field strength was measured by means of a small search coil which could be inserted between the pole pieces near the surface of the polarizing block. In pulling the coil quickly out of the field, the induced electromotoric force was measured on a ballistic galvanometer, giving the result of 14900 Oersted. During continuous runs, water cooling was provided for the magnet coils.

Measurements of the single and double transmission effects were performed with a BF_3 counting tube placed in the beam in such a way that the neutrons would traverse at most the diameter of the tube. Hence it is essentially a 1/v-detector. In order to use the measured results to calculate the polarization of the neutron beam, the integrals of the equations (3.5), (3.6) and (3.7) were determined in the region of neutron velocities between 400 and 7000 m/sec. Contributions to the thermal flux outside this region can safely be neglected. Multiplication and integration of the velocity dependent functions were performed graphically. In the double transmission experiment the neutron beam once more passed through a polarizing block exactly like the first one. A duplicate of the polarizing magnet was not available, and a smaller magnet, producing a field strength of 5200 Oersted, was applied for the second polarizer. In the formula (3.7) for the double transmission experiment, the factor g^2 should be replaced by $g_1 g_2$ in the case of different field strengths. Measurements were performed, first with both fields at 5200 Oersted, and then with the first magnet at 14900 Oersted. The results are quoted in table 4, where the errors indicated are the statistical standard devitions.

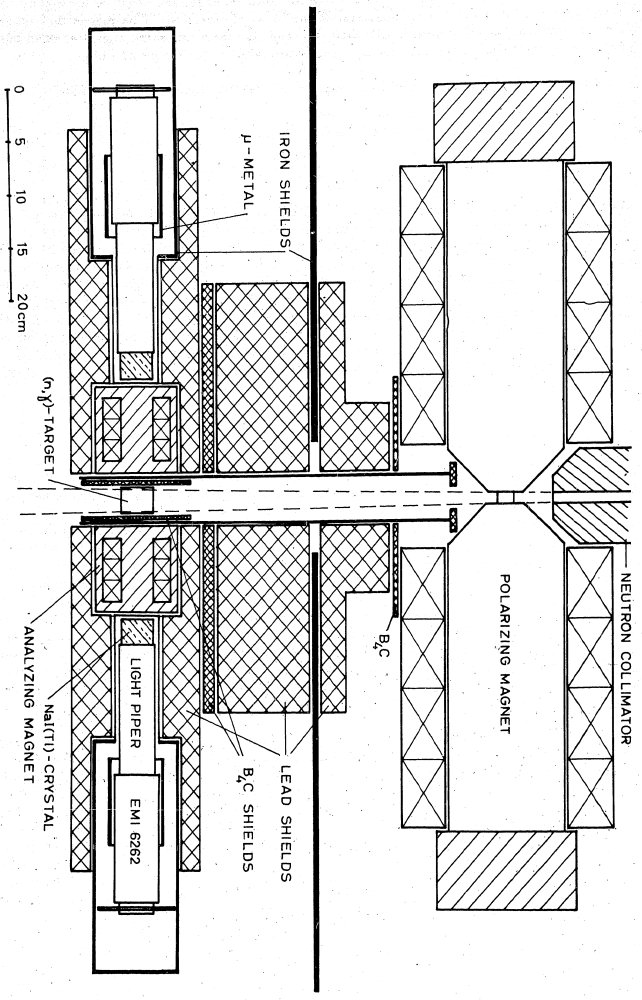

Figure 11.
Experimental set-up for the polarization experiment, as seen from above.

TABLE 4.

Experimental results from measurements of neutron polarization.

Experiment	H_1 Oersted	H_2 Oersted	Observed transmission effect in %	Transmission effect from equation (3.6) or (3.7)	Calculated correction factor f	g_1	g_2
Single transmission effect $\bar{\eta} = \frac{I_m - I_u}{I_u}$	14900		5.25 ± 0.10	$0.0676\ f$	0.775 ± 0.015	0.67 ± 0.02	
Double transmission effect	5200	5200	2.73 ± 0.20	$0.107\ g_2^2$			0.505 ± 0.02
$\frac{I_m^{(2)} - I_s^{(2)}}{I_u^{(2)}}$	14900	5200	3.49 ± 0.20	$0.107\ g_1 g_2$		0.65 ± 0.04	

The integrals of equation (3.5) were calculated for both a 1/v-detector and a total absorption detector. For the polarization of the neutrons detected we get, using the values of table 4:

$$P_n(1/v) = 0.325\ \frac{g}{1+\bar{\eta}} = 20.4\% \pm 0.8\% \qquad (5.1)$$

$$P_n(\text{total}) = 0.283\ \frac{g}{1+\bar{\eta}} = 18.0\% \pm 0.8\% \qquad (5.2)$$

All the (n,γ)-targets that were actually used had absorbing and scattering properties far from these extremes. For the further calculations, the value $P_n = 19$ % was considered as a satisfactory approximation.

Between polarizer and target the neutrons travel 40 cm through an approximately homogeneous magnetic field of about 100 Oersted. This field, which insures that the neutrons keep their direction of polarization, is produced by two parallel iron plates that pick up part of the stray field from the magnet.

The target is generally a thin walled aluminium cylinder of 35 mm diameter and 25 mm high, containing the element to be studied. For some materials such a thick target would result in too many scattered neutrons producing unpolarized γ-rays in the target and the surroundings. Then its extension in the direction of the neutron beam is reduced.

If the capturing material is ferromagnetic it can depolarize the neutrons before absorption. For iron- and nickel-targets the non-ferromagnetic compounds Fe_2O_3 and $NiSO_4$ were chosen. As small ferromagnetic impurities can reduce the polarization considerably, the targets were studied for depolarizing action by placing them at the position of the iron shim in the double transmission experiment. It was found that the neutron beam had 65% of its original polarization after having passed through 23 mm of the Fe_2O_3-target. When the target was placed in its ordinary position, the average polarization of the neutrons captured was reduced by 78%. The other materials, including the $NiSO_4$-powder, gave no depolarizing effect.

The directions of greatest circular polarization of the γ-rays are given by an axis through the

(n,γ)-target, parallel to the incident neutron spin, which is defined by the magnetic field direction of the polarizing magnet. Radiation emitted in both directions along this axis are detected by NaI(Tl)-crystals after having passed through analyzers consisting of 8 cm long pieces of iron magnetized in the direction of transmission. The crystals, the cores of the analyzing magnets and the maximal size of the target, constitute parts of a cylinder with diameter 35 mm.

As shown in figure 11, both ends of each iron core are formed as flat discs fitting into an outer cylinder. The coil producing the magnetic field is placed within the cylinder and around the core, which forms the narrowest part of the magnetic circuit. A few separate windings serve for the measurement of the magnetic induction, which is found to be 18300 gauss, corresponding to 86.3 % of saturation. The polarization is then $P_a = 1.96$ % at 7 MeV, and is slowly varying with energy above 3 MeV, as indicated by figure 10.

An estimate for the sensitivity of the experiment can now be obtained by insertion of the derived polarization quantities in equation (1.12) combined with (2.21) for $\cos\Theta = 1$:

$$\frac{I' - I''}{I' + I''} = P_\gamma \, P_a = R \, P_n \, P_a = 0.0037 \, R \qquad (5.3)$$

at 7 MeV. I is the γ-ray intensity as measured by the crystals. It is seen that in order to determine the magnitude of R, which is between 0 and 1, extremely small relative variations in the intensity should be measured. Furthermore, the sensitivity of the method is considerably reduced by background and scattering.

Each detector consists of a cylindrical NaI(Tl)-crystal, 35 mm in diameter and 25 mm high, coupled to an EMI 6262 photomultiplier. Systematic errors may arise if the pulse height is influenced by the inversion of the magnetic fields, because this effect can simulate polarization. Therefore, long light pipers are used to bring the photomultipliers away from the magnets, and the tubes are surrounded by μ-metal and soft iron shields. The EMI venetian blind photomultipliers employed are reported by Wardley (1952) to be less influenced by magnetic fields than other types. The influence is mainly due to magnetic deviation of the electron current between the photocathode and the first dynode, since this is by far the largest interelectrode distance in the tube. Ordinarily 180 volts, being the highest voltage allowed, is applied between these electrodes. By lowering this voltage to 1/20 of the usual value, the sensitivity to magnetic fields was increased accordingly. Using a radioactive source, the pulse discrimination was set by trial to the position of highest magnetic sensitivity. Relative changes in the counting rates due to inversion of the magnetic fields were less than $5 \cdot 10^{-4}$, corresponding to less than $3 \cdot 10^{-5}$ for the actual experiment in the worst case. In the next section is quoted the result of a "symmetry control" experiment, performed with a titanium target placed 12 cm from the ordinary position, but still in the neutron beam, so that the γ-rays passing from target to detector would not pass through the analyzer core. The measurements showed the expected absence of asymmetry, but the statistical accuracy is poor, so that no decisive conclusion can be drawn from this experiment alone. As mentioned below, series of observations were carried out in such a way that systematic errors due to reversal of magnetic fields would cancel out.

Heavy shielding of lead and boron carbide serve to reduce the intense background radiation, which is largely due to γ-rays resulting from neutron capture in and scattering from the polarizing iron block. The effect of neutrons scattered from the target is reduced by boron containing plastic plates, placed between target and analyzing magnets.

Figure 12 shows a block diagram of the electronic apparatus used.
The pulses from the two photomultipliers are applied to two identical channels consisting of cathode follower, linear amplifier, single channel discriminator and scaler. In channel No. 1 the scaling factor is 8, 16 or 32, and in channel No. 2. it is twice this value. The output pulses from the scalers can be led to the mechanical registers A og B. The switching between these registers is performed by means of a relay circuit at every 100th pulse from scaler No. 2. At the same moments the current in the analyzer magnets is reversed.

The analyzer magnets are oppositely coupled, meaning that the γ-intensity $I'(1)$ in channel No. 1. is registered at the same time as $I''(2)$ in channel No. 2, and vice versa. As channel No. 2. is used as a monitor, the number of counts per period in channel No. 1. is given by

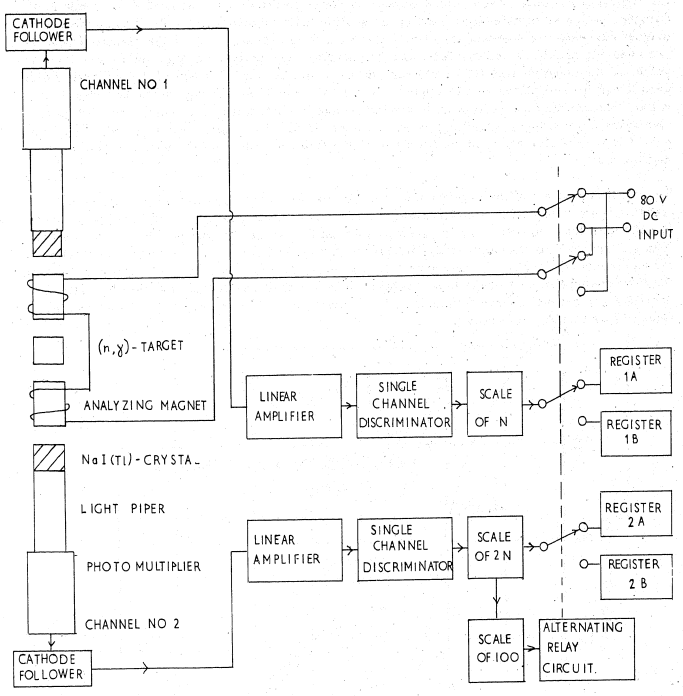

Figure 12.
Block diagram of the electronic circuit for the polarization experiment.

$$N_a' \propto \frac{I'(1)}{I''(2)} \qquad (5.4)$$

$$N_a'' \propto \frac{I''(1)}{I'(2)} \qquad (5.5)$$

and using equation (5.3), we get for the observed asymmetry:

$$\left.\begin{aligned} \frac{N_a' - N_a''}{N_a' + N_a''} &= \frac{2 R \, P_n \, P_a}{1 + (R \, P_n P_a)^2} \\ &\cong 2 R \, P_n \, P_a \quad \text{for } R \, P_n \, P_a \ll 1 \end{aligned}\right\} \qquad (5.6)$$

This condition is fulfilled as shown by equation (5.3).

By observation of opposite polarization in the two channels, fluctuations due to changes in neutron flux or in background are compensated.

The numbers of counts N'_a and N''_a are observed alternatively, and the data are accumulated on the registers A and B. Each period with one definite polarizer current is of about 3 minutes' duration, which is adjusted by means of the scaling factor in channel No. 2. When analyzer magnet currents are inversed frequently, errors due to different drift in the electronics of the two channels should be unimportant. If both polarizer and analyzer change field directions, the values of the counting rate N_a should remain the same, but the influence of the magnetic fields upon the photomultipliers will be opposite in the two cases. An average of the two polarization values thus obtained will compensate for the change in photomultiplier sensitivity. Measurements are always done with a certain polarizing field direction for a longer period. The next period is then performed with opposite polarizing field, in order to eliminate possible systematic errors.

The resolving power of the experimental set-up was found by measurements of the spectra from titanium, iron, sulphur and aluminium, which have quite prominent high energy γ-rays. In neither of these spectra was complete resolution of a single γ-ray performed, but by trial it was found that curves calculated with a resolution of 14.5% give the best agreement with the experimental results. By using the cross sections for NaI, as given by Bell (1955, fig. 17), the total absorption of γ-rays in a crystal of 25 mm length was calculated, together with the contributions from the three different types of interaction. These properties are shown in figure 13 as functions of energy.

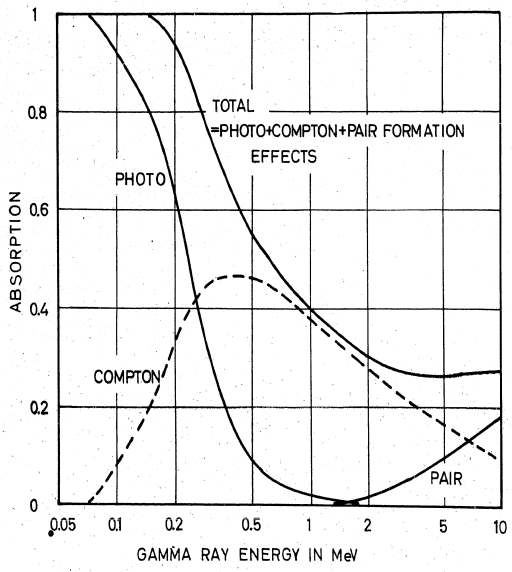

Figure 13.
Absorption of γ-rays in 25 mm of NaI.

In the region of high energy neutron capture γ-rays, i.e. from about 5 to 10 MeV, the Compton and pair formation cross sections are of the same order of magnitude. Compton electrons are widely distributed, as shown in figure 14 for γ-rays of 7 MeV. In the small crystals used, most of the annihilation quanta resulting from the positrons will escape. The pulses due to pair formation will then correspond to a single peak at an energy $2m_ec^2$ lower than the γ-ray energy. This peak makes energy discrimination possible.

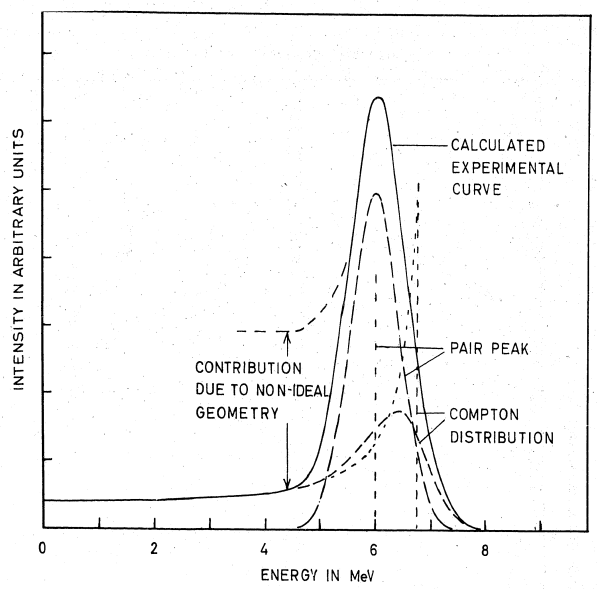

Figure 14.
Pulse spectrum of a 7 MeV γ-ray in a 25 mm long crystal of NaI(Tl). Pair and Compton contributions are shown in the ideal case and for a resolution of 14.5 %. The full drawn curve is the expected experimental distribution.

The ideal theoretical spectrum of figure 14 was folded with a gaussian distribution with half width equal to 14.5% of the total energy. The resulting distribution of the photomultiplier pulses is shown. The γ-ray spectra for the elements studied could then be constructed, by use of the energy and intensity data given by Kinsey, Bartholomew and Walker (1951 c, 1952), Kinsey and Bartholomew (1953 abe) and Groshev, Adyasevich and Demidov (1955 b).

Measurements of the spectra were performed with the analyzing magnets removed. Contributions from slow neutrons scattered into the counters were determined by comparison with a graphite target, and subtracted. Four experimental pulse distributions are shown in figure 15. Curves, as the one in figure 14, were used to construct these spectra, but in order to obtain approximate agreement below the highest peaks, one must introduce an additional contribution to the single γ-ray spectrum. Such a contribution will result from electrons escaping from the crystals and from γ-rays scattered in the target and in the surroundings of the detectors. The correction is shown as a broken line in figure 14.

The poor resolving power is mainly due to the fact that the crystals used were quite small for the study of high energy γ-rays. By use of a collimator, and without the light piper, the resolution could be improved somewhat, but these changes would imply a too large decrease in intensity. Within experimental errors, the photomultiplier pulse height was found to be a linear function of energy.

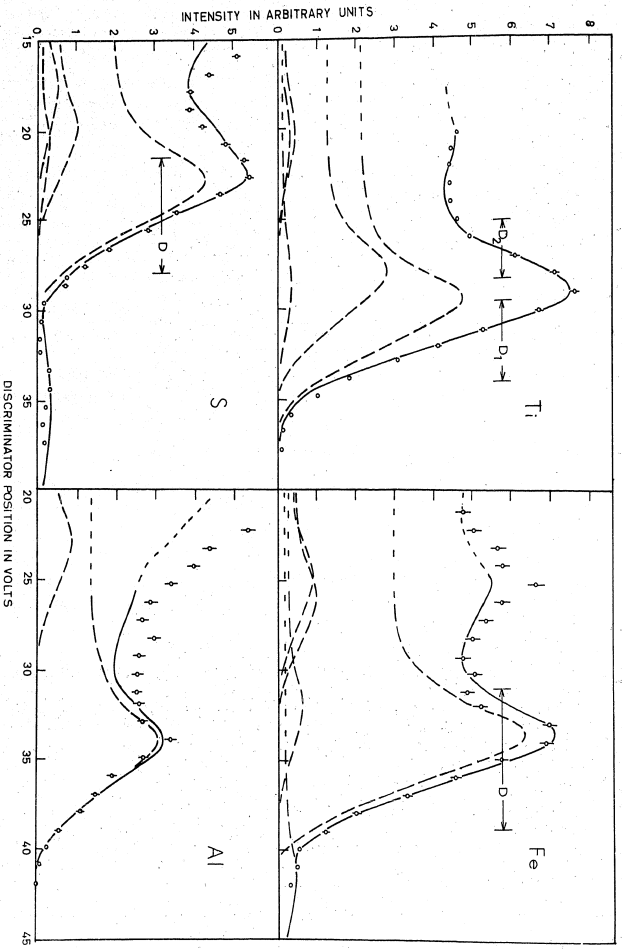

Figure 15. Experimental γ-ray spectra. Discriminator positions used in the polarization measurements are shown.

6. Treatment of experimental data.

During the polarization measurements, several γ-rays are simultaneously detected. Instead of $R\,P_n\,P_a$ of equation (5.6), one then measures the average quantity:

$$\overline{R\,P_n\,P_a} = P_n \sum_i \alpha_i R_i P_{ai} \tag{6.1}$$

where α_i is the relative contribution of the i-th γ-ray, and $\sum_i \alpha_i = 1$. As P_a is slowly varying with energy, a good approximation is

$$\overline{R} \cong \sum \alpha_i R_i \qquad \text{for } P_a \cong \text{constant} \tag{6.2}$$

Generally, R_i is unknown for all the γ-rays in the spectrum. If the radiation X is predominant, i.e. if α_X is large, an approximate determination of R_X is obtained from a measurement of

$$\frac{1}{2\,P_n\overline{P_a}}\,\frac{N'_a - N''_a}{N'_a + N''_a} = \overline{R} \cong \alpha_X R_X + \sum_{i \neq X} \alpha_i R_i \tag{6.3}$$

where the sum is taken over all γ-rays except X, and the values of R_i may be anything between +1 and - 1/2. Using constructed spectra like the ones in figure 15, the best discrimination of pulses could be chosen, and the intensities α_i for the different γ-rays entering the single channel discriminator were easily evaluated.

For the experiment it must be appreciated that N_a of equation (5.6) is the counting rate of γ-rays that are not scattered, produced by capture in the target of the incoming neutron beam plus the non-depolarized part of the scattered neutrons. The asymmetry actually observed is

$$Q = \frac{1}{2}\,\frac{N'_t - N''_t}{N'_t + N''_t} \tag{6.4}$$

where N_t is the total counting rate which consists of direct and scattered γ-rays from the target and γ-rays due to capture of neutrons scattered from the target as well as background. The difference in the numerator is due to polarization only, thus $N'_t - N''_t = N'_a - N''_a$. Equation (6.3) and (6.4) together with the abbreviation $N = (N' + N'')/2$ give

$$\overline{R} = \frac{1}{P_n\,\overline{P_a}} \cdot \frac{N_t}{N_a}\,Q \tag{6.5}$$

If we define N_b = counting rate of γ-rays that are not scattered, produced by neutrons captured in the target after depolarizing scattering, $N_a + N_b$ represents the direct γ-rays originating in the target.

The correction factor $\beta = N_a/(N_a + N_b)$, due to depolarization of neutrons scattered in the target, can be calculated. For the repeated scattering of an already scattered neutron we obtain the probability $(\sigma_s/\sigma_t)(1-e^{-\sigma_t \eta \overline{r}})$, where σ_s and σ_t are scattering and total cross sections respectively, η is the atomic density of the target, and $\overline{r}$ is the average distance that the neutron must travel to escape from the target. Considering multiple scattering and depolarization, we get the correction factor

$$\beta = 1 - 2\,\chi\,\frac{\sigma_s}{\sigma_t}\,(1 - e^{-\sigma_t \eta \overline{r}}) \tag{6.6}$$

The spin flip probability χ is given by Meyerhof and Nicodemus (1950):

$$\chi = \frac{2}{3}\,\frac{\sigma'_{inc}}{\sigma_s} \tag{6.7}$$

Here σ'_{inc} is the incoherent scattering cross section due to spin effects only. A scattering nucleus with angular momentum zero has $\chi = 0$. For the targets employed, β was very near, or equal to 1.

The relative contribution of the γ-rays originating in the target, and detected without being scattered, is given by $\delta = (N_a + N_b)/N_t$. This quantity can be found indirectly by an experiment in which the analyzing magnets and some of the shielding around the detecting crystals is removed. Measurements were performed with the ordinary targets, and for correction purposes with a graphite target, which does not produce γ-rays. In comparing observations with and without thin boron shields in front of the counter, it was possible to determine the contribution to the counting rate from neutrons scattered from the targets, followed by capture in the crystals. By insertion of a cadmium foil in the neutron beam, it was found that the epithermal neutrons did not contribute to the counting rate by a measurable amount.

The resulting γ-ray intensity was multiplied by the calculated transmission through the analyzer, yielding $N_a + N_b$. From measurements with the analyzing magnets in the ordinary positions N_t was determined. In this way the factor δ was found for all the targets and for all the discriminator positions used to select γ-rays. It had magnitudes from 9.5% for calcium up to 91% for chromium. The complete correction factor needed for the determination of $\overline{R}$ from Q as given by equation (5.6) is

$$P_n \overline{P}_a N_a/N_t = P_n \overline{P}_a \beta\delta \tag{6.8}$$

In the determination of the numerical values of the quantities given in (6.8), the relative errors were estimated to be smaller than 8% for P_n, 2% for $\overline{P}_a$, 3% for β, and 5% for δ. When the relative error of x is denoted by $\Delta(x)/x$, and considered as a standard deviation, the root mean square error of (6.8) becomes

$$\frac{\Delta(P_n \overline{P}_a \beta \delta)}{(P_n \overline{P}_a \beta \delta)} = \sqrt{\left[\frac{\Delta(P_n)}{P_n}\right]^2 + \left[\frac{\Delta(\overline{P}_a)}{\overline{P}_a}\right]^2 + \left[\frac{\Delta(\beta)}{\beta}\right]^2 + \left[\frac{\Delta(\delta)}{\delta}\right]^2} \cong 10\ \% \tag{6.9}$$

The measured quantity Q has the standard deviation

$$\Delta(Q) = \sqrt{\left[\Delta_1(Q)\right]^2 + \left[\Delta_2(Q)\right]^2} \tag{6.10}$$

where $\Delta_1(Q)$ is the statistical error of counting, and $\Delta_2(Q)$ is due to the reduced accuracy which results when the counts taken during each period are registered as an integral multiple of the scaling factor. When the register counts the number n, the correct value may be anywhere between n-1 and n+1. In a certain counting period, let u_1 be the number of pulses incident upon the scaler before the first register count, and u_2 the number of pulses after the last count. Then $(v = u_1 + u_2 + 1 - u_{sc})$ is the single error for this measurement. For a great number of measurements K, u_1 and u_2 are supposed to be uniformly distributed between zero and the scaling factor u_{sc}. The root mean square error for the arithmetic mean is then

$$\Delta(v) = \sqrt{\frac{\sum v^2}{K(K-1)}} = \sqrt{\frac{\sum_{u_1=0}^{u_{sc}-1} \sum_{u_2=0}^{u_{sc}-1} (u_1+u_2+1-u_{sc})^2}{u_{sc}^2 (K-1)}} \cong \frac{u_{sc}}{\sqrt{6(K-1)}} \tag{6.11}$$

The corresponding errors in the total number of counts N'_t is $K\Delta(v)$, when K is the number of periods for one register. As the deviations in N'_t and N''_t are equal and opposite, the error in the measured quantity $N'_t - N''_t$ is equal to $2K\Delta(v)$. The number of register pulses per period is about 200 in channel No. 1, where the measurement of $N'_t - N''_t$ is performed. This gives $N_t \cong 200\ K\ u_{sc}$. In setting $K-1 \cong K$, we get

$$\Delta_2(Q) = \frac{\Delta_2(N'_t - N''_t)}{4N_t} = \frac{K\Delta(v)}{2N_t} \cong \frac{1}{40}\sqrt{\frac{u_{sc}}{3N_t}} \tag{6.12}$$

The standard deviation due to counting is $\Delta_1(Q) = 1/\sqrt{4N_t}$, and the total error becomes

$$\Delta(Q) = \frac{1}{2}\sqrt{\frac{1}{N_t}\left(1 + \frac{u_{sc}}{1200}\right)} \tag{6.13}$$

Even at the highest scaling factor applied, $u_{sc} = 32$, the error due to scaling is negligible compared with $\Delta_1(Q)$.

Each complete determination of Q consisted of between 15 and 40 separate series of measurements. When Q is determined from each of these, the root mean square error is

$$\Delta(Q) = \sqrt{\frac{\sum_i N_{ti}(Q_i - \overline{Q})^2}{(K_s - 1)\sum_i N_{ti}}} \tag{6.14}$$

where K_s is the number of measuring series. Generally, this error was of the same magnitude as $1/\sqrt{4N_t}$, indicating that no fluctuations other than the statistical counting rate variation were of any importance. For the quotation of the results in the next section, the largest of the two errors has been chosen.

The experimental value of $\overline{R}$ has the relative standard deviation

$$\frac{\Delta(\overline{R})}{\overline{R}} = \sqrt{\left[\frac{\Delta(Q)}{Q}\right]^2 + \left[\frac{\Delta(P_n \overline{P}_a \beta\delta)}{P_n \overline{P}_a \beta\delta}\right]^2} \tag{6.15}$$

In all the cases studied, the counting statistics were the largest contributor to the error in $\overline{R}$.

7. Measurements.

Measurements were taken with the JEEP running at a power level between 200 and 450 kW. A few times 10^7 neutrons per second were emitted from the collimator. The γ-ray counting rates were from 300 to 3000 pulses per minute. In order to obtain standard deviations of Q as low as 10^{-4}, continuous counting must be carried on for weeks or months on each target.

In table 5 the results from measurements on 12 different γ-rays are quoted. First the emitting nuclei are listed, and the second and third columns give the γ-ray terms and energies taken from the papers of Kinsey, Bartholomew and Walker (1952), and Kinsey and Bartholomew (1953 abe). Then the experimental values obtained for Q are quoted, together with the standard deviation. In the fifth column is listed the correction factor $P_n \overline{P}_a \beta\delta$, which shows large fluctuations, mainly due to the correction factor δ, being quite small for the measurement of radiation with low intensity. The corresponding value of $\overline{R} = Q/(P_n \overline{P}_a \beta\delta)$, is given in column 6, also with standard deviation. From constructed γ-ray spectra the relative contributions to $\overline{R}$ were found from the various energies of the spectrum, as shown by equation (6.3). They are listed in the 7th column together with the maximum uncertainties which are due to the γ-rays not studied. Finally, the last column gives the derived value of R for the γ-ray under investigation.

The table first gives the result of a "symmetry control" experiment, which has already been mentioned in section 5.

For the 6.18 MeV neutron capture γ-ray from wolfram, all the related spin properties are known. Kinsey and Bartholomew (1953 e) showed that it is due to the ground state transition in W^{183}, as illustrated in the decay scheme of figure 36. W^{182} is an even-even nucleus, so that the compound state has spin 1/2 and even parity. Walchli (1953) gives the ground state spin $J_f = 1/2$ for W^{183} and its nucleon configuration was put up by Mayer and Jensen (1955), who place the extra nucleon in a $p_{\frac{1}{2}}$-state, having odd parity. Then the radiation is of electric dipole type, and according to table 2, $R_D = 1$. The theoretical value for the measurement is $\overline{R}_{th} = 0.80 \pm \begin{bmatrix}+0.20\\-0.10\end{bmatrix}$ as compared to the obtained $\overline{R}_{exp} = 0.60 \pm 0.16$. This result verifies the theoretical prediction for the direction and magnitude of the circular polarization. However, the uncertainty in the numerical agreement with theory is still quite large.

For the determination of spin values by means of measuring the circular polarization of γ-rays, we shall assume that the theory gives a quantitatively correct value for R. The most suitable

TABLE 5.

Results of the polarization experiment.

Emitting Nucleus	γ-ray term X	γ-ray energy in MeV	Experimental asymmetry Q Units of 10^{-5}	Correction factor $P_n F_a \beta\delta$ Units of 10^{-3}	Experimental value of $\sum \alpha_i R_i = \overline{R}_{exp}$ Units of 10^{-2}	Theoretical value of $\sum \alpha_i R_i = \overline{R}_{th}$ Units of 10^{-2}	Derived value of R_X
Ti	Symmetry Control Experiment		6 ± 13				
S^{33}	G	5.44	-31 ± 17	0.71	-44 ± 24	$82R_G + \begin{bmatrix}+18\\+9\end{bmatrix}$	$-\frac{1}{2}$
Ca^{41}	C	6.42	-14 ± 11	0.35	-40 ± 30	$91R_C + \begin{bmatrix}+9\\-4.5\end{bmatrix}$	$-\frac{1}{2}$
Ti^{49}	F	6.75	-12 ± 7.5	1.93	- 6 ± 4	$69R_F + 22R_G + \begin{bmatrix}+9\\-4.5\end{bmatrix}$	$-\frac{1}{2}$
Ti^{49}	G	6.41	59 ± 16	1.96	30 ± 9	$50R_F + 40R_G + \begin{bmatrix}+10\\-5\end{bmatrix}$	+ 1
Cr^{54}	A	9.72	-39 ± 20	2.55	-15 ± 8	$68R_A + 31R_B + \begin{bmatrix}+1\\-0.5\end{bmatrix}$	$\simeq -\frac{1}{2}$
Cr^{54}	B	8.88	34 ± 13	2.15	16 ± 6	$13R_A + 66R_B + \begin{bmatrix}+21\\-10.5\end{bmatrix}$	$+\frac{1}{4}$
Fe^{57}	E	7.64	42 ± 6.5	0.54	78 ± 14	$87R_E + \begin{bmatrix}+13\\-6.5\end{bmatrix}$	+ 1
Ni^{59}	A	9.00	-45 ± 39	1.80	-25 ± 22	$82R_A + \begin{bmatrix}+18\\-9\end{bmatrix}$	$-\frac{1}{2}$
Cu^{64}	A	7.91	41 ± 12	1.62	26 ± 8	$78R_A + 18R_B + \begin{bmatrix}+4\\-2\end{bmatrix}$	$\simeq +0.45$
Cu^{64}	B	7.63	- 3 ± 15	1.66	-2 ± 9	$51R_A + 30R_B + \begin{bmatrix}+19\\-9.5\end{bmatrix}$	$-\frac{1}{2}$
Zn^{65}	E	7.88	-10.5 ± 9	0.50	-21 ± 18	$77R_E + \begin{bmatrix}+23\\-11.5\end{bmatrix}$	$-\frac{1}{2}$
W^{183}	D	6.18	45.5 ± 11	0.76	60 ± 16	$80R_D + \begin{bmatrix}+20\\-10\end{bmatrix}$	+ 1

target materials for these experiments have relatively large capture cross sections, combined with the emission of γ-rays that are strong compared to the rest of the spectrum. Most of the elements fulfilling these requirements are found in the region of atomic number 11 to 30. For each γ-ray studied, the derivation of R_X as given in table 5, and the spin properties obtained from this value, will be discussed in chapter V.

CHAPTER IV

COINCIDENCES AND ANGULAR CORRELATION OF GAMMA RAY CASCADES

When the coincidence method is applied to the study of the lowest excited levels in nuclei resulting from capture of neutrons, it is necessary to observe the simultaneous emission of high energy γ-rays of about 7 MeV and of lower energy γ-rays of 1 MeV or less. This combination implies certain complications for the measurement of angular correlation between the γ-rays. An attempt to carry out these experiments is described in the following.

1. Theory.

The theory of angular correlations has been extensively treated by Biedenharn and Rose (1953) and Frauenfelder (1955), and here we shall only review the main results of practical interest for the experimentalist. A γ-ray cascade where two photons, γ_1 and γ_2, are successively emitted from the same nucleus, is schematically shown in figure 16.

The multipole orders are L_1 and L_2. Along a given axis of quantization, the successive nuclear spins J_a, J_b and J_c will have the components m_a, m_b and m_c respectively. Such a double cascade shall be denoted by the γ-ray terms as γ_1, γ_2 or by the spin values as $J_a\,(L_1)J_b(L_2)J_c$. Each component of the disintegration, $m_a \rightarrow m_b \rightarrow m_c$, possesses a certain angular correlation, and the γ-rays from the various components may interfere. The probability that γ_2 is emitted into the solid angle $d\Omega$ at an angle β with respect to γ_1 is, similarly to the equation (2.2) of the preceding chapter, given by

$$W(\beta)\,d\Omega = \sum_{m_a m_c}{}' \left| \sum_{m_b} \left\langle a \left| H_1 \right| b \right\rangle \left\langle b \left| H_2 \right| c \right\rangle^* \right|^2 d\Omega \qquad (1.1)$$

where Σ' means summation over all unmeasured radiation properties, such as polarization. In the matrix elements, H_i is the interaction Hamiltonian for the emission of the γ-ray γ_i, and a, b, c stands for the properties of the states A, B, C of figure 16 respectively. It is seen that an experimental study of $W(\beta)$ can establish a connection between these properties.

In evaluating equation (1.1), one arrives at the result

$$W(\beta) = 1 + \sum_{\nu} a_\nu P_\nu (\cos\beta) \qquad (1.2)$$

Here the functions $P_\nu(\cos\beta)$ are the Legendre polynomials of order ν, and ν takes all even values from 2 upwards. The highest term for which a_ν is different from zero is given by the selection rule

$$\nu_{max} = \mathrm{Min}(2J_b, 2L_1, 2L_2) \qquad (1.3)$$

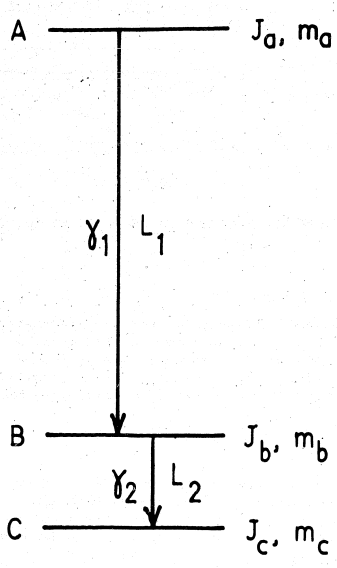

Figure 16.
Energy level scheme for a double γ-ray cascade.

For pure multipole transitions the coefficients a_ν can be separated into two factors, each of them depending upon one single transition only:

$$a_\nu = F_\nu (L_1 J_a J_b) \cdot F_\nu (L_2 J_c J_b) \tag{1.4}$$

where F_ν is expressed by the product of a Clebsch-Gordan and a Racah coefficient:

$$F_\nu (L J_a J_b) = (-1)^{J_a - J_b - 1} (2J_b+1)^{\frac{1}{2}} (2L+1) \left(LL1(-1)\middle| LL\nu 0\right) W(J_b J_b LL; \nu J_a) \tag{1.5}$$

Tables of the functions $F_\nu (L' J_a J_b)$ have been evaluated by Biedenharn and Rose (1953), so that any angular correlation function can immediately be written down.

As in the case of circularly polarized γ-radiation, competing radiations of different multipole orders can interfere and produce a correlation distribution which is very different from either of the distributions resulting from pure multipole transitions. When one of the transitions is mixed, consisting of radiations with wave amplitudes b_1 and b_2 as defined in section 2 of chapter III, the angular correlation function can be expressed as

$$W(\beta) = \frac{b_1^2 W_1 + b_2^2 W_2 + 2 b_2 b_2 W_{12}}{b_1^2 + b_2^2} \tag{1.6}$$

where W_1 and W_2 are the correlation functions for the pure cascades, as described above. For the case that the transition between the levels A and B is a mixture of the multipole orders L_1 and L_1', the contribution due to interference is:

$$W_{12} = \sum_\nu (-1)^{J_b - J_a - 1} \left[(2J_b+1)(2L_1'+1)(2L_1+1)\right]^{\frac{1}{2}} G_\nu (L_1 L_1' J_a J_b) F_\nu (L_2 J_c J_b) P_\nu (\cos\beta) \tag{1.7}$$

The sum is taken over all positive even numbers, and ν satisfies the rule (1.3). Also the functions G_ν have been tabulated by Biedenharn and Rose (1953). W_{12} has the same order of magnitude as the quantities W_1 and W_2. It is seen that an intensity ratio as small as $(b_1/b_2)^2 = 0.01$, corresponding to the coefficient $2b_1b_2/(b_1^2 + b_2^2) = \pm 0.2$ for W_{12}, can produce a correlation function which is quite different from the case of $b_1 = 0$.

In the case of a γ-ray cascade where one of the transitions is a pure dipole, formula (1.3) shows that only the coefficient a_2 of the expansion (1.2) is different from zero. We then have

$$W(\beta)_{L_1 = 1} = 1 + a_2 P_2(\cos\beta) = 1 - \frac{a_2}{2} + \frac{3}{2} a_2 \cos^2\beta \tag{1.7}$$

The only unknown, a_2, can be determined from a measurement of the anisotropy of the coincidences:

$$A \equiv \frac{W(\pi) - W(\pi/2)}{W(\pi/2)} = \frac{3a_2}{2-a_2} \tag{1.8}$$

In a decay scheme like the one of figure 16, the level B may also be obtained by transitions other than γ_1, or the state B may decay in different ways. The disintegration rate of the cascade shall be called N_o. Then $N_o/\varkappa_i$ is the total disintegration rate of γ_i, where $\varkappa_i$ is the contribution of the cascade to this transition. Using the symbols ω_i and ε_i for the solid angle and efficiency, respectively, of the detector measuring the radiation γ_i, we get for the net counting rates of the two detectors:

$$\left.\begin{aligned} N_1 &= N_o \omega_1 \varepsilon_1 / \varkappa_1 \\ N_2 &= N_o \omega_2 \varepsilon_2 / \varkappa_2 \end{aligned}\right\} \tag{1.9}$$

When angular correlation is neglected, the coincidence rate becomes

$$C = N_o \omega_1 \varepsilon_1 \omega_2 \varepsilon_2 \tag{1.10}$$

Random coincidences occur as a result of the accidental overlap of two pulses in the coincidence circuit. The resolving time t_r is equal to the maximum time separation for which two pulses are registered as coincident. For two square pulses of equal duration this is equal to the pulse length. If the counting rate is one pulse per channel per second, the chance of getting a false coincidence is equal to 2 t_r per second. With total counting rates N_1' and N_2', the chance coincidence rate is

$$C_{ch} = 2 N_1 N_2 t_r \tag{1.11}$$

The ratio of true to chance coincidences is

$$\frac{C}{C_{ch}} = \frac{\varkappa_1 \varkappa_2}{2 t_r N_o} \tag{1.12}$$

which shows that the statistical accuracy of a coincidence experiment is not indefinitely improved by increasing the source strength, unless the electronic circuit or the detectors are also improved.

2. Experimental set-up.

For the present experiment a narrow but intense beam of neutrons falling upon a small target of the material to be studied is needed. A small target is advantageous because scattering of the γ-rays can produce false contributions to the angular correlation. The higher the intensity of the beam, the smaller the target can be made.

The neutron source is a graphite scatterer in one of the isotope channels of JEEP. For intensity reasons the target should be placed as near to this source as possible. However, in the vicinity of the reactor wall the neutron and γ-ray background is very high, and the ratio of total to background counts is considerably improved by moving the apparatus farther away from the channel opening. The counting apparatus is actually placed 3 metres from the reactor wall, and about 7 metres from the graphite scatterer. The main outline of the set-up is shown in figures 17 and 18. At the position of the (n,γ)-target the neutron beam is cylindrical, with a diameter of 7 mm. This is also the inner diameter of the aluminium tube containing the target material. The target length, varying between 9 and 35 mm, is dependent upon the neutron absorption cross section.

The two scintillation counters viewing the target consist of 38 mm diameter by 25 mm high NaI(Tl)-crystals mounted on RCA 6655 photomultipliers without light pipers. Crystal No. 2,

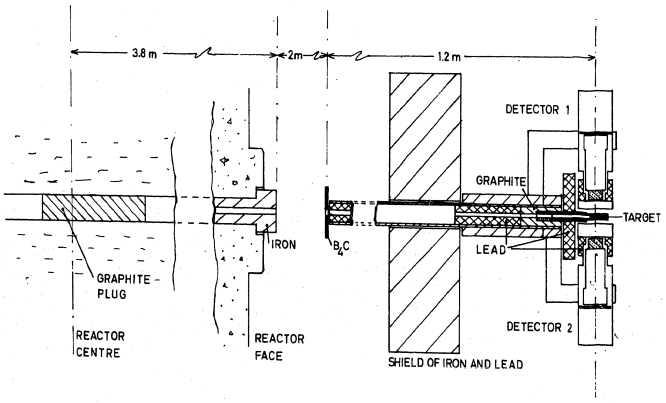

Figure 17.
Main outline of the coincidence and angular correlation experimental set-up.

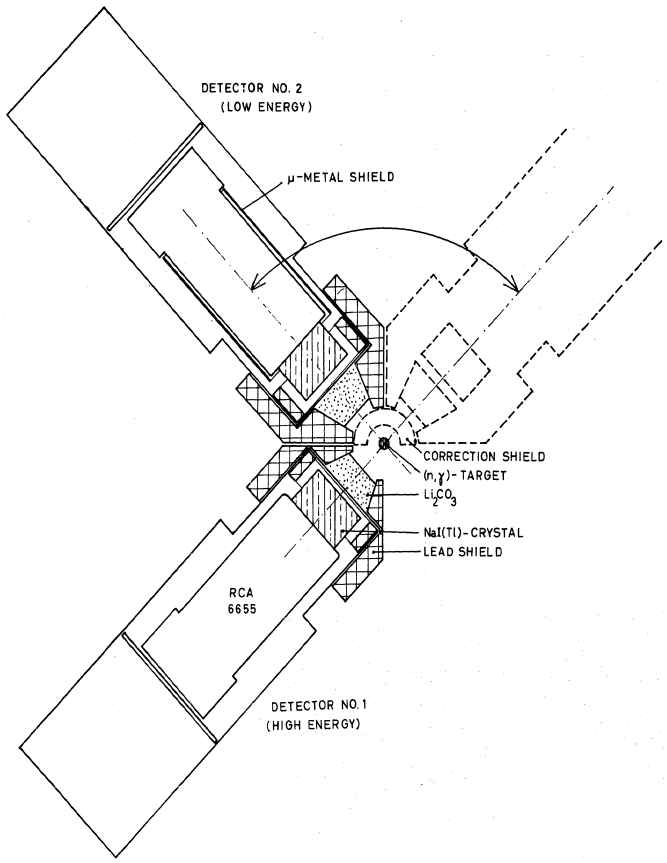

Figure 18.
Target and detectors seen in a plane perpendicular to the neutron beam.

which is used for measuring the lower energy γ-rays, is placed a little farther from the target than No. 1. During angular correlation measurements, detector No. 1. was stationary, and detector No. 2 could be moved in a circle with the target as centre. As the measurements consist in observing the asymmetry, only the positions $\beta = \pi/2$ and $\beta = \pi$ were used. These positions were chosen so that the change of distance between target and crystal, due to the weight of the detector, should be a minimum. Both boxes containing the detectors are made from soft iron tubes, and in addition the movable detector No. 2 has a μ-metal shield around the upper part of the photomultiplier. Thus the influence of the earth's magnetic field will not produce changes in the counting rate as the detector is moved.

The detectors are surrounded by lead shielding, as shown in figure 18. Especially γ-rays emitted from one crystal into the other should be avoided. When a high energy γ-ray is producing an electron pair in one crystal, and the corresponding annihilation quant gives a pulse in the other, a false coincidence can be recorded. Correction measurements are performed by placing a shield in front of the low energy counter in such a way that only the direct low energy γ-rays are attenuated. Photons passing from one crystal to the other in the $\pi/2$-position are unaffected by this shield, which is drawn with a broken line in figure 18. In order to reduce the intensity of scattered neutrons reaching the crystals, shields of Li_2CO_3 are placed between target and counter. Boron, which has a higher absorption cross section, could not be used for this purpose, since it emits γ-rays of 0.478 MeV following neutron capture, as reported by Ajzenberg and Lauritsen (1955).

As a consequence of the large solid angles which are necessary, the absence of a γ-ray collimator, and scattering in the shielding surrounding the crystals, the resolving power of the detectors is only about 15% at 1 MeV.

A coincidence circuit was built to receive pulses from NaI(T1)-crystals. The resolving time ought to be at the most 50 millimicroseconds mμ sec to give an acceptable ratio between true and chance coincidences. On the other hand, resolving times of the order of 10 mμ sec would hardly be obtainable, as NaI(T1)-crystals give pulses with a rise time of about 250 mμ sec and distributed amplifiers were not at our disposal.

A block diagram of the electronic circuit employed is shown in figure 19.
From the photomultiplier, the pulse is fed via a cathode follower to the linear amplifier of the type A.E.R.E. 1049B. Both differentation and integration time selectors were set to 320 mμ sec. From the amplifier, identical pulses are fed to the single channel discriminator and to the input of the fast coincidence circuit. Some details of the latter instrument are shown in figure 19, and figure 20 illustrates the form of the pulses that are counted, for various points of the circuit. Very large amounts of scattered low-energy γ-rays occur in the present experiment. Pulses with approximately half the height of the ones that should be studied are removed by discrimination before entering the fast coincidence circuit. The rest is amplified to about 50 volts and fed to a clipper circuit which gives an output corresponding to the rise of a few volts only of the input pulse. This rise takes place within 10 to 20 mμ sec and as the clipper tube E180F is a very fast broadband amplifier pentode, the output pulses should rise to maximum height within the same time. A pulse forming delay line of a length corresponding to 20 mμ sec, is coupled to the output and shortcircuited at the end. In the ideal case it produces a square pulse of 40 mμ sec duration, but the actual pulse has trapezoidal form. Coincidences between the pulses from two identical clippers are recorded by a 6BN6-circuit, as described by Fischer and Marshall (1952). As seen from figure 20, the time elapsing between the start of the original pulse and the start of the clipper pulse, is strongly dependent upon pulse height and discriminator position. Therefore, only pulses of approximately uniform height can be studied by this coincidence circuit. In fact, a height variation of $\pm$ 20 % can be allowed.

The real selection of pulses is performed by a single channel discriminator which has a fixed lower discrimination of 20 volts, This height corresponds to the ideal input pulse for the fast coincidence circuit. The width of the single channel can be up to 4 volts. It has been experimentally verified that no coincidences are lost at this width. A slow triple coincidence circuit gives an output pulse when the two discriminators admit pulses at the same time as a fast coincidence occurs. To the first approximation the number of random coincidences can be calculated from equation (1.11) when the resolving time t_r is given by the fast coincidence circuit, and N_1 and N_2 are counting rates obtained from the two single channel discriminators. At very high

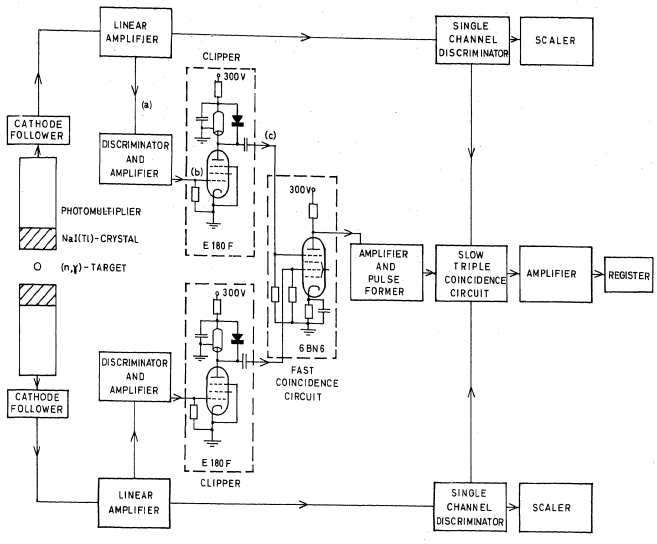

Figure 19.
Block diagram of the electronic circuit for the coincidence measurements.

counting rates, when N_1 or N_2 is comparable to $1/t_s$, where t_s is the resolving time of the triple coincidence circuit, the formula for N_{ch} fails. In the present case, t_s is of the order of 5 μ sec.

The resolving time of the fast coincidence circuit is determined by the voltage at which the 6BN6-tube is triggered, and by the form of the input pulses. When they are triangular, very short resolving times can be obtained if only the upper part triggers the circuit. The available cathode ray oscilloscopes were not fast enough to show the actual form of the pulses incident upon the coincidence tube. The resolving time can be measured by other methods, however. By placing different delay lines in the two channels, and measuring the coincidence rate as a

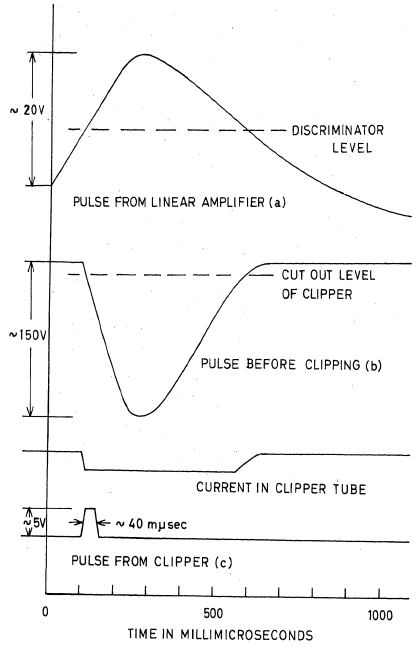

Figure 20.
Pulse forms at certain points in the electronic circuit of figure 19.

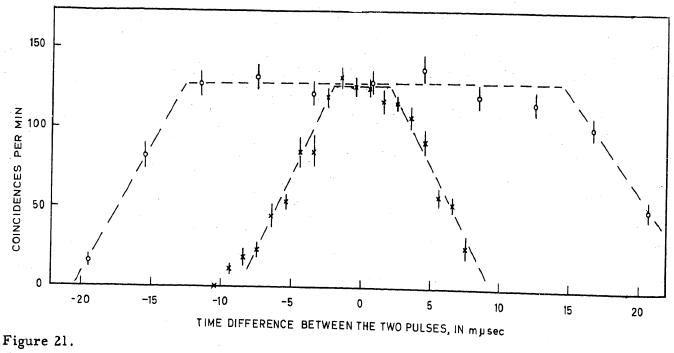

Figure 21.
Coincidences obtained with different delay of the pulses in the two channels.

function of the delay difference, curves like the ones in figure 21 are obtained. When all the pulses fed to the coincidence tube are equal, the measured curve should have a flat top with vertical edges. Due to the fact that a spectrum of pulses is incident upon each channel, also the shortened pulses have somewhat different heights, and the edges of the experimental curves are sloping. Pulse forming delay lines of 10 and 20 mμ sec were used, giving the two curves of figure 21. The narrowest curve indicates that the shorter pulses have triangular form, or a very short flat top. The fact that the two curves have the same coincidence rate at maximum, indicates that all the true coincidences are counted.

When different sources are used for the two counters, only random coincidences occur, and by means of formula (1.11) the resolving time is determined:

$$t_r = \frac{C_{ch}}{2 N_1 N_2} \qquad (2.1)$$

In this way the resolving times t_r = 8 mμsec and t_r = 35 mμsec respectively were measured, in rough agreement with the curves of figure 21.

The broader pulses, giving the 35 mμsec resolving time, were used in the actual experiment. Although the random coincidences are more numerous in this case, the smaller probability of losing any true coincidences justifies this choice.

As all the pulses fed to the fast coincidence circuit should be equal, or only varying very little from a standard size, the selection of various γ-ray energies is performed by keeping the single channel discriminator in a fixed position while the photomultiplier voltage is altered by means of a fine potentiometer. A calibration curve for the relative pulse height as a function of the voltage is shown in figure 22. It is seen that the logarithm of the pulse height is very nearly a linear function of the high tension.

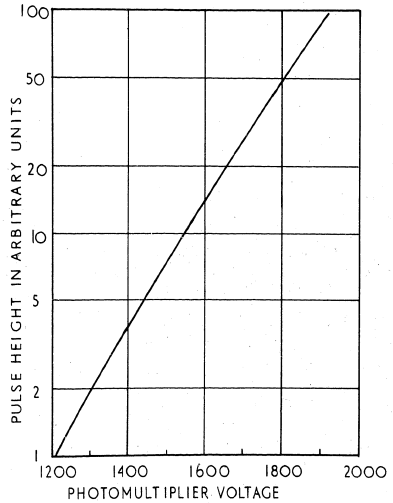

Figure 22.
Photomultiplier pulse height as a function of the voltage applied to the tube.

3. Treatment of experimental data.

The data obtained are first corrected for accidental coincidences C_{ch}, which are readily calculated from formula (1.11). The influence of cosmic rays was measured and found to be negligible compared to the effect to the targets. Scattered neutrons can be captured in the NaI(Tl)-crystals, and resulting γ-ray cascades can give rise to unwanted coincidences. In order to measure this effect, the actual target was replaced by a paraffine scatterer, giving no capture radiation. Coincidences due to scattering from the targets were estimated and subtracted. This contribution was of the order of one percent of the total coincidence rate when the lithium shields were applied in front of the crystals.

For the comparison of different coincidence rates it is advantageous to use the value

$$C'' = \frac{C}{N'_1 \; N'_2} \tag{3.1}$$

instead of the measured coincidence rate C. Here N'_1 and N'_2 are single counting rates, obtained when background and perturbing activities have been subtracted. To the first approximation this procedure corrects for small variations in the sensitivities of the counters and in the distance between the counters and the target.

False coincidences can be due to a high energy γ-ray which produces a Compton recoil pulse in one counter, and after scattering enters the other crystal, producing the second pulse. Formula (4.2) of chapter III shows that the energy of a γ-ray Compton scattered at 90° or more is always less than $m_e c^2 = 0.51$ MeV. In figure 18 it is clearly seen that all false coincidences of this type must be due to scattering angles equal to or larger than 90°, corresponding to energies smaller than 0.51 MeV measured by the second detector.

As has already been mentioned, false coincidences can also be due to high energy γ-rays producing electron pairs in one counter, where the annihilation of the positrons gives rise to quanta detected in the other counter. The energy of these quanta is $m_e c^2 = 0.51$ MeV.

In the present experiment, detector No. 1 is set to count high energy γ-rays of several MeV. The low energy γ-rays, causing false coincidences can, therefore, only be detected in counter No. 2. The two aforementioned causes of false coincidences can be corrected for by means of the lead shield mentioned in section 2. When accidental and background coincidences are subtracted, let $C'(x, \beta)$ be the measured coincidence rate, where the correction shield is placed between the target and counter x. When x = 0, no extra shielding is applied. Counter angle is denoted by β, as before. The measured coincidence rate can be separated into the true and false parts:

$$C'(0, \tfrac{\pi}{2}) = C_2(\tfrac{\pi}{2}) + C_{12}(\tfrac{\pi}{2}) \tag{3.2}$$

Here, $C_c(\beta)$ is due to the cascade only, and $C_{12}(\beta)$ results from γ-rays originating in counter 1, and being detected in counter 2. Using the shield, one can also measure the quantities

$$C'(2, \tfrac{\pi}{2}) = T_2 \, C_c(\tfrac{\pi}{2}) + C_{12}(\tfrac{\pi}{2}) \tag{3.3}$$

$$C'(2, \pi) = T_2 \, C_c(\pi) + T_{12} \, C_{12}(\pi) \tag{3.4}$$

$$C'(1, \pi) = T_1 \, C_c(\pi) + T_1 \, T_{12} \, C_{12}(\pi) \tag{3.5}$$

where T_1 and T_2 are the transmissions through the lead shield of the high and low energy cascade γ-rays respectively, and T_{12} is the transmission of the γ-rays passing from one counter to the other in the position $\beta = \pi$. The quantity T_1 can be determined from the single counting rates of the high energy γ-rays passing through the shield. T_2 and T_{12} are not easily measured, since scattering of the higher energy γ-rays will strongly influence the observation. When T_1 is known, we get from equations (3.1) to (3.4) the desired ratio

$$\frac{W'(\pi)}{W'(\frac{\pi}{2})} = \frac{C_c(\pi)}{C_c(\frac{\pi}{2})} = \frac{(1/T_1)\,C'(1,\pi) - C'(2,\pi)}{C'(0,\frac{\pi}{2}) - C'(2,\frac{\pi}{2})} \tag{3.6}$$

W' is the measured correlation function. In the derivation of equation (3.5) we have neglected the fact that T_1 for the γ-rays of the cascade can be slightly different from the average value for the γ-rays producing annihilation quanta that are counted as coincidences. However, the γ-ray cross section for lead varies very slowly with energy in the region between 4 and 10 MeV, so this error can be considered as unimportant.

The symmetry axes of the two counters form a definite angle β. Since both the target and the detectors have finite dimensions, γ-ray pairs with relative angles somewhat different from β can be detected as coincidences. Feingold and Frankel (1955) have developed the theory of geometrical corrections in angular correlation experiments. They give methods for calculating the coefficients h_ν of the experimental distribution

$$W'(\beta) = 1 + \sum_{\nu>0} h_\nu \, P_\nu(\cos\beta) \tag{3.7}$$

when the coefficients a_ν of the theoretical distribution (1.2) are given. In the application of these corrections to the present experiment, the detectors are considered as circular discs with their axes going through the centre of the source. The source is considered part of a straight line perpendicular to the axes of both counters, and it extends equally on either side of the centre. When only the coefficient a_2 is different from zero, the experimental angular correlation function for a target of 30 mm length is

$$W'(\beta) = 1 + 0.814 \, a_2 \, P_2(\cos\beta) + 0.042 \, a_2 \, P_4(\cos\beta) + \cdots\cdots \tag{3.8}$$

A good approximation is obtained when this expansion is cut off after the third term. The ideal anisotropy A as defined by (1.8) can be expressed in terms of the experimental anisotropy A':

$$A = \frac{1.201 \, A'}{1 - 0.087 \, A'} \tag{3.9}$$

(Target length = 30 mm)

The complete error in the anisotropy, due to the approximate validity of the corrections, is estimated to be smaller than 2 %. This is of very little importance when compared to the experimental errors due to the statistics of counting.

By scattering in the target and in the surrounding material, the γ-rays can change direction, and produce coincidences with a false angular correlation. When discrimination between different γ-ray energies is performed, this error is not serious, since scattering by more than a few degrees will reduce the energy of the γ-ray so much that it will not be counted by the detector. The effect of this scattering is that the angular correlation is "smeared out", and the numerical value of the anisotropy is reduced.

Absorption or reduction of the γ-ray energy by interactions in the target itself is on the average more important for the γ-ray pairs which give coincidences in the 180° position, than for those which give coincidences in the 90° position. Thus more coincidences are lost at $\beta = 180^\circ$ than at $\beta = 90^\circ$. The measured anisotropy will be somewhat more negative than the true one. For the present experiment it was estimated that the largest contribution due to this effect would not amount to more than half a percent in the anisotropy.

4. Measurements.

For the study of decay schemes, one of the counting circuits is adjusted to count pulses from a certain γ-ray. In the other circuit, the coincidence spectrum is scanned by measurements during a stepwise alteration of the photomultiplier voltage. The structure of this spectrum reveals which γ-rays are coincident with the γ-ray chosen by the first counter. Observation of the coincidence spectrum can be used to choose the best position of the discriminators (i.e. the best photomultiplier voltage) for special experiments like the angular correlation measurement. The single counting rate spectrum which is obtained at the same time shows the positions and relative intensities of the most intense γ-rays emitted by the target.

TABLE 6.

Results of the coincidence and angular correlation experiments.

Decaying Nucleus	Cascade	γ-ray energies in MeV Higher	Lower	Approximate value of A_1 (± 0.1)	Correction shield applied	Experimental anisotropy A'	Corrected anisotropy A
Cl^{36}							
	(B,V)	7.79	0.77	2.8		0.088±0.015	0.107±0.018
	(C,U)	7.40	1.16	1.2		0.076±0.021	0.092±0.025
Ti^{49}	(F+G,V)	{6.77 / 6.41}	1.39	0.97			
	(G,W)	6.41	0.33	0.88	X		
	(G,U)	6.41	1.75	0.1			
Cr^{54}	(B,U)	8.88	0.84	1.02		-0.27 ±0.05	-0.32 ±0.06
Ni^{59}	(B,U)	8.53	0.45	0.45	X	0.36 ±0.10	0.46 ±0.12
Cu^{64}	(B,V)	7.63	0.28	1.03	X	0.032±0.065	0.039±0.080
	(C,U)	7.30	0.60	1.38	X	-0.22 ±0.055	-0.26 ±0.06
Zn^{65}	(E,U)	7.88	0.052	<0.002	X		

Coincidence spectra were taken for nuclei having strong neutron capture γ-rays emitted to low lying energy states. In table 6 are first given the nuclei which were investigated. The second, third and fourth columns contain the terms and the energies of the γ-ray cascades that were studied. A cascade consisting of γ-ray γ_1 followed by γ-ray γ_2 is denoted by (γ_1, γ_2). Figures 23, 24, 25 and 26 show some experimental spectra.

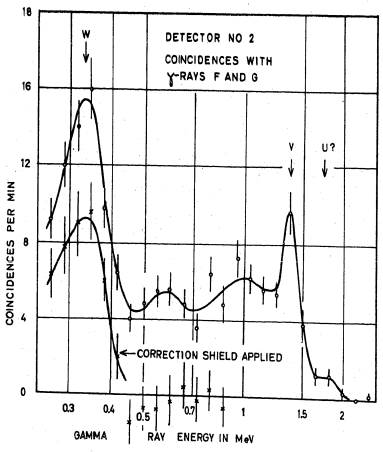

Figure 23.
Coincidence spectra obtained for Ti.

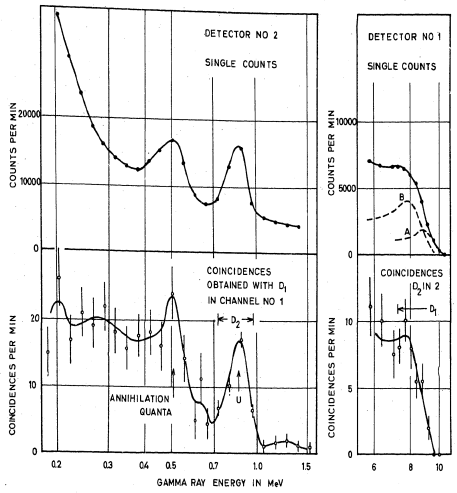

Figure 24.
Singles and coincidence spectra for Cr.

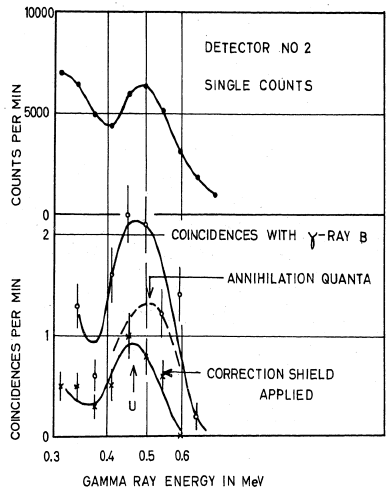

Figure 25.
Singles and coincidence spectra for Ni.

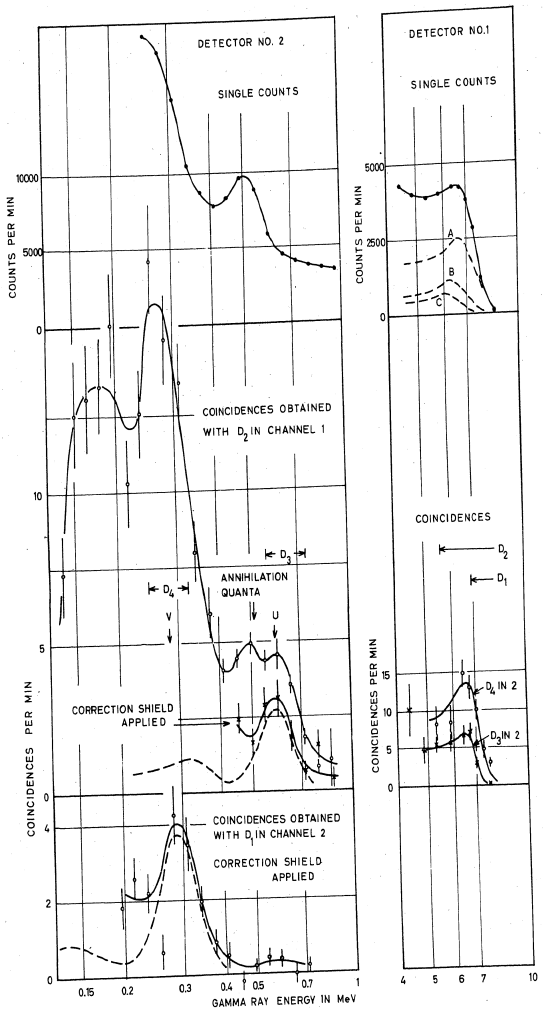

Figure 26.
Singles and coincidence spectra for Cu.

The curves are given without background, and for the coincidence rates random coincidences have also been subtracted. Standard deviation is indicated on coincidence points. The discriminator positions indicated were used in the measurements of the coincidence spectra, and in the angular correlation studies. The spectra have partly been decomposed into the contributions from the various γ-rays. At high energies the decomposition was performed as described in section 5 of chapter III. The low energy γ-ray lines consist of a photopeak and a continuous Compton electron distribution. Their form has been given by Maeder, Müller and Wintersteiger (1954). Annihilation quanta contribute to the measured spectra. In the angular correlation studies this influence was eliminated by additional measurements using the correction shield.

The quantity $\varkappa_1$ being the relative contribution of the high energy γ-ray to the cascade, can be experimentally determined. From a combination of equations (1.9) and (1.10) one gets

$$\varkappa_1 = \frac{C}{N_1 \omega_2 \varepsilon_2} \tag{4.1}$$

Here C is the coincidence rate obtained when the discriminator is set to admit the photopeak of the lower energy γ-ray γ_2 minus the effect of scattering and annihilation quanta. N_1 is the counting rate in channel No. 1, being due to γ_1 only. The efficiency ε_2 for the photopeak of a γ-ray in a $1\frac{1}{2}$" diameter, 1" long NaI(Tl)-crystal has been given by Kalkstein and Hollander (1954). If $\varkappa_1$ becomes larger than one, this means that more than one cascade contributes to the coincidence rate. When the intermediate state B of figure 16 can disintegrate in two or more different ways, or when this state has a lifetime which is comparable to the resolving time of the coincidence circuit, one finds $\varkappa_1 < 1$. Calculated values of $\varkappa_1$ are given in the fifth column of table 6. The experimental uncertainty in the determination of this quantity is about 0.1.

Measurements of angular correlations were performed with the JEEP running at a level of 450 kW. Coincidence rates obtained without the correction shield were between 3 and 20 coincidences per minute. Single counting rates were 10000 per minute or more. For counter No. 2, the larger part of this was background due to scattered γ-rays of higher energy. Counter No. 1, detecting the high energy γ-rays, had at the most 10 % background. Every 5th or every 15th minute the position of the movable detector was changed. Only the two angles $\beta = \pi/2$ and $\beta = \pi$ were used. When correction for annihilation quanta was necessary, the four coincidence rates $C'(0,\pi/2)$, $C'(2,\pi/2)$, $C'(2,\pi)$ and $C'(1,\pi)$ were observed. Also the background and the influence of a paraffine scatterer were measured. Series of observations were taken with the stationary counter in various positions.

Table No. 6 indicates the cases in which the correction shield was applied. The experimental anisotropy, as well as the anisotropy corrected for the geometrical extension of the source and the detectors, are given in columns 7 and 8.

A discussion of the results follows in the next chapter.

CHAPTER V

RESULTS

1. Cl^{36}

The level scheme of this nucleus has been investigated by Paris, Buechner and Endt (1955) who studied the proton spectrum emitted from the (d, p)-reaction on chlorine. In figure 27 are shown the two lowest excited levels in Cl^{36}.

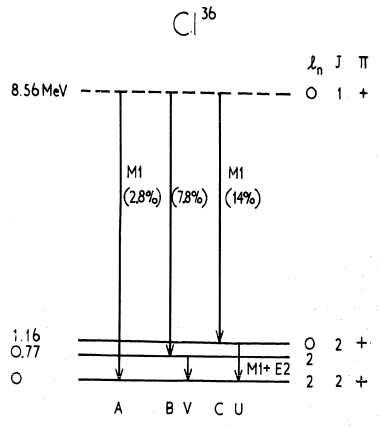

Figure 27. Decay scheme for Cl^{36}.

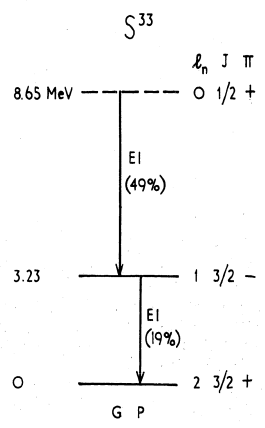

Figure 28. Decay scheme for S^{33}.

Neutron-capture γ-rays emitted from chlorine have been studied by Kinsey, Bartholomew and Walker (1952), by Groshev, Adyasevich and Demidov (1955 b) and by Braid (1956). There is some discrepancy between the relative intensities quoted in these papers. In figure 27 the intensities and nuclear spin values are taken from the paper by Groshev et al. Using a coincidence method, Recksiedler and Hamermesh (1954) verified the existence of the cascades shown in the figure.

In the present coincidence experiment a 30 mm long target of hexachlorobenzene (C_6Cl_6) was used. An attempt to separate the high energy γ-ray B from the γ-ray C was unsuccessful. With the counter No. 1 set to measure essentially no radiation with energy lower than C, coincidences were obtained with the photopeak of the γ-ray U at 1.16 MeV. Coincidences were also measured with the γ-ray V at 0.77 MeV, but the photopeak of this radiation is masked by the Compton electron peak of U, which has very nearly the same energy. The value $\varkappa_1 = 1.2$, obtained for the cascade (C,U), shows that all the γ-rays C are followed by emission of U. As $\varkappa_1 > 1$, detector No. 1 probably counts a small amount of γ-rays with energy lower than C, contributing to the coincidence rate through another cascade.

Angular correlation measurements on the cascade (C,U) yield the anisotropy $A = 0.092 \pm 0.025$. The a priori most probable multipole transitions are given by 1(M1)2(M1)2, corresponding to a theoretical anisotropy of -0.288. The experimental value can apparently best be explained by considering the angular momentum difference $\Delta l_n = 2$ of the transition U, for which the l_n selection rule (II,2.20) predicts a reduced dipole transition probability. Agreement with the experimental value is obtained for the mixed cascade 1(1)2(86% M1, 14 % E2)2. The pure cascade 1(1)2(2)2 gives the right anisotropy, but complete forbidden-ness for the M1 transition is rather improbable.

With the discriminator set to receive the photopeak of the 0.77 MeV γ-ray, the value $\varkappa_1 = 2.8$ is obtained for the (B,V)-cascade. This shows that these coincidences are also mainly due to the (C,U)-cascade. Angular correlation measurements give about the same result as in the former case. If the cascade (B,V) contributes appreciably to the coincidence rate, this one will also have a positive anisotropy.

Polarization studies were not carried out for chlorine as the γ-rays are too closely spaced in the high energy region to be separated from each other to an acceptable extent.

2. S^{33}.

The high energy γ-ray spectrum following capture of thermal neutrons in sulphur has been studied by Kinsey and Bartholomew (1952) and by Groshev, Adyasevich and Demidov (1955 b). By far the most intense high energy transition is the 5.44 MeV γ-ray which is emitted in 48 of 100 cases of neutron capture. In both papers it is identified as the transition from the capturing state to the 3.23 MeV level in S^{33}, which was found by Holt and Marsham (1953 a) and by Paris, Buechner and Endt (1955) in the study of the (d,p)-reaction.

The 5.44 MeV γ-ray G was studied by the polarization method. Neutrons were captured in pure sulphur melted into a standard aluminium target container. The separation of the γ-ray from the rest of the spectrum was fairly good, as indicated in figure 15. As this photon energy is comparatively low, the background was quite high in the present case.

S^{32} is an even-even nucleus, thus the capturing state has $l_n = 0$, and $J_c = \frac{1}{2}$ with even parity. Holt and Marsham (1953 a) found, by angular distribution measurement of the protons emitted from the (d,p)-reaction, that the 3.23 MeV level is a p-state. The possible values for the transition $J_c(L)J_f$ are then $\frac{1}{2}(E1)\frac{1}{2}$ or $\frac{1}{2}(E1)\frac{3}{2}$ giving the polarization ratios $R_G = +1$ and $R_G = -\frac{1}{2}$ respectively. As seen from table 5, the latter value gives $\overline{R}_{th} = -0.41 + \begin{bmatrix} +0.018 \\ -0.09 \end{bmatrix}$ in agreement with the experimental result $\overline{R}_{exp} = -0.44 \pm 0.24$. Figure 28 shows a simplified decay scheme for S^{33}.

In the compilation of nuclear moments by Walchli (1953), spin $\frac{3}{2}$ is given for the ground

state of S^{33}. This corresponds to the $d\frac{3}{2}$-state predicted by shell theory, as seen from figure 2 for the case of 17 neutrons. Accordingly, the γ-ray P emitted to the ground state is also an E1-transition. The state at 3.23 MeV may be interpreted as the odd neutron being lifted to the $2p\frac{3}{2}$-state of the nuclear shell model.

3. Ca^{41}.

The lowest excited level of this nucleus is situated at 1.95 MeV, according to Braams (1954) who performed an analysis of the protons emitted in the (d,p)-reaction on calcium. An angular distribution study on the same reaction, carried out by Holt and Marsham (1953 b), showed that this level is a p-state. The transition from the capturing state to the 1.95 MeV level is represented by the 6.42 MeV γ-ray C found by Kinsey and Bartholomew (1952, 1954).

Polarization experiments were performed using a target of standard size, consisting of pure calcium powder in an aluminium container. The relative background was very high due to the low capture cross section of calcium.

Ca^{40} is an even-even nucleus, and J_c must be $\frac{1}{2}$. As J_f corresponds to a p-state, only the possibilities $R_C = 1$ and $R_C = -\frac{1}{2}$ exist. The value $\overline{R}_{exp} = -0.40 \pm 0.30$ in agreement with $\overline{R}_{th} = -0.46 + \begin{bmatrix} +0.09 \\ -0.045 \end{bmatrix}$ was obtained. J_f then equals $\frac{3}{2}$.

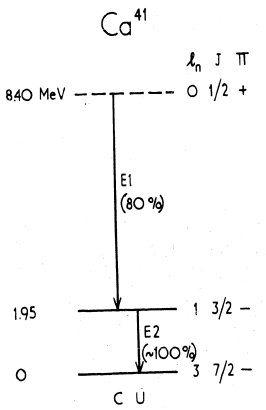

Figure 29. Decay scheme for Ca^{41}.

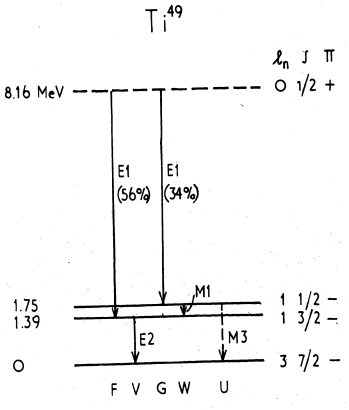

Figure 30. Decay scheme for Ti^{49}.

For the ground state of Ca^{41}, Walchli (1953) gives $J = \frac{7}{2}$, corresponding to one neutron in the $1f\frac{7}{2}$ shell. When it is lifted to the $p\frac{3}{2}$ level of the next shell, the first excited state of 1.95 MeV is obtained. Braid (1956) found a γ-ray with an energy of 1.93 MeV, and intensity of about 98 photons per 100 neutrons captured. This is clearly the ground state transition U of the first excited state. According to the spin value measured it must consist of E2-radiation.

The capture cross section of calcium is too small to allow coincidence studies to be performed.

4. Ti^{49}.

By neutron capture in this nucleus, two prominent γ-rays F and G with energies 6.77 and 6.41 MeV respectively, are emitted. They were detected by Kinsey and Bartholomew (1953 a, 1954) who identified them with the decay to the two excited states at 1.35 and at 1.70 MeV found by Pieper (1952). Braid (1956) and Reier and Shamos (1955), by the scintillation method, found γ-rays of 0.33, 1.39 and 1.75 MeV, obviously corresponding to the transition between these states and to the ground state transition of each of them respectively.

These assignments were checked by means of a simple coincidence measurement performed with a 30 mm long target of pure titanium powder. With channel No. 1 set to detect both the two high energy γ-rays, the coincidence spectrum of figure 23 was obtained by varying the voltage on detector No. 2. Photopeaks of the 0.33 and 1.39 MeV γ-rays are clearly found. An indication of the γ-ray at 1.75 MeV is also present. By using these rough measurements the values of $\varkappa_1$ given in table 6 were calculated for the cascades (F+G,V), (G,W) and (G,U) shown in the decay scheme of figure 30. The results strongly indicate that the decay scheme is correct. It should be kept in mind, however, that the error in $\varkappa_1$ may be about 0.1.

Polarization measurements were carried out with a target consisting of pure titanium powder filling a standard target container of aluminium. The two different discriminators applied are shown in figure 15. Although it was not possible to separate the two γ-rays, conclusions can be drawn from measurements at two discriminator settings, giving different weights to the two γ-rays.

Angular distribution measurements on the (d,p)-reaction on titanium have been performed by Bretscher et al. (1954), who assign angular momentum $l_n = 1$ to the levels at 1.35 MeV and at 1.70 MeV. Thus, a direct transition to one of these levels must be electric dipole, with $R = 1$ or $-\frac{1}{2}$ corresponding to $J_f = \frac{1}{2}$ or $\frac{3}{2}$ respectively. By setting $\overline{R}_{exp} = \overline{R}_{th}$ in table 5, two equations are obtained, giving the solutions $R_F = -0.53$, $R_G = +1.4$. The correct values must then be $R_F = -\frac{1}{2}$ and $R_G = +1$. The derived spin values are given in figure 30. For the ground state of Ti^{49}, Walchli (1953) gives $J = \frac{7}{2}$, and according to the shell model it is a $f\frac{7}{2}$-state. From a comparison of figures 2 and 30, it is seen that the 1.39 and 1.75 MeV levels probably constitute the doublet consisting of $J = 1 - \frac{1}{2}$. The γ-rays W and V must be M1- and E2-transitions respectively, and the transition U, if it exists, is of the M3 type.

5. Cr^{54}.

In the neutron capture γ-ray spectrum of chromium, measured by Kinsey and Bartholomew (1953 a), only the two highest energy γ-rays A and B with energies of 9.72 and 8.88 MeV respectively, can with certainty be assigned to Cr^{54}. A γ-ray U of 0.83 MeV was observed by Braid (1956) and by Reier and Shamos (1955), indicating that the nucleus decays to the ground state by means of the cascade (B, U), as shown in figure 31.

That this is actually the case was shown by a coincidence measurement, using a 28 mm long target of chromium powder. The spectra of figure 24 clearly show the coincidences between the two γ-rays, and the value of $\varkappa_1 \cong 1$ given in table 6 indicates that all the 8.88 MeV γ-rays take part in the cascade.

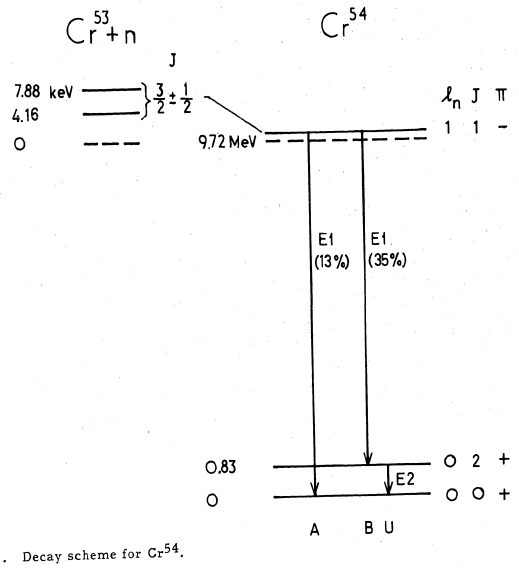

Figure 31. Decay scheme for Cr^{54}.

Both angular correlation and polarization experiments were performed with chromium. As the γ-rays A and B are of very high energy, the background is comparatively small for these measurements. The ground state spin of Cr^{53} is $\frac{3}{2}$, as quoted by Walchli (1953), and it has odd parity according to the shell model. No definite resonance is known to have a dominating influence upon the capture cross section, so that J_c may be 1 or 2, or a mixture of both. For Cr^{54}, being an even-even nucleus, the ground state spin is zero. Angular correlation measurements on the cascade (B, U) yielded the anisotropy $A = -0.32 \pm 0.06$, which agrees very well with the theoretical value for the cascades 1(1)1(1)0 and 1(1)2(2)0, both giving $A = -0.33$. No other possible cascade has a negative anisotropy.

For the polarization experiment the target was of standard size, consisting of metallic chromium powder. Two different discriminator positions were used, giving the values of $\overline{R}_{th}$ presented in table 5. When these expressions are set equal to the experimental values $\overline{R}_{exp}$, the solutions $R_A = -0.36$ and $R_B = +0.31$ are obtained. R_A may be equal to $-\frac{1}{2}$ or $+\frac{1}{2}$ corresponding to $J_c = 1$ or $J_c = 2$ respectively. The experimental result shows that the former case at least is the more important of the two. As already shown by the angular correlation experiment, thermal neutron capture in the state $J_c = 1$ is predominating. Emission of A from $J_c = 2$ is rather improbable, since this would be a quadrupole transition. The actual value of R_A, therefore, must be very near to $-\frac{1}{2}$. According to the angular correlation experiments the 0.83 MeV state can have $J = 1$ or 2, corresponding to $R_B = -\frac{1}{4}$ or $+\frac{1}{4}$ respectively. The polarization experiment confirms the latter case.

resonance levels of Cr^{53} quoted in the nuclear level compilation by Way et al. (1955) are indicated in figure 31, but nothing is known about their widths, and the value $J_c = 1$ cannot be assigned to a definite resonance. The value J = 2 for the 0.83 MeV level confirms the rule mentioned in section 3 of chapter II, assigning spin 2 to the lowest excited states of even-even nuclei. As also $\ell_n = 0$ and even parity is the rule, this is indicated in the figure.

6. Fe^{57}.

By neutron capture in iron, a very intense γ-ray of energy 7.64 MeV is emitted. It was detected by Kinsey and Bartholomew (1953 a, 1954) who state that it is most probably the ground state transition from the capturing level.

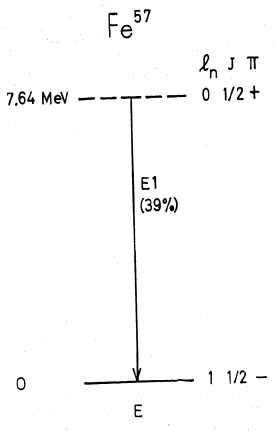

Figure 32. Decay scheme for Fe^{57}.

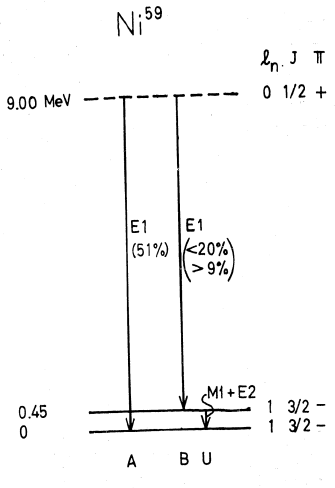

Figure 33. Decay scheme for Ni^{59}.

Fe_3O_2-powder in a standard target container of aluminium was used for the polarization measurements. As mentioned earlier these observations had to be corrected for depolarization of the neutrons passing through the target material.

Fe^{56} is an even-even nucleus, having spin 0, and the ground state of Fe^{57} has $\ell_n = 1$, as found by measurements of angular distribution in the (d,p)-reaction, performed by Black (1953) and by McFarland et al. (1955). Thus the ground state γ-ray E is of the E1 type. The polarization experiment clearly gives the result $R_E = +1$, corresponding to $J_f = \frac{1}{2}$. This value is in disagreement with the single particle shell model, which predicts that the extra neutron is in a $p\frac{3}{2}$-state. If the level scheme of figure 2 is correct for the neutrons in the iron atom, the spin of the ground state must be a result of interactions between several nucleons.

7. Ni^{59}.

Of the high energy capture γ-rays from nickel, measured by Kinsey and Bartholomew (1953 a), only the 9.00 MeV ground state transition A in Ni^{59} could with certainty be assigned to this nucleus. The second highest γ-ray B, of energy 8.53 MeV, can either be the ground state transition in Ni^{61}, or a transition to the level at about 0.45 MeV in Ni^{59}, found by studies of the (d,p)-reaction by McFarland, Bretscher and Shull (1953) and by Pratt (1954).

Polarization measurements were only performed for the highest energy γ-ray. The target consisted of pure $NiSO_4$ filled into an aluminium box of standard type. The use of a non-ferromagnetic target material results in a small capture-to-scattering cross section ratio. At 9.00 MeV the background is very low, but also the γ-ray intensity was small. It was found that R_A is negative. As Ni^{58} is an even-even nucleus, giving $J_c = \frac{1}{2}$, and the very intense ground state γ-ray is clearly a dipole transition, only the possibilities $J_f = \frac{1}{2}$ and $J_f = \frac{3}{2}$ exist. The latter case agrees with the measurement. It also agrees with the nuclear shell model which predicts a $p\frac{3}{2}$-state for Ni^{59}. The odd parity corresponds to the ground state transition being of electric dipole type.

Coincidence measurements on the γ-ray B at first sight only revealed the expected annihilation peak. However, as this peak is higher than what corresponds to the observed counting rate N_1 in the high energy γ-ray detector, a contribution from the 0.45 MeV γ-ray U, which has been detected by Braid (1956), is suggested. A coincidence spectrum was taken with the correction shield in front of detector No. 2. This spectrum contains all the false coincidences. When it is subtracted from the original curve, only true coincidences, illustrated by the lowest curve in figure 25, are left. From the intensity of the cascade (B,U), the value $\varkappa_1 = 0.45$ is obtained. This can be explained in various ways. The decay of the 0.45 MeV level may be so slow that only part of the cascade is recorded by the coincidence circuit, or this state may, in part, decay to a lower lying excited level. It is also possible that 55 % of the γ-ray peak B obtained by Kinsey and Bartholomew (1953 a) corresponds to the ground state decay in Ni^{61}, and the rest is emitted from Ni^{59}. The measured intensity of the (B,U)-cascade contradicts the result of Pratt (1954) who found the spin $J = \frac{7}{2}$ for the 0.45 MeV level. In that case the transition B would be of octupole type, which could not cause an intensity comparable to the electric dipole transition A to the ground state.

The angular correlation measurements on the cascade (B,U) yielded the anisotropy $A = 0.46 \pm 0.12$. All pure cascades with spin $J_b = \frac{1}{2}, \frac{3}{2}$ or $\frac{5}{2}$ for the 0.45 MeV level have zero or negative anisotropy. If this level is supposed to have the same parity as the ground state, as is generally the rule for low excited states, the only possible cascade giving the correct anisotropy is $\frac{1}{2}(1)\frac{3}{2}(35\ \%\ M1;\ 65\ \%\ E2)\frac{3}{2}$. The proposed decay scheme is shown in figure 33.

8. Cu^{64}.

Kinsey and Bartholomew (1953 b) studied the radiation following capture of neutrons in copper. The three highest energy γ-rays A, B and C have energies of 7.91, 7.63 and 7.30 MeV respectively. Of these, A and C were assigned to the nucleus Cu^{64}, where A is the ground state transition, and C is the transition to the 0.51 MeV level found by Hoesterey (1952) in the study of (d,p)-reactions. If the γ-ray V of 0.28 MeV, observed by Reier and Shamos (1955), is assumed to form a cascade together with B, the level scheme of figure 34 is obtained.

This scheme has been confirmed by coincidence measurements, using a copper target of 9 mm length. The obtained coincidence spectra are shown in figure 26. By use of the correction shield some details of the pure coincidence spectra were resolved. The γ-ray at 0.60 ± 0.05 MeV has not earlier been observed. We may safely conclude that it is the γ-ray U, corresponding to the decay of the 0.51 MeV level studied by Hoesterey (1952). The part of the coincidences being due to annihilation and scattering was calculated from measurements with the correction shield applied. The calculated values of $\varkappa_1$ are approximately equal to one,

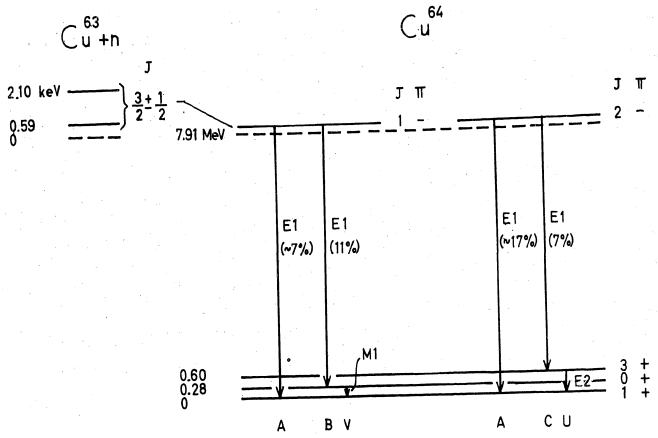

Figure 34. Tentative decay scheme for Cu^{64}.

indicating that B and C in whole take part in the cascades. For the γ-ray pair (C,U), the high value of H_1 may be due to the influence of a γ-ray with energy lower than C, also coincident with U.

Polarization measurements were performed with a target of metallic copper, which because of its high density was only 10 mm long in the direction of the neutron beam, and 20 mm broad. The γ-ray intensity was quite high, but separation of the different high energy γ-rays was difficult to perform. From the experimental results quoted in table 5 are found the most probable values $R_A = +0.45$ and $R_B = -0.50$. The influence of R_C is smaller than the statistical errors, but the agreement with the two experimental values is best if $R_C = -0.5$.

The ground state of Cu^{63} has spin $\frac{3}{2}$ according to Walchli (1953), and a $p\frac{3}{2}$-state is predicted by the nuclear shell model. Then the capturing state has spin 1 or 2 with odd parity. For the ground state spin of Cu^{64}, Lemonick and Pipkin (1954) found the value J = 1 by means of the atomic beam resonance method. The lowest shell model configuration of 29 protons and 35 neutrons is given by (proton $2p\frac{3}{2}$) (neutron $1f\frac{5}{2}$)^3 having even parity. Thus the γ-ray A is an electric dipole transition. From table 2 is seen that the possible values for R_A are $-\frac{1}{4}$ and $+\frac{3}{4}$, corresponding to $J_c = 1$ and 2 respectively. If x is the part of the γ-ray A which is emitted from the compound state with spin $J_c = 2$, the experimental results yield $x = 0.70 \pm 0.15$. Because of their high intensities, both the γ-rays B and C can be assumed to be E1-transitions. The value $R_B = -\frac{1}{2}$ is in agreement with both the transitions 1(E1)0 and 2(E1)3.

Corresponding to these transistions, the cascade (B,U) can be 1(E1)0(M1)1 or 2(E1)3(E2)1, with

theoretical anisotropies 0 and -0.242 respectively. In none of these cases is mixing of multipole orders probable. Angular correlation measurements were carried out for both the cascades (B,U) and (C,V). The method of the correction shield was applied. According to the experimental results for copper in table 6, the cascades are obviously (B,U) = 1(E1)0(M1)1 and (C,V) = 2(E1)3(E2)1. These results are indicated in the decay schemes of figure 34. The anisotropy -0.242 would also be obtained for the cascade 2(1)2(1)1. However, if 2 were the spin value of the 0.60 MeV level, also the cascade 1(1)2(1)1 having A = +0.288 would contribute appreciably. The resulting anisotropy in that case would be about +0.06.

Two neutron resonances, obtained from Hughes and Harvey (1955), are indicated in figure 34. As very little is known about their widths and about other positive or negative resonances contributing to the thermal neutron capture, the spins 1 and 2 cannot be assigned to definite resonances.

9. Zn^{65}.

The rádiation emitted by neutron capture in zinc has been studied by Kinsey and Bartholomew (1953a), who found an intense γ-ray of energy 7.88 MeV. This is very near the binding energy of a neutron in Zn^{65}, so it may be interpreted as the ground state transition in that nucleus. The intensity of the transition indicates that it is of dipole type. Following the β^+-decay of Ga^{65}, Crasemann (1954) found a γ-ray of 0.052 MeV. If this is a ground state transition in Zn^{65}, it is also possible that the γ-ray E of 7.88 MeV is a transition to the 0.052 MeV level.

Polarization measurements were carried out with a standard size target of metallic zinc. The observations were hampered by considerable neutron scattering in the target, and relatively high background.

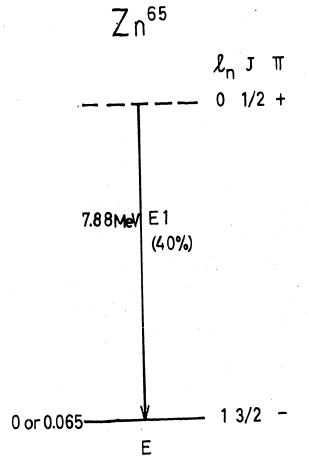

Figure 35. Decay scheme for Zn^{65}. It is not known whether the γ-ray E leads to the ground state or not.

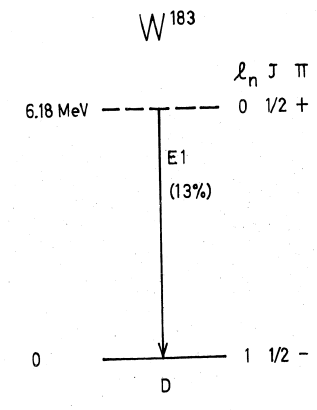

Figure 36. Decay scheme for W^{183}.

Zn^{64}, being an even-even nucleus, has zero spin, yielding $J_c = \frac{1}{2}$. As E is a dipole transition, the final spin must be $\frac{1}{2}$ or $\frac{3}{2}$, corresponding to $R_E = +1$ or $-\frac{1}{2}$ respectively. The negative value of $\overline{R}_{exp}$ agrees with the latter case, and it can be concluded that the γ-ray E produces a state with spin $\frac{3}{2}$. The nuclear shell model predicts the spin $\frac{5}{2}$ for the ground state of Zn^{65}. However, the spin $\frac{3}{2}$ may be obtained by coupling between the three neutrons in the $(1f\frac{5}{2})^3$-configuration, or it is possible that the configuration $(2p\frac{3}{2})^3\ (1f\frac{5}{2})^4$ has the lowest energy. It is therefore not possible to tell whether the γ-ray E is a transition to the ground state or to the 0.052 MeV level.

An investigation with the coincidence apparatus gave the result $\mathcal{N}_1 < 0.002$ for the two γ-rays E and U, being the 0.052 MeV transition. This means that either the cascade (E,U) does not exist, or the emission of U takes place with such a long lifetime that most coincidences are not counted with the present experimental set-up.

10. W^{183}.

The polarization measurement on this nucleus was discussed in Chapter III, section 7. As the angular momentum properties were known in advance, this observation was used to check the experimental method.

11. Conclusion.

It has been experimentally verified that circularly polarized γ-radiation is emitted as a result of the capture of polarized thermal neutrons. Within experimental errors, the observations were in accordance with theory. For a number of cases it has been shown that the measurement of circularly polarized γ-rays can successfully be used as a means for obtaining nuclear spin properties. Theoretical values of the degree of circular polarization have also been evaluated for the case of mixed multipole orders. Mixing was, however, not experimentally observed, since only the simplest cases could be studied with the apparatus employed. Actually, all the γ-rays studied were of electric dipole type. Other multipole orders should not then influence the measurements.

The possible methods for the measurement of circular polarization have been briefly discussed. For the present experiment, the method of measuring the transmission through magnetized iron was chosen. The experimental efficiency was very small, mainly due to the fact that only about 2 of the 26 electrons in the iron atom can be polarized. Very small changes in counting rates had to be measured, and long counting periods were required. The energy discrimination of the γ-rays was not very good, since care must be taken to get high intensity.

The angular correlation method was applied, with some success, to the study of γ-ray cascades following the capture of slow neutrons. The techniques were mainly conventinal ones, but some special experimental difficulties occurred. When the source is a target which captures neutrons, its specific activity is quite low. A compromise must then be found between the distortion of the correlation function due to the scattering in a big target, and low intensity due to a small target. Very high background counting rates occurred in the detector measuring low energy γ-rays. When radiation of energy 0.5 MeV or less was measured in one of the detectors, false coincidences were obtained as a result of annihilation quanta produced by high energy γ-rays in the other detector. Energy discrimination was difficult for the complicated γ-ray spectra resulting from neutron capture. A few cases of mixed multipole radiation were observed in the angular correlation measurements.

The excited nuclear energy levels that are most easily studied by the techniques mentioned, are the lowest lying ones, being obtained by single transitions from the capturing state. The γ-rays corresponding to these transitions have comparatively high energy, and they are fairly easy to isolate from the other γ-energies by discrimination.

The results obtained were quite rough. In some cases only the sign of the circular polarization or of the angular correlation anisotropy could be determined with certainty. Still, it was possible to draw conclusions about angular momentum properties from such results. Especially useful was the combination of the two methods, as illustrated by the cases of Cr^{53}, Ni^{59} and Cu^{64}.

ACKNOWLEDGEMENTS.

It is a pleasure for the writer to express his gratitude to Director G. Randers who allowed this work to be carried out at the Joint Establishment for Nuclear Energy Research.

Thanks are extended to Dr. J.A. Goedkoop for his encouraging interest in the present work, and for his help in reading through and correcting the manuscript.

The writer is also very much indebted to Dr. A. Lundby, Dr. A. Patro and Dr. J.P. Davidson for stimulating discussions, and to Mr. H. Strand and Mr. A. Sunde for valuable help with the electronic equipment. It is not possible to mention all collaborators by name, but thanks are also extended to all those of the JENER staff who took part in making the present work possible.

REFERENCES.

F. Ajzenberg and T. Lauritsen — 1955: Rev. Mod. Phys. 27, 77.

K. Alder — 1952: Helv. Phys. Acta. 25, 235.

P. Argyres and C. Kittel — 1953: Acta Metall. 1, 24.

G.E. Bacon — 1955: Neutron Diffraction, Clarendon Press, Oxford.

P.R. Bell — 1955: Beta and Gamma Ray Spectroscopy, ed. K.Siegbahn, North Holland Publ. Comp., Amsterdam, p.133.

S. Bernstein, L.D. Roberts, C.P. Stanford, J.W.T. Dabbs and T.E. Stephenson — 1954 a: Phys. Rev. 94, 1243.

S. Bernstein; L.D. Roberts, -, J.W.T. Dabbs and C.P. Stanford — 1954 b: Phys. Rev. 95, 105.

S. Bernstein; J.W.T. Dabbs, L.D. Roberts and - — 1955; Phys. Rev. 98, 1512.

R.A. Beth — 1936: Phys. Rev. 50, 115.

L.C. Biedenharn, J.M. Blatt and M.E. Rose — 1952: Rev. Mod. Phys. 24, 249.

L.C. Biedenharn and M.E. Rose — 1953: Rev. Mod. Phys. 25, 729.

L.C. Biedenharn, M.E. Rose and G.B. Arfken — 1951 a: ORNL-986, U.S. Atomic Energy Commission.

L.C. Biedenharn, M.E. Rose and G.B. Arfken — 1951 b: Phys. Rev. 83, 683.

C.F. Black — 1953: Phys. Rev. 90, 381.

J.M. Blatt and V.F. Weisskopf — 1952: Theoretical Nuclear Physics, Wiley, New York.

A. Bohr — 1952: Kgl. Dan. Mat. Fys. Medd. 26, No. 14.

A. Bohr and B.R. Mottelson — 1953: Kgl. Dan. Mat. Fys. Medd. 27, No. 16.

C.M. Braams — 1954: Phys. Rev. 94, 763.

T.H. Braid — 1956: Phys. Rev. 102, 1109.

M.M. Bretscher, J.O. Alderman, A. Elwyn and F.B. Shull — 1954: Phys. Rev. 96, 103.

M.T. Burgy, D.J. Hughes, J.R. Wallace, R.B. Heller and W. Woolf — 1950: Phys. Rev. 80, 953.

J.M. Cassels — 1950: Progress in Nuclear Physics I , ed. O.R.Frisch, Butterworth-Springer, London, p.185.

E.U. Condon and G.H. Shortley — 1935: The Theory of Atomic Spectra, The University Press, Cambridge.

B. Crasemann — 1954: Phys. Rev. 93, 1034.

C.M. Davisson — 1955: Beta and Gamma Ray Spectroscopy, ed. K.Siegbahn, North Holland Publ. Comp., Amsterdam, App.I.

A.M. Feingold and S. Frankel — 1955: Phys. Rev. 97, 1025.
J. Fischer and J. Marshall — 1952: Rev. Sci. Inst. 23, 417.
H. Frauenfelder — 1955: Beta and Gamma Ray Spectroscopy, ed. K.Siegbahn, North Holland Publ. Comp., Amsterdam, p. 531.

M. Goldhaber and A.W. Sunyar — 1951: Phys. Rev. 83, 906.
S.B. Gunst and L.A. Page — 1953: Phys. Rev. 92, 970.
L.V. Groshev; B.P. Adyasevich, - and A.M. Demidov — 1955 a: Session of the Academy of Sciences, Moscow, 4, 270.
L.V. Groshev, B.P. Adyasevich and A.M. Demidov — 1955 b: Proc. Internat. Conf. on Peaceful Uses of Atomic Energy, 2, 39.

O. Halpern — 1951 a: Nature, 168, 782.
O. Halpern — 1951 b: Phys. Rev. 82, 753.
O. Halpern, M. Hamermesh and M.H.Johnson — 1941: Phys. Rev. 59, 981.
O. Halpern and T. Holstein — 1941: Phys. Rev. 59, 960.
O. Halpern and M.H. Johnson — 1939: Phys. Rev. 55, 898.
O. Haxel, J.H.D. Jensen and H.E. Suess — 1950: Z. Physik, 128, 251.
W. Heitler — 1954: The Quantum Theory of Radiation, Clarendon Press, Oxford.

D.C. Hoesterey — 1952: Phys. Rev. 87, 216.
J.R. Holt and T.N. Marsham — 1953 a: Proc. Phys. Soc. A. 66, 462.
J.R. Holt and T.N. Marsham — 1953 b: Proc. Phys. Soc. A. 66, 565.
D.J. Hughes, M.T. Burgy and W.E. Woolf — 1950: Phys. Rev. 80, 481.
D.J. Hughes and J.A. Harvey — 1955: BNL-325, U.S. Atomic Energy Commission.

D.J. Hughes, J.R. Wallace and R.H. Holtzmann — 1948: Phys. Rev. 73, 1277.

M.I. Kalkstein and J.M. Hollander — 1954: UCRL-2764, U.S. Atomic Energy Commission.

B.B. Kinsey, G.A. Bartholomew and W.H. Walker — 1951 a: Can. Journ. Phys. 29, 1.
B.B. Kinsey, G.A. Bartholomew and W.H. Walker — 1951 b: Phys. Rev. 82, 380.
B.B. Kinsey, G.A. Bartholomew and W.H. Walker — 1951 c: Phys. Rev. 83, 519.
B.B. Kinsey, G.A. Bartholomew and W.H. Walker — 1952: Phys. Rev. 85, 1012.
B.B. Kinsey and G.A. Bartholomew — 1953 a: Phys. Rev. 89, 375.
B.B. Kinsey; G.A. Bartholomew and - — 1953 b: Phys. Rev. 89, 386.
B.B. Kinsey; G.A. Bartholomew and - — 1953 c: Can. Journ. Phys. 31, 49.
B.B. Kinsey; G.A. Bartholomew and - — 1953 d: Can. Journ. Phys. 31, 1025.
B.B. Kinsey and G.A. Bartholomew — 1953 e: Can. Journ. Phys. 31, 1051.
B.B. Kinsey and G.A. Bartholomew — 1954: Phys. Rev. 93, 1260.
P.F.A. Klinkenberg — 1952: Rev. Mod. Phys. 24, 63.

A. Lemonick and F.M. Pipkin — 1954: Phys. Rev. 95, 1356.
J.S. Levin and D.J. Hughes — 1956: Phys. Rev. 101, 1328.
F.W. Lipps and H.A. Tolhoek — 1954 a: Physica, 20, 85.
F.W. Lipps and H.A. Tolhoek — 1954 b: Physica, 20, 395.
R.P. Lowde — 1954: Proc. Roy. Soc. A. 221, 206.

D. Maeder, R. Müller and V. Wintersteiger — 1954: Helv. Phys. Acta, 27, 3.
M.G. Mayer — 1950: Phys. Rev. 78, 16.
M.G. Mayer and J.H.D. Jensen — 1955: Elementary Theory of Nuclear Shell Structure, Wiley, New York.

C.E. McFarland, M.M. Bretscher and F.B. Shull — 1953: Phys. Rev. 89, 892.
C.E. McFarland, F.B. Shull, A.J.Elwyn and B. Zeidman — 1955: Phys. Rev. 99, 655.

R.W. Meier, P. Scherrer and G. Trumpy — 1954: Helv. Phys. Acta, 27, 577.
W.E. Meyerhof and D.B. Nicodemus — 1950: Phys. Rev. 82, 5.
C.O. Muehlhause — 1951 a: Phys. Rev. 83, 235.
C.O. Muehlhause, C.T. Hibdon and - — 1951 b: Phys. Rev. 83, 235.

C.O. Muehlhause, C.T. Hibdon and - — 1952: Phys. Rev. 87, 222.

C.H. Paris, W.W. Buechner, P.M. Endt — 1955: Phys. Rev. 100, 1317.

J. Pelser — 1954: Physica 21, 22.
G.T. Pieper — 1952: Phys. Rev. 88, 1299.
W.W. Pratt — 1954: Phys. Rev. 95, 1517.

A.L. Recksiedler and B. Hamermesh — 1954: Phys. Rev. 96, 109.
M. Reier and M.H. Shamos — 1955: Phys. Rev. 100, 1302.
M.E. Rose — 1949: Phys. Rev. 76, 678.
M.E. Rose — 1955: Multipole Fields, Wiley, New York.
M.E. Rose, G.H. Goertzel, B.I. Spinrad, J. Harr and P. Strong — 1951: Phys. Rev. 83, 79.

G. Scharff-Goldhaber — 1953: Phys. Rev. 90, 587.
C.G. Shull and E.O. Wollan — 1951: Phys. Rev. 81, 527.
C.G. Shull, E.O. Wollan and W.C. Koehler — 1951: Phys. Rev. 84, 912.
J.A. Spiers — 1948: Nature, 161, 807.
C.P. Stanford, T.E. Stephenson, L.W. Cochran and S. Bernstein — 1954: Phys. Rev. 94, 374.
J. Steinberger and G.C. Wick — 1949: Phys. Rev. 76, 994.

T. Teichmann — 1950: Phys. Rev. 77, 506.
H.A. Tolhoek and J.A.M. Cox — 1953: Physica 19, 101.

H.E. Walchli — 1953: ORNL-1469, U.S. Atomic Energy Commission.

J. Wardley — 1952: Transactions of the Instruments and Measurements Conference, Stockholm, p. 198.

K. Way, R.W. King, C.L. McGinnis and R. van Lieshout — 1955: TID-5300, U.S. Atomic Energy Commission.
V.F. Weisskopf — 1951: Phys. Rev. 83, 1073.
E. Wigner — 1931: Gruppentheorie, Vieweg, Braunschweig.

L. Wolfenstein — 1949 a: Phys. Rev. 75, 342.
L. Wolfenstein — 1949 b: Phys. Rev. 75, 1664.

Declassified in Part - Sanitized Copy Approved for Release @ 50-Yr 2013/10/24 : CIA-RDP81-01043R002400120007-1

UNCLASSIFIED

JENER REPORT NO. 47.

JOINT ESTABLISHMENT FOR NUCLEAR ENERGY RESEARCH

Kjeller near Lillestrøm, Norway.

Enclosure 2
Despatch No. 5
AmEmbassy, Oslo

4201181

ABSOLUTE NEUTRON AND GAMMA-RAY SPECTRA OF JEEP MEASURED BY MEANS OF NUCLEAR EMULSIONS

By

S. SELIM-YOUNIS

Kjeller, April 1957.

UNCLASSIFIED

CONTENTS

Figure Legends.

Absolute Neutron and Gamma-ray Spectra of JEEP measured by means of Nuclear Emulsions.

by

S. Selim- Younis.[+]

Summary:

Nuclear emulsions have been irradiated at the opening of the central channel (5/11) of JEEP. Calculations from 2000 recoil- and 100 deuteron photoproton- measured tracks gave the following results:

1) The total fast neutron flux at the opening is (2.2 ± 0.4) neutrons per cm^2. sec. watt.

The energy distribution of the emitted neutrons shows a degradation from the thermal fission neutrons. The spectrum fits better with the formula:

$$n(E) = (2.9 \pm 0.5).\ \sqrt{E}\ \exp(-1.035\ E + 0.038\ E^2)$$

neutrons/ cm^2. sec. watt. Mev interval,

where E is the neutron energy in Mev.

2) The total flux of gamma rays, with energies greater than 2.5 Mev is (40 ± 30) photons per cm^2. sec. watt.

The absolute spectrum, neglecting the line structure, decreases exponentially with the energy and probably contains more hard rays around 8 Mev than the expected fission gamma rays. The approximated fit to the spectrum is:

$$n(k) = (230 \pm 210).\ \exp(-0.8\ k)$$

photons/ cm^2. sec. watt. Mev interval,

where k is the photon energy in Mev.

Introduction:

The determination of the neutron and gamma-ray spectra of a nuclear reactor is of interest in several respects. The energy spectrum of the prompt neutrons from the slow neutrons fission of U^{235} has been well

---

[+] On leave from the Egyptian Atomic Energy Commission, Cairo.

determined before [1-7]. The best fit for the number of neutrons emitted with an energy of E Mev per unit energy interval is given by the empirical formula:

$$n(E) = A.\ \exp(-1.035\ E).\ \sinh\sqrt{2.29E}$$

where A is a constant. The spectrum has a maximum around 0.7 Mev and an average neutron energy of 2.0 Mev[8]. The gamma ray spectrum accompanying thermal U^{235} fission has not been determined with the same accuracy. Recent measurements [9-12] suggest that the total gamma energy release is between 7 and 12 Mev per fission. The spectrum is continuous, approximately exponential, with a sharp cut- off at about 8 Mev.

Measurements have been performed on the fast neutron spectra of different reactors[3,6,15,16]. For hard gamma rays, less has been published[16,17]. As regards JEEP, Grimeland[18] and Pelser[19] have determined the thermal neutron spectrum from a fast neutron channel. Bogaardt et al[20] have measured the neutron density distribution along the irradiation channels; Klepp and Popović[21] determined the gamma flux distribution.

The aim of the present work is a preliminary determination of the absolute energy distributions of fast neutrons and of hard gammas (which give rise to photo- neutrons in the heavy water). The beam under investigation was that coming out from the central channel no. 5, south.

In experiments with reactors, the high background of secondary effects makes electronic devices too less suitable for such a study. For this reason we have used the nuclear photographic plates, a technique in which one can avoid troubles arising from the background.

Two main reactions were taken into consideration, namely:

a) the deuteron photo disintegration for the determination of the gamma rays spectrum. The reaction is as follows:

$$D + h\nu \longrightarrow n + p + \varepsilon \qquad (1)$$

where ε = 2.2 Mev is the deuteron binding energy. The cross section of the reaction is of the order of 10^{-27} cm^2. Such a method has been used and described in details before[22]. In short, a nuclear photographic plate is soaked in heavy water till saturation, thus getting about 10^{23} D- nuclei per cm^3 in the emulsion. The wet plate is then exposed to the collimated beam. Reaction (1), along with others involving the nuclei in the emulsion (Ag, Br, .. etc), will take place. The emitted photo protons will have an

angular distribution of the form: $a + b. \sin^2 \theta$.

To eliminate the less frequent disturbing photo protons, another similar plate is soaked in ordinary water till saturation, irradiated and treated exactly under the same conditions as the heavy water plate. The difference of events between the two plates ($D_2O - H_2O$), limiting the measurements to backward tracks in order to avoid the recoils, gives the photo protons from the deuteron disintegration. Since the emitted particles in reaction (1) are nearly of the same mass and the gamma momentum can be neglected in this energy range ($h\nu < 10$ Mev), the photon energy is given by:

$$h\nu = 2 E_p + \varepsilon = 2 E_n + \varepsilon \qquad (2)$$

where $E_p = E_n$ = the kinetic energy of the emitted nucleon. Thus, knowing the energy of the proton, one can deduce the photon energy, and, knowing the cross section as a function of $h\nu$ [23], one can calculate the intensity of the reacting gamma rays.

b) The recoil protons, or deuterons, in the forward direction, which are scattered elastically by the neutrons ($\sigma \simeq 10^{-24}$ cm^2) are used to determine the neutron spectrum. This method has been used by different investigators[24, 25]. Knowing the number of reactions in a certain neutron energy range, and the n-p (or n-d) scattering cross section as a function of that energy one could calculate the neutron spectrum.

Experimental Part:

1) Preparation of the plates:

Kodak NTA nuclear plates (200 μ thickness) were used. For every set of exposures three plates from the same batch were cut to a size of about 2.5 x 2.6 cm^2. One plate was then soaked in H_2O, another in D_2O for several hours to ensure saturation, and the third one kept in dry condition. The amount of the water taken up was carefully determined for each plate [22]. For these particular emulsions, the mean quantity of water was (82 ± 5) mg/cm^2 of emulsion; from this one could find the excess D- (or H-) nuclei in the emulsion.

In the case of the neutron spectrum measurements, in order to reduce the excess proton tracks of energy 0.6 Mev arising from the interaction of

thermal neutrons with the N^{14} present in the emulsion according to the reaction $N^{14}(n, p)C^{14}$, the plates were enclosed in cadmium cassettes of thickness 1 mm. By taking the difference between the forward tracks in the H_2O and dry plates, these spurious tracks are further eliminated.

On the other hand, for measurements of the gamma ray spectrum, aluminium cassettes were used during the irradiation so as to minimize the gammas arising from capture in the cassette material.

In each cassette a few drops of (light or heavy) water were placed so as to ensure saturation. The cassettes were then exposed to the beam, for equal periods of time, under the same geometrical configuration.

II) Experimental arrangement:

Figure (1) shows the irradiation arrangement. The beam passes through a graphite- iron collimator, about 200 cm long, with an opening of 2 x 4 cm^2. The uncertainity in the incidence angle of the direct beam is, therefore, less than 2^o. The exposure time was either 1 minute at 350 kw, giving a track population of about 3000 tracks/mm^2 of the emulsion surface, or 20 minutes at 24 watts (after 5 hours of reactor's shut-down), giving about 10 tracks/mm^2.

III) Treatment of plates:

The irradiated plates were treated in the following way:

1. Washed in running water for a short time.
2. Soaked in Ilford ID-19 (1 : 3 by volume) at 4^oC for 30 minutes.
3. Transfered to ID-19 (1 : 3 by volume) at 18^oC for 25 minutes with slight rocking.
4. Washed in running water for a minute.
5. Soaked in cool acid hardener during 15 minutes.
6. Washed in water for a minute.
7. Fixed, for 7 hours, in a 30% hypo- neutral solution at 20^oC.
8. Washed in cool running water for 2 hours.
9. Left to dry at room temperature.

IV Measurement Technique:

After the plate had been dried, the direction of the beam was marked

on the surface and this was taken as the Y- axis throughout subsequent measurements. A Watson binocular[+] microscope with a mechanical stage was used. The microscope was fitted with a 50x fluorite, oil- immersion objective (N.A. = 0.95), compensated with a pair of 6x eye- pieces. The measurements of projected lengths of the tracks were made using a calibrated 6x scale eye- piece, and those the depths of the tracks by the micrometer drum. The projected emission angles between the tracks and the Y- axis were measured by a pointer- goniometer device.

Certain areas on the plates, confined to a region 4 mm from the edge nearest to the neutron source were examined. This was done to avoid excessive selective attenuation[25]. Tracks whose beginnings and ends lay in the emulsion, and whose lengths were greater than the minimum detectable value, (6 μ), were all recorded for the calculations.

Treatment of the data:

For calculating the true lengths and emission angles of the tracks it is necessary to determine the shrinkage S, of the emulsion due to processing. For dry plates, this has been determined by direct measurements of the emulsion before and after processing. For wet plates, both this method and the alpha-track method[22] using a U^{233}- solution, have been used. The results of these measurements were:

$$S_{dry} = 2.8 \pm 0.2$$

$$S_{wet} = 9.7 \pm 0.6$$

Thus, for each track, one can calculate the true length ℓ and the true angle θ using the relations:

$$\ell = \sqrt{\ell'^2 + h^2 s^2} \qquad (3)$$

$$\cos\theta = \cos\vartheta \cdot \cos\alpha, \qquad (4)$$

where ℓ' is the projected length, h the depth of the track, ϑ the projected angle of emission, and α is dip angle.

To transform the true lengths of the tracks into energy, the range- energy relation of the emulsion must be known. For the dry plates, we have used the data given by Kodak. For the wet emulsions, however, the range- energy curve

---

+ I wish to thank Forsvarets Forskningsinstitutt, Kjeller for lending me the microscope.

is shifted from the values for dry emulsions by a constant lengthenning factor f which depends upon the water content in the emulsion and which is nearly constant allover the proton energy domain up to 12 Mev[22]. It might be mentioned[+] here that f is nearly the same for alpha tracks as for protons in this energy range.

In order to determine f, we soaked some plates in a diluted solution containing U^{233} (E_α = 4.82 Mev, Range = 19.5 μ in dry emulsions) [++] for several hours, to allow saturation of the emulsion with water. The plates were then processed and treated in the way described. Figure 2 gives the range distribution of 170 alpha- tracks in the wet emulsion. The calculated mean range is 29 μ, corresponding to a lengthenning factor f = 1.5. This value has been used for all wet plates.

Results:

1) Neutrons:

Only forward tracks emitted in a circular cone of an opening angle $\Theta = 20^\circ$ have been considered. The tracks in the corresponding backward cone were subtracted so as to eliminate - within statistical inaccuracy - the effect of the (n,p) and (γ,p) reactions. This procedure assumes that the ejected protons from the last two reactions are symmetric in those two laboratory cones. In any case, this effect contributes fewer than 3% of the forward tracks. The track- difference results in recoil energy- intervals. Then we calculate the escape probability factor k which corrects for those tracks leaving the emulsion[22]. For an isotropic distribution of the recoil protons in the centre of mass system, and a constant scattering cross section in an energy interval around E, the total number of neutrons falling per cm^2 per second per energy interval is given by:

$$n'(E) = \frac{N\,k\,/\,F}{c\cdot n\,v\,t} \qquad (5)$$

where N is the total number of recoils,
k is the escape correction,
F is a factor which depends on the angular distribution. It is given by

---

[+] Own measurements (unpublished).

[++] I wish to thank the Chemistry Department for providing me with the solution.

$(1 - \cos^2 20^\circ)$ in the case of recoil protons and, in the case of recoil deuterons, it is obtained by interpolating data deduced from the curves given in reference (26).

σ is the scattering cross section at energy E[26],

n is the number of H- (or D-) nuclei/cm^3,

v is the volume of the emulsion,

and t is the exposure time.

Table 1 gives the calculations for 1100 recoil protons measured in: (1) a plate soaked in ordinary water, and (2) a dry plate. Both plates were exposed for one minute at a power level of 350 kw.

Figure 3 shows the absolute neutron spectrum plotted as log $(n(E)/E)$ against E. The experimental points fit better with a curve of the form:

$$f(E) = aE^2 + bE + c$$

which is valid only for energies less than 12 Mev. To determine the constants a and b, the slope of the given curve: $\frac{\partial f(E)}{\partial E} = 2aE + b$ at the points E = 1.0 and E = 6.5 Mev were measured. These gave the values:

$$a = 0.0165 \quad \text{and} \quad b = -0.45.$$

The spectrum will thus have the distribution:

$$n(E) = A' \sqrt{E} . \exp(-1.035\ E + 0.038\ E^2) \qquad (6)$$

For comparison, the fission curve:

$$n(E) = A . \sinh \sqrt{2.29\ E} . \exp(-1.035\ E) \qquad (7)$$

is also plotted in figures 4 and 5. The constants A' and A were so chosen that the two curves coincide with the experimental results at E = 0.6 Mev. The deviation of the thermal fission neutrons in relation (7), from the experimental points is very clear. There is a general displacement of the distribution towards the lower energy side. The experimental point at the lowest energy (E = 0.32 Mev) is abnormally low. This is because the recoil tracks in this energy have a length of about 6 μ, and may therefore escape detection. The maximum estimated correction for the number of these tracks will not exceed a factor of 1.5.

The numerical value for A' making the area under the curve given by relation (6) equal to the area under the experimental histogram, was also calculated. Relation (6) then becomes:

$$\frac{N(E) = (2.9 \pm 0.5) . \sqrt{E} . \exp(-1.035E + 0.038\ E^2)}{\text{neutrons/cm}^2 . \text{ sec. watt. Mev.}} \qquad I$$

TABLE I.

Neutron Energy Distribution (1100 recoil proton- tracks).

Recoil energy interval Mev	$\bar{E}$ Mev	E_n Mev	net no. of events N (1)	(2)	σ	correction escape factor, k (1)	(2)	n'(E) x10^4 (1)	(2)	n(E)
0.20 - 0.39	0.3	0.32	118	2	7.9	1.00	1.00	6.80	0.55	0.72 ± 0.07
0.40 - 0.79	0.6	0.64	278	73	5.79	1.00	1.00	11.12	14.00	1.49 ± 0.08
0.80 - 1.19	1.0	1.06	140	53	4.31	1.00	1.01	7.31	13.15	1.16 ± 0.08
1.20 - 1.59	1.4	1.49	97	30	3.57	1.00	1.01	6.13	8.98	0.91 ± 0.08
1.60 - 1.99	1.8	1.92	52	12	3.10	1.00	1.02	3.87	4.22	0.53 ± 0.07
2.00 - 2.39	2.2	2.35	43	13	2.80	1.01	1.02	3.50	5.21	0.52 ± 0.07
2.40 - 2.79	2.6	2.77	35	6	2.55	1.01	1.03	3.14	2.60	0.41 ± 0.06
2.80 - 3.19	3.0	3.20	14	5	2.32	1.01	1.03	1.39	2.44	0.22 ± 0.05
3.20 - 3.59	3.4	3.62	11	6	2.12	1.01	1.04	1.21	3.17	0.22 ± 0.05
3.60 - 3.99	3.8	4.05	7	1	1.96	1.02	1.04	0.82	0.56	0.10 ± 0.03
4.00 - 4.39	4.2	4.48	5	2	1.83	1.02	1.05	0.63	1.22	0.10 ± 0.03
4.40 - 4.79	4.6	4.90	7	0	1.72	1.02	1.06	0.94	0.00	0.10 ± 0.03
4.80 - 5.19	5.0	5.33	3	2	1.62	1.03	1.07	0.44	1.46	0.09 ± 0.04
5.20 - 5.59	5.4	5.75	4	0	1.53	1.03	1.09	0.62	0.00	0.06 ± 0.025
5.60 - 5.99	5.8	6.18	0	2	1.46	1.04	1.10	0.00	1.66	0.05 ± 0.025
6.00 - 6.39	6.2	6.61	2	0	1.38	1.04	1.11	0.34	0.00	0.03 ± 0.02
6.40 - 6.79	6.6	7.03	1	1	1.32	1.05	1.13	0.19	0.91	0.05 ± 0.025
6.80 - 7.19	7.0	7.46	1	1	1.26	1.05	1.14	0.18	0.96	0.05 ± 0.025
7.20 - 8.19	7.7	8.20	2	0	1.18	1.06	1.15	0.20	0.00	0.02 ± 0.01

$\bar{E}$: mean proton energy in the interval considered.

E_n: corrected mean neutron energy $1/4. = \bar{E} / \overline{\cos^2 \theta} = \bar{E} \dfrac{\int dp}{\int \cos^2 \theta \, dp}$

where dp is the angular distribution of the recoils in the laboratory system $\propto 2\pi \sin\theta . d\theta$. The limits of the integral are taken from 0^o to 20^o. Therefore, $E_n = 1.065 \bar{E}$.

n'(E): number of neutrons falling/cm^2. sec., at 350 kw, per one neutron energy interval (i.e. 0.213 Mev).

n(E): calculated number of neutrons/cm^2. sec. per watt per one Mev interval. The given values are obtained from the results of the two plates 1 and 2 taking the statistical weight into consideration. The errors in n(E) are merely the statistical fluctuations.

σ: scattering cross section in barns.

where E is the neutron energy measured in Mev. Here the error in the constant A' contains all sources of uncertainities (e.g. statistical, uncertainities in water contents, in cross section, . . . etc.).

From the distribution it is clear that the maximum neutron energy is:

$$\bar{E}_n = \frac{\sum E_i\, n(E)}{\sum n(E)} = 1.9 \pm 0.4 \text{ Mev.}$$

Extending the calculations to the other plates, one can determine the total fast neutron flux with energies more than 0.2 Mev. Table 2 gives the results of these calculations for four plates, the first two of which were mentioned before. The mean neutron flux is:

$$\phi = (2.2 \pm 0.4) \quad \text{neutrons/cm}^2\text{. sec. watt.} \qquad \text{II}$$

TABLE II.

Fast neutron flux at the channel opening.

No.	Description of plate	measured area mm^2	number of recoils	flux ϕ, neutrons/ cm^2. sec. watt.
1	H_2O plate at 350 kw, irradiation of 27/4-56	0.5	820	2.60 ± 0.57
2	dry plate at 350 kw, irradiation of 27/4-56	0.9	250	3.85 ± 1.36
3	D_2O plate at 350 kw, irradiation of 27/4-56	0.9	825	1.50 ± 0.35
4	H_2O plate at 24 w, irradiation of 9/5-56	65	50	2.73 ± 0.82
			mean:	2.20 ± 0.40

2) Gamma Rays:

To avoid any recoil tracks interfering with the deuteron photoprotons, only backward tracks ($\theta \geq 90^\circ$) were considered. Similar areas in D_2O- and H_2O- plates of the same exposure series were measured. The difference between the two measurements is - within statistical fluctuations- due to the deuteron photo protons.

Arranging the tracks into energy intervals, one can calculate the energy of the interacting photon by using equation (2). Again, taking into consideration the escape correction factor for different angular zones, one obtains the real number of interactions in the backward hemisphere. This number is clearly half the total number in the 4π space, since the distribution is symmetric around the 90° -axis. The total number of photons n(k), with an energy k and corresponding to an energy group of photo protons, is given by:

$$n(k) = \frac{2 \sum^{\theta} [N(E,\theta).k(\theta)]}{\sigma(k).n.v.t} \qquad (8)$$

where $N(E,\theta)$ is the net number of tracks at certain intervals of energy and angle,
$k(\theta)$ is the escape correction factor,
k is the photon energy = 2 E + 2.2 Mev,
$\sigma(k)$ is the deuteron photo cross section at an energy k,
n is the number of D- nuclei/cm^3,
v is the examined volume of the emulsion,
and t is the exposure time.

Calculations were applied to 100 measured tracks, the results of which are shown in table III.

TABLE III

Energy distribution of gamma rays (100 tracks)

Photon energy k Mev	n(k) photons/cm^2. sec.watt.Mev
2.8	19.7 ± 4.5
3.6	18.1 ± 6.5
4.8	10.6 ± 5.9
6.0	1.0 ± 0.55
7.2	1.3 ± 0.55
8.4	0.43 ± 0.16
9.6	0.12 ± 0.075

(errors given are only statistical)

Figures 6 and 7 show the distribution. Owing to the very poor statistics, no definite conclusions could be drawn but, one might observe an excess of photons around 8 Mev, which is higher than the expected distribution of gamma rays from

thermal fission of U^{235}. If this is so, the explanation is probably the presence of capture- gamma rays in the beam. A very approximated empirical distribution of the gamma rays at the channel opening is given by the formula:

$$\underline{n(k) = (280 \pm 210).\ \exp(-0.8\ k)} \qquad \text{III}$$
$$\text{photons/cm}^2\text{.sec.watt.Mev}$$

The calculated total gamma flux, with energies greater than 2.5 Mev, in this case is:

$$\underline{I = (40 \pm 30)\ \text{photons/cm}^2\text{.sec.watt}} \qquad \text{IV}$$

Discussion:

Although the statistics, especially for gamma rays, is still poor, an idea about the spectra as well as the fluxes could be given. The technique is so simple that a one day work spent on exposures will be enough for measurements leading to a high statistical accuracy. The only difficulty arises from microscopy which is tedious. Since we considered at first tracks in all directions (total$\simeq$8000), a relatively long time was spent to obtain the above results. The effort (about 3.5 month x man) could be reduced to about the half if one would limit himself to only the forward cone for neutrons, and only to the backward tracks for gamma rays.

Acknowledgements:

The author is deeply indepted to the Director of JENER for kindly providing him with all facilities. He wishes also to thank Mr. Palm of the workshop, and the personnel of the reactor operating group for their help.

Thanks are due to Dr. J. Goedkoop for reading the manuscript.

References:

1) L. Cranberg, G. Frye, N. Nereson and L. Rosen: Phys. Rev. 103/662 (1956).
2) L. Cranberg and N.G. Nereson: LA- 1916 (1955).
3) L. Rosen: U.N. Geneva Conference 4/97 (1955).
4) T. W. Bonner, R.A. Ferrell and M.C. Rinehart: Phys. Rev 87/1032 (1952).
5) D.L. Hill: Phys. Rev. 87/1034 (1952)
6) B.E. Watt: Phys. Rev. 87/1037 (1952).
7) R.B. Leachman: Phys. Rev. 101/1005 (1956).
8) J.S. Fraser: AECL-329/ 39 (1956), G.C. Hanna: AECL-329/ 3 (1956).
9. P.E. Cavanagh and H.J. Dunster: A.E.R.E. Progress Reports 17/21 (1949) 18/17 (1950).
10) J.E. Francis and H.J. Gamble: ORNL-1879/ 20 (1955).
11) J. Kirkbridge: NRDC/58 (1955).
12) C. Moak: unpublished, quoted in reference 13.
13) R. Stephenson: Introduction to Nuclear Engineering, McGraw Hill Co, New York (1954)
14) R.L. Gamble: quoted in reference 7.
15) C. Eggler, C.M. Huddleston, V.E. Krohn and G.R. Ringo: Nucl. Science and Engineering 1/391 (1956).
16) U.S. Government Printing Office: Research Reactors, o-346804/pp 30, 108, 109 (1955)
17) J.W. Motz: Phys. Rev. 86/753 (1952)
18) B. Grimeland: JENER Report-16 (1953): -28 (1954)
JENER Publication-12 (1956)
19) J.Pelser: Physica, 21/22 (1955).
20) M. Bogaardt, W. Hälg and J. Pelser: JENER Report-21 (1953).
21) H.B. Klepp and D.D. Popović: JENER Report-25 (1954).
22) H. Wäffler and S. Younis: Helv. Phys. Acta 24/483 (1951).
23) J.S. Levinger: Phys. Rev. 97/970 (1955).
24) E. P. Ferreira and P.J. Waloschek: U.N. Geneva conference 2/124 (1955)
25) L. Rosen: Nucleonics 11/no. 7 p32 (1953).
26) D.H. Hughes and J.A. Harvey: BNL-325 (1955).

St. 1537
HHE/RL
30.4.1957

Fig. 1. Irradiation arrangement

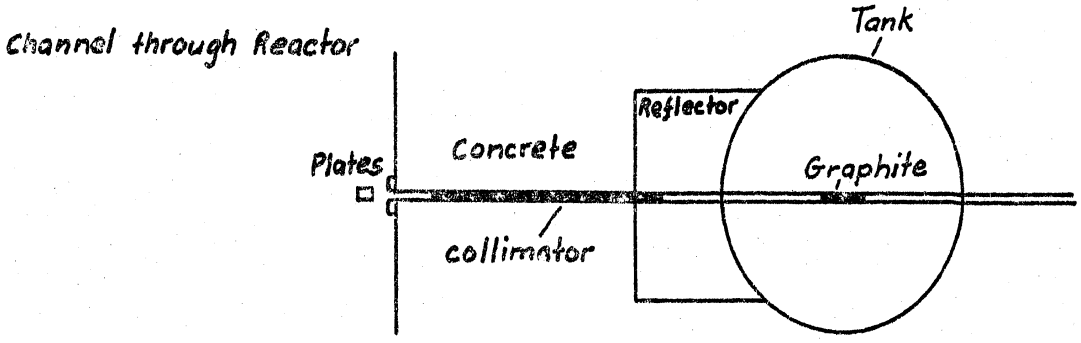

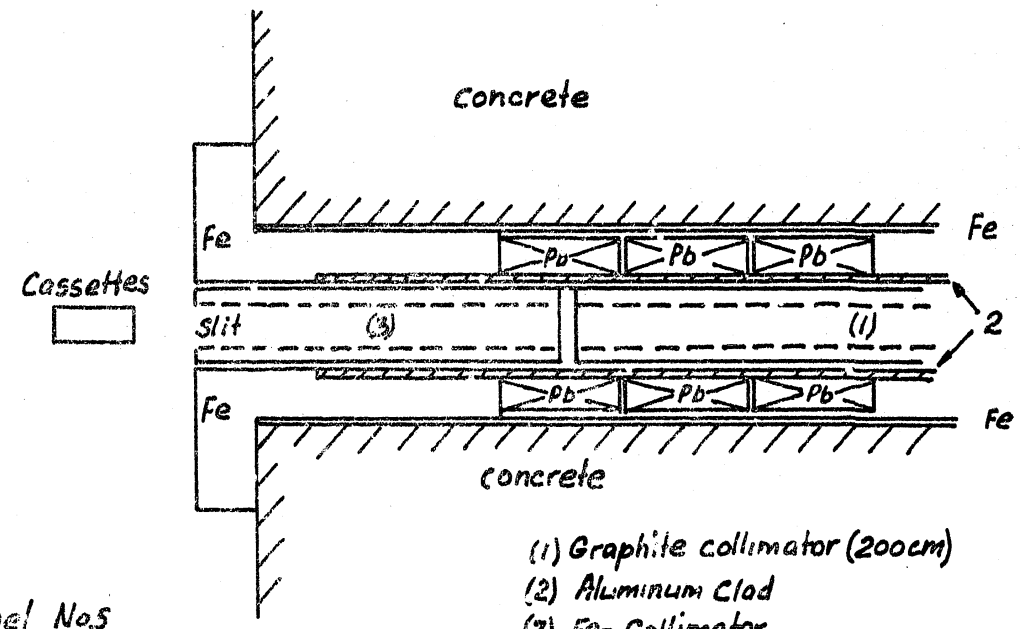

Range Distribution of U^{233}-solution α-tracks in wet emulsion:
170 tracks.

Fig.2.

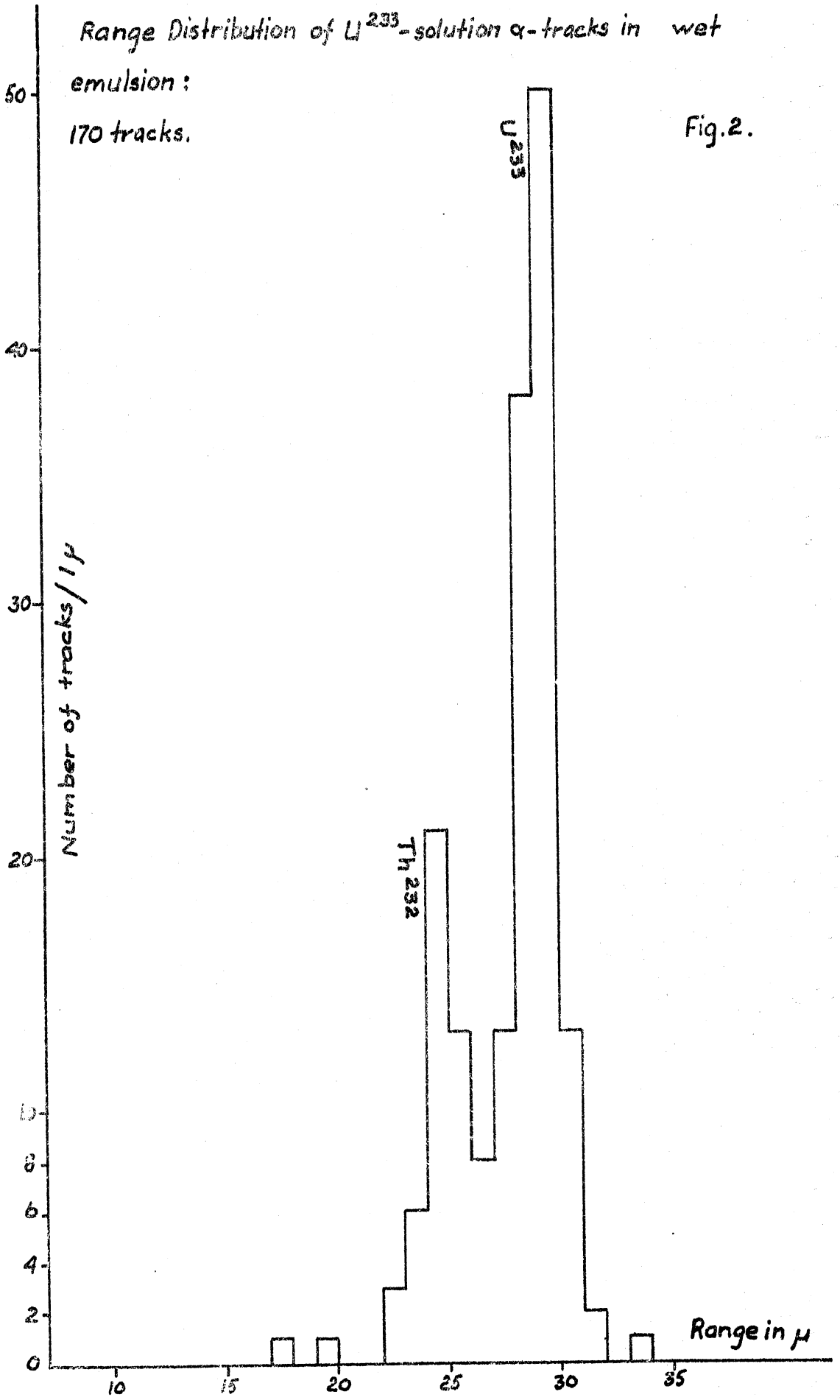

Fig 3: Absolute Fast Neutron Spectrum:

$\log \frac{n(E)}{\sqrt{E}}$ vis E

——— $n(E) = 3.5\sqrt{E}\, e^{-1.035E + 0.038E^2}$

— — — $n(E) = 1.86 \sinh\sqrt{2.29E}\, e^{-1.035E}$

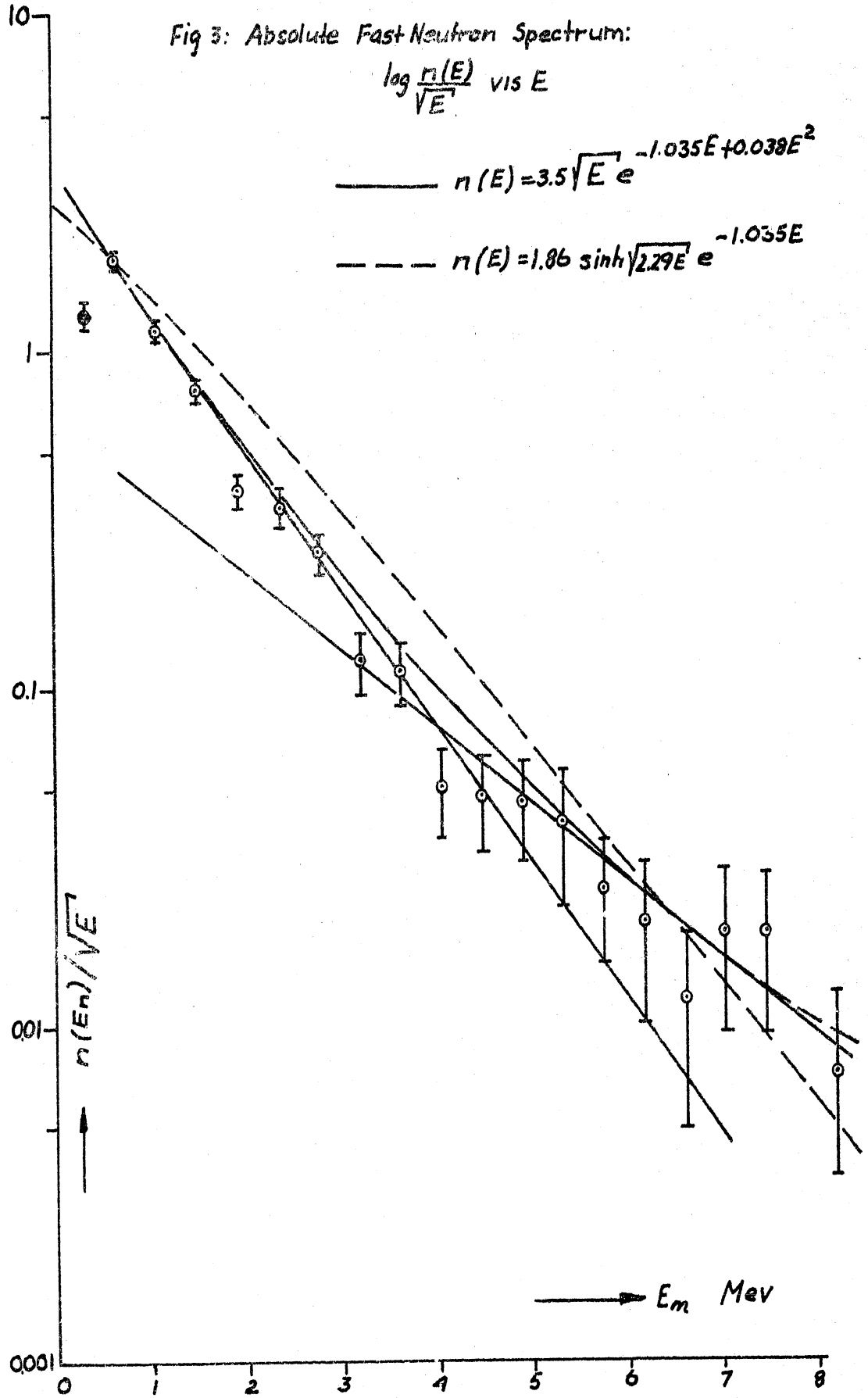

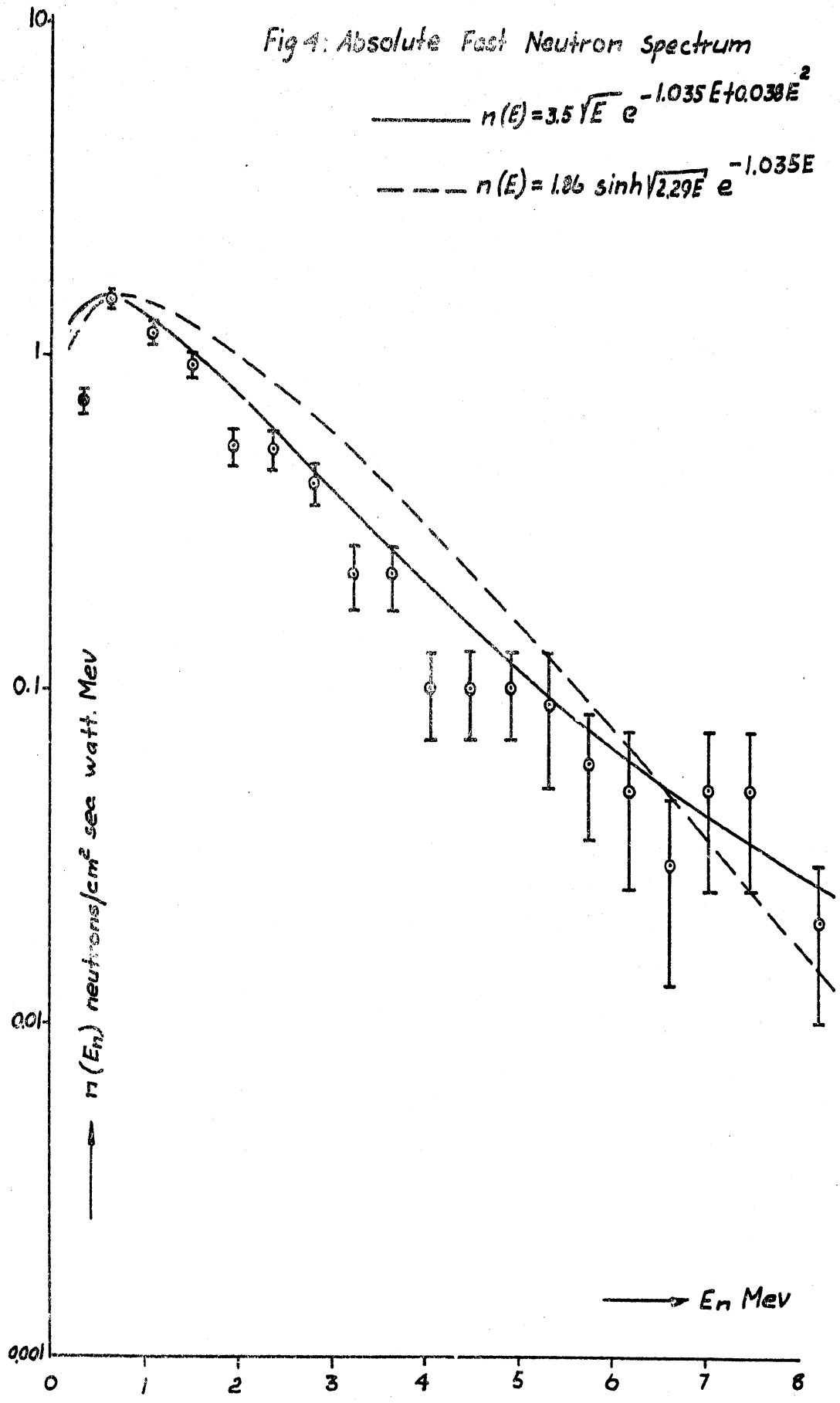

Fig 4: Absolute Fast Neutron Spectrum

——— $n(E) = 3.5\sqrt{E}\, e^{-1.035E + 0.038E^2}$

— — — $n(E) = 1.86 \sinh\sqrt{2.29E}\, e^{-1.035E}$

Fig .5 : Absolute Neutron Energy Spectrum

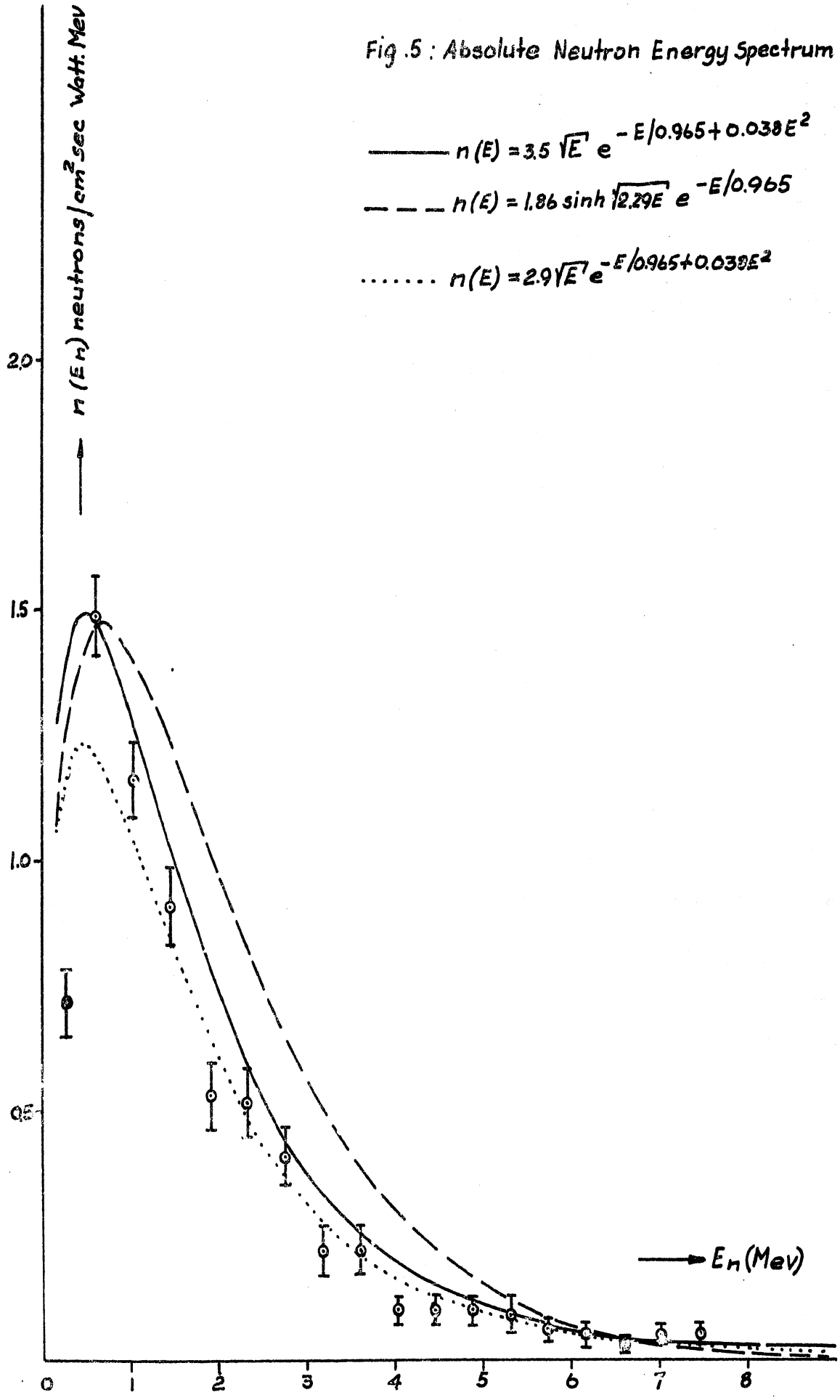

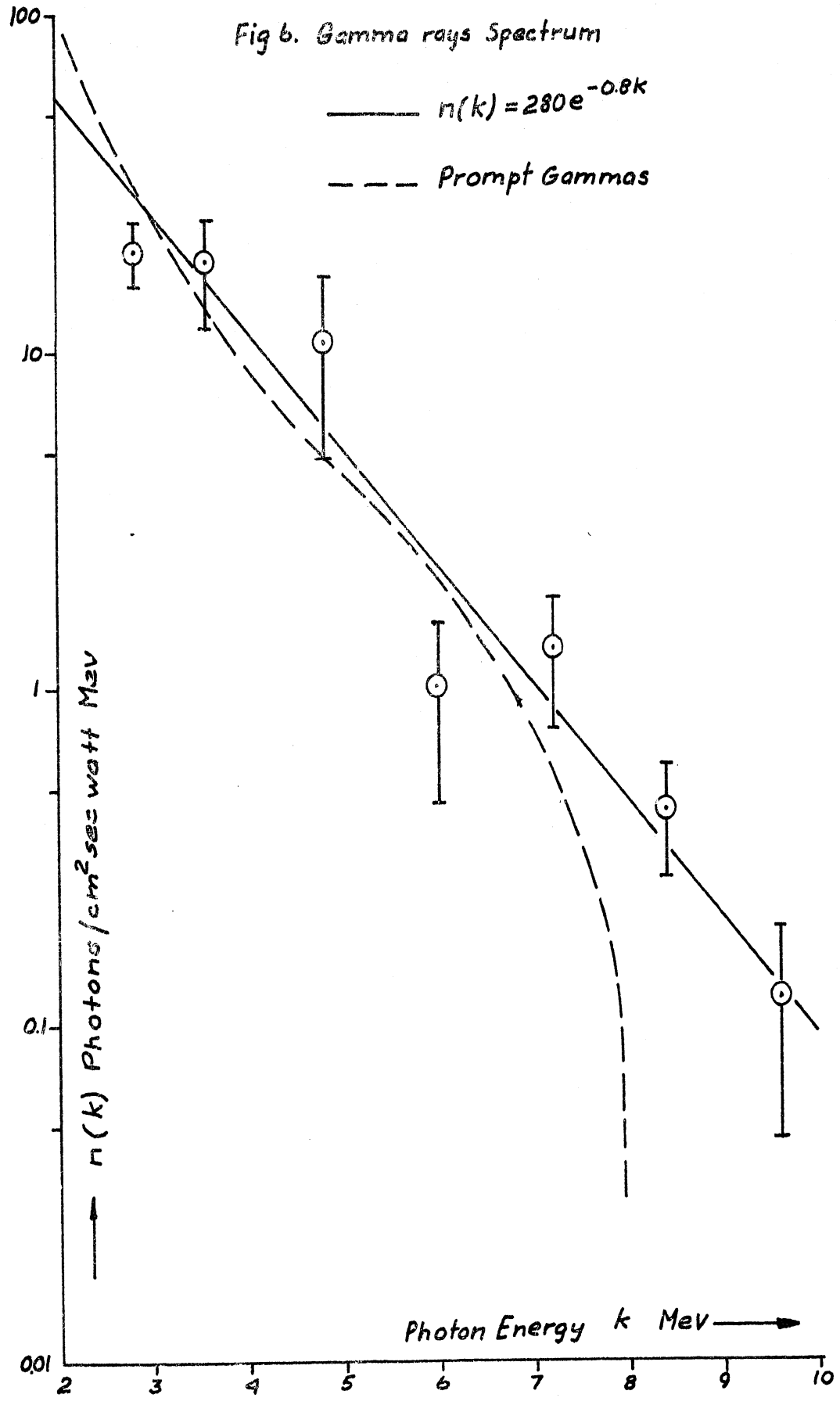

Fig 6. Gamma rays Spectrum

Fig 7: Absolute Gamma.rays Energy Spectrum

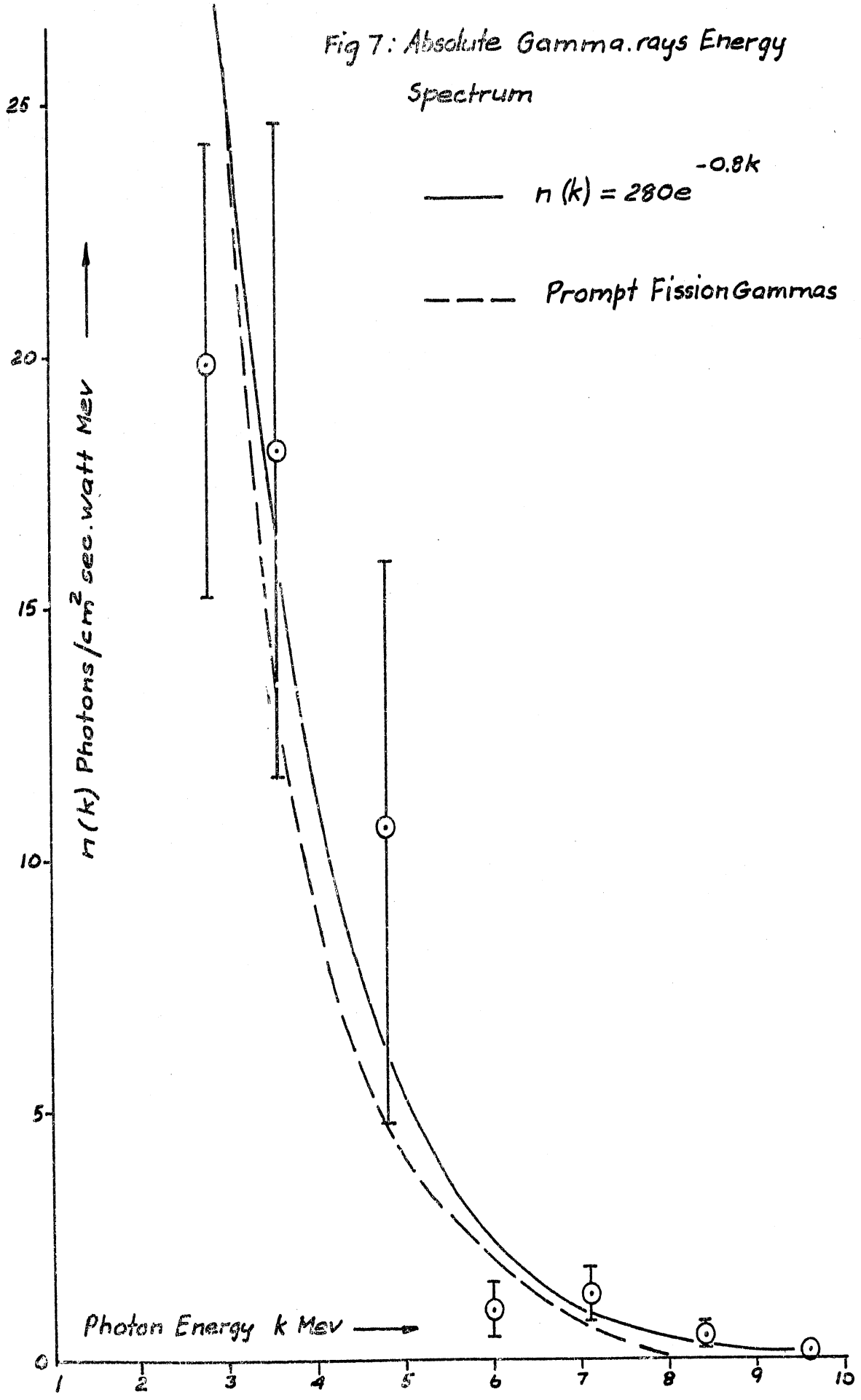

UNCLASSIFIED

JENER REPORT NO. 54

JOINT ESTABLISHMENT FOR NUCLEAR ENERGY RESEARCH
Kjeller near Lillestrøm, Norway.

SEPARATION OF U AND Pu FROM Zr, Nb, Ru AND Cs ON A COLUMN OF MANGANESE DIOXIDE.

By

D. CVJETICANIN AND N. CVJETICANIN

Kjeller, April 1958.

UNCLASSIFIED

CONTENTS

Separation of U and Pu from Zr, Nb, Ru and Cs on a Column of Manganese Dioxide

by

D. Cvjeticanin and N. Cvjeticanin

Abstract

The adsorption of U, Pu, Zr, Nb, Ru, Sr-Y and Cs was examined to provide a good separation of uranium and plutonium from the fission products mentioned.

It was established that it is quantitatively possible to wash UO_2^{++} and PuO_2^{++} from a column of manganese dioxide with 0.1 N HNO_3. Under the same conditions, 99.2% of Zr^{95}, Nb^{95}, Ru^{106} and Cs^{137} was adsorbed.

Introduction

In the aqueous process for the separation of uranium and plutonium from fission products, the most difficult problem is the separation of Zr, Nb, and Ru[1,2]. Because of these difficulties, it is very often necessary to add special steps to a process in order to get a good decontamination from these three elements. Final decontamination of U[3] and Pu[2] from Zr and Nb is obtained by passing the acid solution over a column of silica gel.

Culler[4] used co-precipitation of fission products with manganese dioxide as a preliminary decontamination prior to solvent extraction in reprocessing highly active fuels. Potassium permanganate is added to the feed solution, which is heated, and permanganate is reduced to manganese dioxide. Permanganate and manganese dioxide both oxidize plutonium to PuO_2^{++}. PuO_2^{++} does not adsorb on manganese dioxide. Harmon[5] described a preliminary separation of Ru, Zr and Nb prior to solvent extraction by using potassium permanganate for the oxidation of ruthenium to the volatile tetroxide, which is distilled off from the feed solution. On the other hand, the use of permanganate results in formation of manganese dioxide, which can be used for the removal of Zr and Nb.

It is probable that this process is not the most convenient because of the necessity of separating the precipitate by centrifuging, which is very inconvenient in large-scale experiments and in continuous processing.

The purpose of this work was the examination of the adsorption of U, Pu, Zr, Nb, Ru and some other fission products of interest to the reprocessing and to provide an adequate separation of plutonium and uranium from fission products on a column of manganese dioxide.

Experimental procedure

1. Preparation of manganese dioxide

One of the methods for the preparation of manganese dioxide is to treat potassium permanganate solution with a solution of a manganous salt [6,7] by the reaction:

$$3\ Mn^{++} + 2\ MnO_4^- + 2\ H_2O \rightarrow 5\ MnO_2 + 4H^+$$

G. Forschhammer [6] used a mixture of 2 moles of potassium permanganate and 3 moles of the manganous salt in a dilute solution. A.P. Lunt [7] used a mixture of 400 ml of a saturated solution of potassium permanganate and 400 ml of a saturated solution of manganese sulphate.

In this work, manganese dioxide was prepared by the gradual addition of the solution of manganous sulphate (101.4 gr of $MnSO_4 \cdot H_2O$ in 1 l H_2O) to a solution of the permanganate (63,2 g $KMnO_4$ in 5 l H_2O). After filtration the precipitate was washed with hot water till free from acid, then with 1 l of 3 N HNO_3 and again with water till free from acid. The precipitate was dried for about 20 hours at 110°C. The prepared manganese dioxide was boiled for 5 minutes in 3 N HNO_3 and boiling stopped by the addition of cold distilled water. The precipitate was washed with distilled water until the filtrate was free from acid and then dried for about 80 hours at 110°C. The prepared manganese dioxide was first sieved, and the fraction from 100-140 mesh was used. This fraction contains small amounts of a very fine powder of manganese dioxide easily removable by decantation in water.

2. X-Ray Analysis of Manganese Dioxide

X-ray diagrams were taken with Cu and Mo-irradiation. Only 3-4 faint and diffuse lines were found, indicating that the substance consisted of rather small crystallites (nearly X-ray amorphous). By comparison with the ASTM card index (no. 4-0779), the lattice was identified as γ-MnO_2.

3. Preparation of the Column of Manganese Dioxide

Manganese dioxide (100-140 mesh) was made into a slurry with water and the fine powder removed by decantation. Then it was poured into a 2 mls column. The column was then washed with 50 mls of 1 N HNO_3 and afterwards with distilled water.

4. Procedure

On the column of manganese dioxide, prepared as described above, solutions

of UO_2^{++}, PuO_2^{++}, Pu (IV), Zr^{95} - Nb^{95}, Ru^{106}, Sr^{90}-Y^{90}, Cs^{137}-Ba^{137} were adsorbed separately, and the column washed with HNO_3 in different concentrations.

After washing the column, the quantity of the element in the effluent as well as the quantity adsorbed on the manganese dioxide was determined. In the case of U^{233} and Pu^{239}, only the effluent was analyzed. To determine the quantity of adsorbed element on the column, manganese dioxide was dissolved in dilute HNO_3 containing sodium nitrite, hydroxylamine or hydrogen peroxide, and the solution diluted to a desired volume. Beta and gamma activity were recorded from an aliquot of 0.5-2 mls and alpha activity from an aliquot of 50-100 λ. Alpha activity was measured with a scintillation counter of conventioned type (ZnS screen on the photocathode of an E.M.J. photomultiplier tube) and Beta activity was measured with an ordinary type Philips Geiger-Müller counter.

U^{233} is prepared in the Isotope Department at this Institute.

Pu^{239} was purified by the extraction with 0,2 M TTA (Thenoyltrifluoroacetone) in CCl_4 (8).

The solution of Pu (VI) was prepared using freshly precipitated silver peroxide (9) as oxidizing agent.

Pu (IV) was prepared by evaporating the solution of Pu with nitric acid in the presence of hydrogen peroxide or perchloric acid. This operation was repeated and the residue was dissolved in nitric acid (in this case sodium nitrite could not be used because of the dissolution of MnO_2 in the presence of nitrite). The solution of Zr^{95} - Nb^{95} in 0,5% Oxalic acid (Received from Radiochemical Center, Amersham, England) was treated with conc. nitric acid in the presence of some drops of perchloric acid. The solution was evaporated to dryness to destroy oxalic acid. The operation was repeated several time, at the end the evaporation was carried out with conc. nitric acid. The residue was disolved in 5 N nitric acid. From this solution, the solutions in 0,1 and 1 N nitric acid were prepared by dilution with water.

Ru^{106} was in 8 N nitric acid (Received from Radiochemical Center, Amersham, England). The solutions of Ru^{106} in 0,1, 0,5 and 1 N nitric acid were prepared by dilution the original solution with water.

Sr^{90} and Cs^{137} are separated from a mixture of fission products (10,11).

5. Results

The solution of U^{238}(VI), U^{233}(VI) and Pu^{239}(VI) from 0.001 N HNO_3 (100-200 λ aliquot) was adsorbed on the column of manganese dioxide. The column was

washed with 0.1, 0.5 and 1 N HNO_3. The elution curves for U^{233} (VI) and Pu^{239} (VI) are given in figures 1 and 2. U^{233} (VI) and Pu^{239} (VI) both are qu antitatively eluted.

The experimental data for U (VI), Pu (VI), Zr^{95}-Nb^{95}, Ru^{106}, Sr^{90}-Y^{90} and Cs^{137}-Ba^{137} are given in Table I.

After these experiments, 25 mls of a solution of uranium containing 12.9 g U/ml in 0.1 N HNO_3 was passed through a column, and the column washed with 10 mls of 1 N HNO_3. No Beta or Gamma activity could be detected in the effluent, which means that UX was adsorbed on the column under the conditions mentioned.

At least 25 mls of a solution of UO_2^{++}, Zr^{95}-Nb^{95}, Ru^{106} and Cs^{137} in 0.1 N HNO_3 was passed through a column. After that, the column was washed first with 0.1 N HNO_3 and then with 50 mls 1 N HNO_3. The experimental data are given in Table II.

6. Capacity Determination of Manganese Dioxide for Zr

Zirconium nitrate was dissolved in 4 N HNO_3 and diluted to 1 N HNO_3.

Capacity determinations were carried out by passing about thirty times the amount of Zr necessary to saturate manganese dioxide through a column, washing the column with 50 mls of 1 N HNO_3 and dissolving manganese dioxide in dilute nitric acid plus hydrogen peroxide. Zirconium was determined gravimetrically as ZrP_2O_7 (12).

The obtained value for the capacity was 24 $\pm$ 1 mg/g MnO_2, dried at 110°C.

Discussion

From the results given in Tables I and II, it is seen that Zr^{95}-Nb^{95}, Ru^{106} and Cs^{137} are adsorbed on the column of manganese dioxide and that by using such a column of manganese dioxide, it is possible to separate them from U (VI) and Pu (VI) in a solution of 0.1 N HNO_3.

Separation of uranium from these elements is simple to carry out. When Pu is also present in solution, it is necessary to have an oxidizing agent present to provide PuO_2^{++}; but under these conditions it is probable that some Ru is oxidized to the volatile RuO_4. Perhaps it would be convenient to carry out the oxidation of Pu under conditions similar to the Redox process (4), using $KMnO_4$ or MnO_2 as oxidising agent, or to oxidise Pu at room temperature with silver peroxide or with $S_2O_8^{--}$ Ag^+.

Acknowledgements

This work was performed in the period, June-December, 1957. We are indebted to JENER for the kind hospitality shown us during the work. Our sincere thanks are given to Miss M. Bonnevie-Svendsen for X-ray analysis of manganese dioxide and to Dr. T. J. Barendregt for his constant interest and support during the course of this work.

References

1. F. R. Bruce: International Conference on the Peaceful Uses of Atomic Energy, Vol. 7, P/719 (United Nations, New York, 1956).
2. A. M. Aikin: Chemical Engineering Progress, 53, 82F - 5F (1957).
3. I. R. Flanary: International Conference on the Peaceful Uses of Atomic Energy, Vol. 9, P/539 (United Nations, New York, 1956).
4. F. L. Culler: Ibid, Vol. 9, P/822.
5. M. K. Harmon: H. W. 49544 A (April 3. 1957).
6. I. W. Mellor: Inorganic and Theoretical Chemistry, Vol. XII (Longmans, Green and Co., London, 1932).
7. A. P. Lunt: Analyst, 79, 651 (1954).
8. J. G. Cuninghame and G. L. Miles: J. Inorg. Nucl. Chem., Vol. 3, 54 (1956).
9. G. R. Hall, P. D. Herniman and A. J. Walter: AERE C/R 712.
10. R. O. Lingjærde: JENER Report No. 48, 1957.
11. R. Wolschrijn: JENER Report No. 49, 1957.
12. W. W. Scott: Standard Methods of Chemical Analysis, Vol. I. (D. Van Nostrand Co. Inc., New York, 1939).

St.1985.
DCv.NCv/ASl.
11/4-58.

TABLE I

Element Present	Amount of Eluate		Amount of Element Present in Effluent, in %		
U^{233} (VI) ~ 2,5 mg	20 ml	0.1 N HNO_3	99.5		*
U^{233} (VI) ~ 2,5 mg	10 ml	1 N HNO_3	98.4		*
Pu^{239} (VI) ~ 0,6 mg	20 ml	0.1 N HNO_3	98.8		*
Pu (VI) ~ 0,6 mg	10 ml	1 N HNO_3	100.5		*
Pu (IV) ~ 0,5 mg	22 ml	1 N HNO_3	43		x
Pu (IV) ~ 0,6 mg	10 ml	5 N HNO_3	42.8		x
Zr^{95}-Nb^{95} $6.33 \cdot 10^5$ cpm	10 ml	1 N HNO_3	~ 0.02		o
	+ 10 ml	1 N HNO_3	–		
	+ 25 ml	5 N HNO_3	~ 0.06		
	30 ml conc.	HNO_3	69.6		
Zr^{95}-Nb^{95} $6.30 \cdot 10^5$ cpm	10 ml	1 N HNO_3	0.07		x
Ru^{106} $5.51 \cdot 10^5$ cpm	10 ml	0.1 N HNO_3	0.26		*
	+ 10 ml	0.5 N HNO_3	~ 0.05		
	+ 10 ml	1 N HNO_3	0.5		
	+ 10 ml	5 N HNO_3	17		
Ru^{106} $5.41 \cdot 10^5$ cpm	10 ml	0.5 N HNO_3	3.5		o
	+ 10 ml	0.5 N HNO_3	~ 0.08		
	+ 10 ml	1 N HNO_3	~ 0.09		
	+ 10 ml	5 N HNO_3	6.9		
Sr^{90}- Y^{90} $5 \cdot 10^5$ cpm	10 ml	0.1 N HNO_3	45.4	mostly Sr^{90}	o
	+ 10 ml	0.1 N HNO_3	0.6		
	+ 10 ml	1 N HNO_3	56	mostly Y^{90}	
Cs^{137}-Ba^{137} $4.12 \cdot 10^5$ cpm	10 ml	0.1 N HNO_3	–		o
	+ 20 ml	1 N HNO_3	–		
	+ 10 ml	5 N HNO_3	–		
Ru^{106} $5.4 \cdot 10^5$ cpm (treated with $(NH_4)_2$, S_2O_8 and Ag NO_3 at room temperature)	10 ml	1 N HNO_3	2.7		*

TABLE I continued

The column volume of manganese dioxide was 2 mls and the flow rate was 3 mls/min/cm^2.

(*) The column of manganese dioxide was prepared as previously described, washed with 50 mls of 1 N HNO_3 and then with water until the effluent was free from acid.

(x) The column of manganese dioxide was pre-treated with 1 N HNO_3.

(o) The column was pre-treated with 0.1 N HNO_3.

TABLE II

Element Present in 25 mls			Amount Eluate	Beta Activity in the Effluent in %
U 0.3237 gr				
Zr^{95}-Nb^{95}	841.700	cpm	25 ml 0.1 N HNO_3	0.8
Ru^{106}	2.164.800	cpm		
Cs^{127}	130.560	cpm	+ 50 ml 1 N HNO_3	3.7

FIGURE 1.

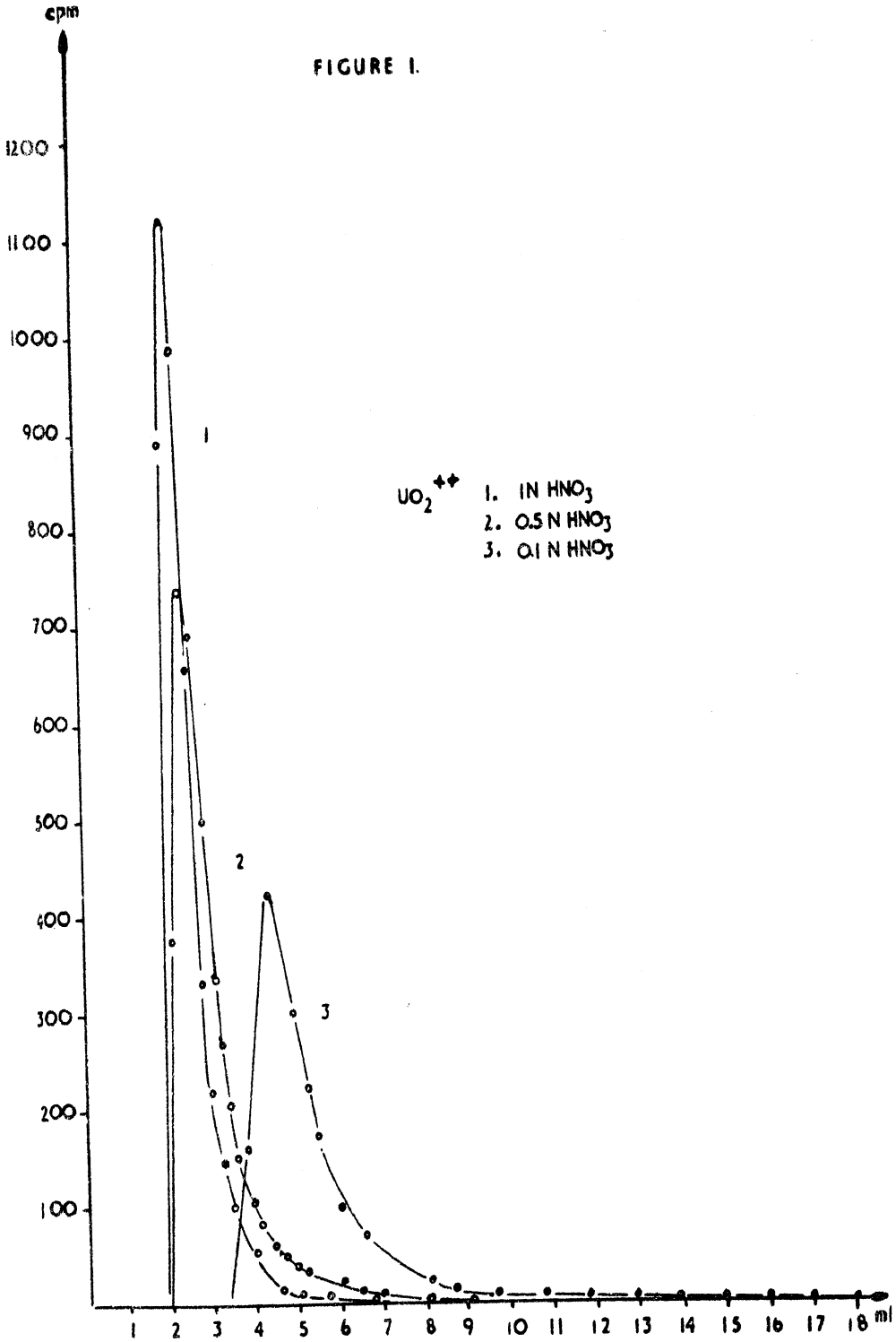

FIGURE 2.